



AMERICAN UNIVERSITY OF BEIRUT

RANITIDINE ABATEMENT IN CHEMICALLY ACTIVATED  
PERSULFATE SYSTEMS: ASSESSMENT OF INDUSTRIAL  
IRON WASTE FOR SUSTAINABLE APPLICATIONS

by  
SAHAR JOSEPH NAIM

A thesis  
Submitted in partial fulfillment of the requirements  
for the degree of Master of Science  
to the Department of Chemistry  
of the Faculty of Arts and Sciences  
at the American University of Beirut

Beirut, Lebanon  
April 2015

AMERICAN UNIVERSITY OF BEIRUT

RANITIDINE ABATEMENT IN CHEMICALLY ACTIVATED  
PERSULFATE SYSTEMS: ASSESSMENT OF INDUSTRIAL  
IRON WASTE FOR SUSTAINABLE APPLICATIONS

by

SAHAR JOSEPH NAIM

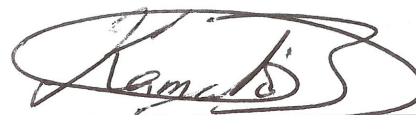
Approved by:



---

Advisor


Dr. Antoine Ghauch, Associate Professor  
Department of Chemistry



---

Member of Committee

Dr. Kamal Bouhadir, Associate Professor  
Department of Chemistry



---

Member of Committee

Dr. Houssam El-Rassy, Associate Professor  
Department of Chemistry

Date of thesis defense: April 28, 2015

# AMERICAN UNIVERSITY OF BEIRUT

## THESIS, DISSERTATION, PROJECT RELEASE FORM

Student Name: \_\_\_\_\_  
Last First Middle

Master's Thesis  
Dissertation

Master's Project

Doctoral

I authorize the American University of Beirut to: (a) reproduce hard or electronic copies of my thesis, dissertation, or project; (b) include such copies in the archives and digital repositories of the University; and (c) make freely available such copies to third parties for research or educational purposes.

I authorize the American University of Beirut, **three years after the date of submitting my thesis, dissertation, or project**, to: (a) reproduce hard or electronic copies of it; (b) include such copies in the archives and digital repositories of the University; and (c) make freely available such copies to third parties for research or educational purposes.

\_\_\_\_\_  
Signature

\_\_\_\_\_  
Date

## ACKNOWLEDGMENTS

I address my sincerest gratitude to my thesis supervisor, Prof. Antoine Ghauch, who has profoundly directed my thesis work with thoughtful guidance, continuous encouragement, constructive criticism, and full patience. I would like to express my appreciation to him for his advice, as he constantly motivates me to remain focused on achieving my goal.

I am grateful to the other members of my thesis committee: Prof. Kamal Bouhadir and Prof. Houssam El Rassy for reviewing my thesis and providing important feedback. I thank as well all the Faculty members and the staff of the Chemistry Department for their academic, administrative, and technical support.

I convey special acknowledgement to the Central Research Laboratory (KAS CRSL) where I pursued many experiments and took advantage of the provided instrumental facilities. I am grateful to the director of the Laboratory Dr. Youssef Mouneimne. I indeed greatly appreciate the best engineer ever Joan Younes for his generous time spent in providing essential technical assistance. Also deep thanks to the manager Rania, as well as the engineers Chady and Samer.

I extend my gratitude to the NAS-USAID, NSF-PEER, URB-AUB, and LNCSR for funding this research project, RYMCO (NISSAN) where industrial iron was collected, and the mechanical engineering department where iFe was sieved. Many thanks also for the AUB Library facilities among which I accessed my resources and to Dr. Amy Zenger for her help in the writing center.

I want to express my gratitude to Habib Baydoun and Al Muthanna Tuqan, the members of Dr. Ghauch research group who have provided early training and guidance. My deeply-felt thanks are to Ghada Ayoub who wasn't only a partner and a group member who I can freely discuss ideas with, but also a friend, a sister, and the biggest supporter. Also, I want to thank all people who were members of Dr. Ghauch research group: Maya, Amer, Hadi, Nadine, Nancy, Alaa, and Nour.

“The only hurdle between you and what you want to be is the support of other people” as quoted by David Joseph Schwartz. This makes me grateful to all my colleges mainly Remi, Malek, Mai, Malak, Tarek, Mohammad, Tharalla, Ghinwa, Daniel, Rasha, Naim, Mazhar and Antranik and all other chemistry graduates, and to other friends who supported me as well: Farah, Sarra, Abbas, Jamil, and Hadir.

Lastly, and above all, my entire gratitude and pride goes to my parents who have strived hard to provide me and my sisters a good education. My words are really short in expressing my acknowledgement to their continuous support for me in all my pursuits. Their love and motivation are always my bedrock. Thanks to my sisters Alexa, Sandra, and Carine for their concern, support, and strength all these years.

## AN ABSTRACT OF THE THESIS OF

Sahar Joseph Naim for Master of Science  
Major: Chemistry

Title: Ranitidine abatement in chemically activated persulfate systems: Assessment of industrial iron waste for sustainable applications

This work assessed the use of industrial iron-based scrap in the activation of persulfate (PS) into sulfate radicals (SRs) for the removal of ranitidine (RAN) (28.5  $\mu\text{M}$ ) from aqueous systems. Knowing that  $\text{Fe}^{2+}$  released from iFe is the main activator toward PS, the optimal molar ratio of  $\text{Fe}^{2+}$ :PS was investigated and appeared to be 1:1. A comparative study between industrial iron (iFe) and commercial iron (cFe) at 2 successive experimental runs, each for 1 h, revealed that iFe present some advantages over cFe in terms of reaction stoichiometric efficiency (RSE) and sludge formation. A low load of iFe (1 mg / 20 mL) was utilized to provide adequate amounts of Fe for PS activation without leaving excessive Fe residuals in water. It was feasible to get almost a complete RAN removal over 1 h reaction with a ratio of dissolved iron species (equivalent to  $\text{Fe}^{2+}$ ):PS of only 0.166:1. The employment of iFe in PS-based AOPs was evaluated at different ionic strength conditions controlled by  $\text{NaClO}_4$  background electrolyte. It was also assessed in chloride-containing solutions and bromide-containing solutions at  $[I] = 100$  mM. Results showed that the increase in ionic strength lowered down the rate of RAN degradation. However, halides appeared enhancing PS activation for RAN removal rather than quenching. The reactivity of bromide was slightly more advantageous than the reactivity of chloride. In both ionic matrices, iFe has sustained its activity with optimum concentration of  $\text{Br}^-$  and  $\text{Cl}^-$  at 1 mM. Total organic carbon (TOC) was analyzed at different PS:iFe molar ratios. It was revealed that the amount of iron corrosion products (ICPs) formed is directly related to the concentration of PS and to the amount of iFe used. Although degradation was successful at low iFe load, mineralization was negligible. However, co-precipitation could be more significant at higher iFe levels. The HPLC/MS chromatograms showed the presence of a RAN intermediate detected at 331 m/z that dissipates gradually throughout the treatment.

# CONTENTS

ACKNOWLEDGMENTS.....	v
ABSTRACT.....	vi
LIST OF ILLUSTRATIONS.....	ix
LIST OF TABLES.....	xii
LIST OF ABBREVIATIONS.....	xiii

## Chapter

I. INTRODUCTION.....	1
A. Literature Review.....	4
1. Occurrence of Pharmaceuticals.....	4
2. Sources of Pharmaceuticals.....	6
3. Fate of Pharmaceuticals in the Environment.....	7
4. Effect of Pharmaceuticals in the Environment.....	10
5. Properties of Ranitidine.....	11
6. Prior to Advanced Oxidation Processes.....	14
a. Fe <sup>0</sup> / H <sub>2</sub> O system.....	14
i. Redox Route (Degradation/ Transformation to Less Harmful Byproducts.....	14
ii. Adsorption/ Co-precipitation Route (Immobilizing).....	15
7. Advanced Oxidation Processes (AOPs).....	17
a. Fe <sup>0</sup> / H <sub>2</sub> O <sub>2</sub> system.....	17
b. Fe <sup>0</sup> / PS system.....	18
B. Objectives.....	22
II. MATERIALS AND METHODS.....	23
A. Chemicals.....	23
B. Chemical Analysis.....	23

C. Experimental Setup.....	26
1. Industrial Iron Boring Scrap Collection.....	26
2. Batch Experiments.....	27
<b>III. RESULTS AND DISCUSSION.....</b>	<b>30</b>
A. Characterization of Iron-Based Particles.....	30
1. Commercial Iron (cFe).....	30
2. Industrial Iron Waste (iFe).....	30
B. Optimization of Fe <sup>2+</sup> :PS Ratio.....	34
1. FeCl <sub>2</sub> vs FeSO <sub>4</sub> .....	34
2. Single Fe <sup>2+</sup> Additions.....	35
3. Sequential Fe <sup>2+</sup> Additions.....	37
C. Evaluation of iFe Efficiency, Sustainability, and Corrosivity.....	40
D. Application of iFe at Low Iron Load in Different Water Matrices Containing Chlorides and Bromides (the Main Sea Water Components).....	44
1. Optimization of Ionic strength (RAN/PS/iFe/NaClO <sub>4</sub> Systems).....	44
a. Non-Controlled Ionic Strength System.....	44
b. Controlled Ionic Strength Systems.....	48
2. Application of iFe in the Presence of Chlorides at Concentrations as that in Brackish Water (RAN/PS/iFe/NaClO <sub>4</sub> /NaCl Systems).....	50
3. Application of iFe in the Presence of Bromides at Concentrations as that for Sea Water (RAN/PS/iFe/NaClO <sub>4</sub> /NaBr Systems).....	54
E. TOC Analysis at Different PS:iFe Molar Ratios.....	59
F. Study of Iron Corrosion Products (ICPs).....	62
G. Characterization of iFe after Reaction.....	64
H. Identification of Transformation Products and Proposed Degradation Scheme	68
<b>IV. CONCLUSION.....</b>	<b>74</b>
<b>BIBLIOGRAPHY.....</b>	<b>76</b>



## ILLUSTRATIONS

Figure.....	Page
<b>Fig. 1.</b> Calibration curve by spectrophotometric method for quantification of PS showing absorbance of the PS-KI complex vs concentration of PS at 40 $\mu\text{M}$ , 50 $\mu\text{M}$ , 60 $\mu\text{M}$ , 80 $\mu\text{M}$ , and 100 $\mu\text{M}$ . Error bars represent standard deviation of six replicates. ....	25
<b>Fig. 2.</b> Calibration curve by AA for quantification of dissolved iron species (equivalent $\text{Fe}^{2+}$ ) showing absorbance vs concentration of $\text{Fe}^{2+}$ at 2 ppm, 5 ppm, 7 ppm, 9 ppm, 12 ppm, and 15 ppm. Error bars represent standard deviation of three replicates. ....	26
<b>Fig. 3.</b> Brake disc skimming and iron boring scrap collection. ....	27
<b>Fig. 4.</b> (a) Picture, (b) SEM image, and (c) EDS analysis of commercial iron powder. ....	30
<b>Fig. 5.</b> (a) Picture and (b) SEM image of non-sieved iron boring scrap from a rotor disc. (c, d) SEM images and (e, f) EDS analysis of the surface of this industrial iron and of the spiral deposit present on it, respectively. ....	31
<b>Fig. 6.</b> (a) Picture of a brake pad. (b) SEM image of a sample taken from the top of the brake pad, and its corresponding (c) EDS analysis.....	33
<b>Fig. 7.</b> Comparison between the percentages of RAN degradation after 10 min of injecting $\text{FeSO}_4 \cdot 7\text{H}_2\text{O}$ and $\text{FeCl}_2 \cdot 4\text{H}_2\text{O}$ at concentrations of 148 $\mu\text{M}$ , 500 $\mu\text{M}$ , and 892 $\mu\text{M}$ . Error bars represent standard deviation of two replicates.....	35
<b>Fig. 8.</b> Variations of (a) RAN and (b) PS due to single $\text{Fe}^{2+}$ injections. Experimental conditions: $[\text{Fe}^{2+}]_0 = 56.4 \mu\text{M}$ , 100 $\mu\text{M}$ , and 142 $\mu\text{M}$ , $[\text{RAN}]_0 = 28.5 \mu\text{M}$ , $[\text{PS}]_0 = 100 \mu\text{M}$ . $\text{pH}_i = 6.42$ , $\text{pH}_f$ (case of 56.4 $\mu\text{M}$ ) = 4.51, $\text{pH}_f$ (case of 100 $\mu\text{M}$ ) = 3.84, $\text{pH}_f$ (case of 142 $\mu\text{M}$ ) = 3.83. Error bars represent standard deviation of two replicates. ....	37
<b>Fig. 9.</b> Variation of (a, c, e) RAN and (b, d, f) PS due to sequential $\text{Fe}^{2+}$ injections. Experimental conditions: $[\text{Fe}^{2+}]_{\text{total}} = 56.4 \mu\text{M}$ (a,b), 100 $\mu\text{M}$ (c,d), 142 $\mu\text{M}$ (e,f), $[\text{RAN}]_0 = 28.5 \mu\text{M}$ , $[\text{PS}]_0 = 100 \mu\text{M}$ . $\text{pH}_i = 6.45$ , $\text{pH}_f$ (case of 56.4 $\mu\text{M}$ ) = 3.7, $\text{pH}_f$ (case of 100 $\mu\text{M}$ ) = 3.61, $\text{pH}_f$ (case of 142 $\mu\text{M}$ ) = 3.95. Error bars represent standard deviation of two replicates. ....	39
<b>Fig. 10.</b> Variation of (a) RAN and (b) PS in 2 runs of 5 mg of cFe (< 150 $\mu\text{m}$ ) vs 5 mg of iFe (53- 150 $\mu\text{m}$ ). (c) The % of average RSE for each run. (d) Concentration of iron species (equivalent $\text{Fe}^{2+}$ ) at the end of the reaction. Inset: Picture of the solutions at $t = 120$ min. Pictures of (e) cFe vs (f) sieved iFe. Experimental conditions: $[\text{RAN}]_0 = 28.5 \mu\text{M}$ , $[\text{PS}]_0 = 100 \mu\text{M}$ , $[\text{cFe}]_0 = [\text{iFe}]_0 = 5 \text{ mg} / 20 \text{ mL} = 4.46 \text{ mM}$ . $\text{pH}_i = 6.5$ , $\text{pH}_f$ (case of cFe) = 6.26, $\text{pH}_f$ (case of iFe) = 6.21. Error bars represent standard deviation of two replicates. ....	42

- Fig. 11.** Variation of RAN in the presence of washed iFe (RAN/PS/WiFe) and non-washed iFe (RAN/PS/iFe). Experimental conditions:  $[RAN]_0 = 28.5 \mu\text{M}$ ,  $[PS]_0 = 100 \mu\text{M}$ ,  $[WiFe] = [iFe] = 1 \text{ mg} / 20 \text{ mL} = 892 \mu\text{M}$ .  $\text{pH}_i = 6.5$ ,  $\text{pH}_f$  (WiFe) =  $\text{pH}_f$  (iFe) = 3.9. Additional control experiments without PS or iFe gives  $\text{pH}_f$  (RAN/PS) = 6.6 and  $\text{pH}_f$  (RAN/iFe) = 7.01. Error bars represent standard deviation of two replicates. .... 45
- Fig. 12.** Variation of (a) RAN, (b) PS, (c) %  $\text{RSE}_{\text{av}}$ , and (d)  $k_{\text{obs}}$  at different ionic strength conditions in the presence of different concentrations of  $\text{NaClO}_4$  where  $[I] = [\text{NaClO}_4]$ . (e) Concentration of iron species (equivalent  $\text{Fe}^{2+}$ ) at the end of the reaction. (f) Conductivities with respect to ionic strength values. Experimental conditions:  $[RAN]_0 = 28.5 \mu\text{M}$ ,  $[PS]_0 = 100 \mu\text{M}$ ,  $[iFe]_0 = 1 \text{ mg} / 20 \text{ mL} = 892 \mu\text{M}$ ,  $[\text{NaClO}_4] = 0, 50 \text{ mM}, 100 \text{ mM}, 250 \text{ mM}, 500 \text{ mM}$ ,  $\text{pH}_i = 6.5$  and  $\text{pH}_f = 4.4 \pm 0.1$ . Error bars represent standard deviation of two replicates. .... 47
- Fig. 13.** Variation of (a) RAN, (b) PS, (c) %  $\text{RSE}_{\text{av}}$ , and (d)  $k_{\text{obs}}$  at different  $[\text{NaCl}]$  at  $[I] = 100 \text{ mM}$ . (e) Concentration of iron species (equivalent  $\text{Fe}^{2+}$ ) at the end of the reaction. Experimental conditions:  $[RAN]_0 = 28.5 \mu\text{M}$ ,  $[PS]_0 = 100 \mu\text{M}$ ,  $[iFe]_0 = 1 \text{ mg} / 20 \text{ mL} = 892 \mu\text{M}$ ,  $[\text{NaClO}_4] = 100 \text{ mM}$ ,  $[\text{NaCl}] = 0, 0.1 \text{ mM}, 1 \text{ mM}, 10 \text{ mM}, 100 \text{ mM}$ .  $\text{pH}_i = 6.5$  and  $\text{pH}_f = 4.0 \pm 0.1$ . Error bars represent standard deviation of two replicates. .... 52
- Fig. 14.** Variation of (a) RAN, (b) PS, (c) %  $\text{RSE}_{\text{av}}$ , and (d)  $k_{\text{obs}}$  at different  $[\text{NaBr}]$  at  $[I] = 100 \text{ mM}$ . (e) Concentration of iron species (equivalent  $\text{Fe}^{2+}$ ) at the end of the reaction. Experimental conditions:  $[RAN]_0 = 28.5 \mu\text{M}$ ,  $[PS]_0 = 100 \mu\text{M}$ ,  $[iFe]_0 = 1 \text{ mg} / 20 \text{ mL} = 892 \mu\text{M}$ ,  $[\text{NaClO}_4] = 100 \text{ mM}$ ,  $[\text{NaBr}] = 0, 0.001 \text{ mM}, 0.01 \text{ mM}, 0.1 \text{ mM}, 1 \text{ mM}, 10 \text{ mM}$ .  $\text{pH}_i = 6.5$  and  $\text{pH}_f = 3.9 \pm 0.1$ . Error bars represent standard deviation of two replicates. .... 56
- Fig. 15.** Variation of the Total Organic Carbon (TOC) obtained after one hour reaction in several systems of RAN/PS/ $\text{NaClO}_4$ /iFe where  $[RAN] = 28.5 \mu\text{M}$  and  $[\text{NaClO}_4] = 100 \text{ mM}$ . Case # 1: different concentrations of [PS] at different masses of iFe. Case # 2: different [PS] at same masses of iFe.  $\text{pH}_i = 6.5$  for both cases. Experimental conditions are summarized in Table 5. Blank solution contains RAN/ iFe (400 mg / 40 mL) gives  $\text{pH}_f = 8.8$ . .... 60
- Fig. 16.** Collected masses of ICPs in different systems of RAN/PS/ $\text{NaClO}_4$ /iFe. Experimental conditions:  $[RAN] = 28.5 \mu\text{M}$ ,  $[\text{NaClO}_4] = 100 \text{ mM}$ ,  $[\text{PS}](\text{mM}):i\text{Fe}(\text{mg}/ 40 \text{ mL})$  is 0:200, 5:100, 10:200, and 20:400 for Sys 1, Sys 2, Sys 3, and Sys 4, respectively. Error bars represent standard deviation of two replicates. .... 64
- Fig. 17.** SEM images and EDS analysis for the collected ICPs precipitates from solutions of RAN/PS/ $\text{NaClO}_4$ /iFe systems. Experimental conditions:  $[RAN] = 28.5 \mu\text{M}$  and  $[\text{NaClO}_4] = 100 \text{ mM}$ . Sys 1:  $[\text{PS}]:[i\text{Fe}]$  is 0:200. Sys 2:  $[\text{PS}]:[i\text{Fe}]$  is 5:100. Sys 3:  $[\text{PS}]:[i\text{Fe}]$  is 10:200. Sys 4:  $[\text{PS}]:[i\text{Fe}]$  is 20:400. [PS] in mM and [iFe] in mg/ 40 mL. .... 65

<b>Fig. 18.</b> (a, b) SEM images and (c, d) EDS analysis showing elemental composition of iFe (53-150 $\mu$ M) before and after 1h reaction, respectively. Experimental conditions: [RAN] = 28.5 $\mu$ M, [NaClO <sub>4</sub> ] = 100 mM, [PS] = 5 mM and iFe = 100 mg / 40 mL = 44.64 mM. ....	66
<b>Fig. 19.</b> SEM images of iFe (53-150 $\mu$ M), after 1 week of the 1h reaction is over, at (a) low magnification and (c) high magnification with corresponding (c) EDS analysis. Experimental conditions: [RAN] = 28.5 $\mu$ M, [NaClO <sub>4</sub> ] = 100 mM, [PS] = 5 mM and iFe = 100 mg / 40 mL = 44.64 mM.....	67
<b>Fig. 20.</b> (a, b) SEM images of the magnification of the metallic oxide expansion of Fig. 17 where EDS analysis is considering (c) the expansion and (d) the nearby surface, respectively. Experimental conditions: [RAN] = 28.5 $\mu$ M, [PS] = 5mM, [NaClO <sub>4</sub> ] = 100 mM, and iFe = 100 mg / 40 mL = 44.64 mM. ....	68
<b>Fig. 21.</b> (a) HPLC Chromatogram showing RAN degradation in the RAN/PS/ <i>Fe</i> <sup>2+</sup> + (sequentially spiked) system: 28.5 $\mu$ M/ 100 $\mu$ M/ 100 $\mu$ M. Presence of an oxidation byproduct initially formed and later disappeared after repetitive <i>Fe</i> <sup>2+</sup> + spiking. (b, c) MS spectra showing RAN peak at 315.2 m/z and the oxidation byproduct peak at 331.2 m/z with their corresponding structures. ....	69
<b>Fig. 22.</b> DAD absorption spectrum of RAN (at t = 0 min) and the oxidation product obtained at 3.7 min (at t = 10 min).....	71
<b>Fig. 23.</b> Proposed degradation mechanism of RAN by sulfate radicals in PS/ <i>Fe</i> <sup>2+</sup> + systems at room temperature.....	73
<b>Fig. 24.</b> Proposed degradation mechanism of RAN by hydroxyl radicals in PS/ <i>Fe</i> <sup>2+</sup> + systems at room temperature.....	74

## TABLES

Table .....	Page
<b>Table 1.</b> Measured Concentrations (MCs) of Some Selected Pharmaceuticals in STP Effluents at Specific Sites .....	5
<b>Table 2.</b> Factors Affecting Pharmaceutical Fate: Physico-Chemical Properties and Environmental Factors [36, 39, 42]. .....	9
<b>Table 3.</b> Physiochemical properties of Ranitidine [54, 63, 64].....	13
<b>Table 4.</b> The emission energies of the elements detected by EDS in industrial iron boring scrap .....	32
<b>Table 5.</b> Experimental conditions corresponding for Case # 1 and Case #2 of Fig. 11: [PS] (mM), iFe (mg/ 40 mL), n(PS):n(iFe), and pH <sub>f</sub> .....	61

## ABBREVIATIONS

**AA:** Atomic Absorption

**AMU:** Atomic Mass Unit

**AOPs:** Advanced Oxidation Processes

**APPI:** Atmospheric Pressure Photoionization

**aq:** aqueous

**av:** average

**BET:** Brunauer–Emmett–Teller

**cFe:** Commercial Iron

**$\sigma$ :** Conductivity

**DAD:** Diode-Array Detector

**DI:** Deionized water

**DMA:** Dimethylamine

**DO:** Dissolved Oxygen

**ECs:** Emerging contaminants

**EDS:** Energy Dispersive X-ray Spectroscopy

**EU:** European Union

**HPLC:** High Performance Liquid Chromatography

**HRs:** Hydroxyl Radicals

**[I]:** Ionic strength

**ICPs:** Iron Corrosion Products

**iFe:** Industrial Iron

**ISCO:** In Situ Chemical Oxidation

**k**: rate constant

**MCs**: Measured Concentrations

**MSD**: Mass Spectrometer Detector

**NDMA**: N-Nitrosodimethylamine

**obs**: observed

**PCBs**: Polychlorinated Biphenyls

**pH<sub>i</sub>**: Initial pH

**pH<sub>f</sub>**: Final pH

**PS**: Persulfate

**PRB**: Permeable Reactive Barrier

**RAN**: Ranitidine

**RNO**: p-Nitrosodimethylaniline

**RSE**: Reaction Stoichiometric Efficiency

**r<sub>t</sub>**: retention time

**SEM**: Scanning Electron Microscope

**SHE**: Standard Hydrogen Electrode

**SMX**: Sulfamethoxazole

**SRs**: Sulfate Radicals

**STPs**: Sewage Treatment Plants

**TCE**: Trichloroethylene

**TOC**: Total Organic Carbon

**USEPA**: United States Environmental Protection Agency

**UV**: Ultraviolet

**Vis**: Visible

**WHO:** World Health Organization

**WiFe:** Washed Industrial Iron

**WWTP:** Waste Water Treatment Plant

**ZVI:** Zero Valent Iron

# CHAPTER I

## INTRODUCTION

Maintaining water quality is considered a highly crucial issue particularly after the adverse stresses subjected on existing natural water resources. The increment of anthropogenic activities in the city development, agriculture, and industry has added into the water supplies hundred thousands of harmful compounds that threatened its quality and urged for the improvement in the water treatment strategies [1].

Historically, primitive water remediation methods, such as sand filtration, were only accounting for turbidity, color and taste of water. In the 19<sup>th</sup> century, with the perception of the microbial content of drinking water and its effect on health, the need of eliminating deadly waterborne diseases led to the introduction of chlorine and ozone disinfection for attaining safe free-microbial drinking water. Later in the 20th century, because of the development of gas chromatography and mass spectrometry, the detection of hazardous chemicals, such as disinfection byproducts in chlorinated water, became feasible [2].

As a consequence, assessing the severity of the chemical content of drinking water became indispensable and many international recommendations were set to regulate these chemicals. Up until the 1990's, focus was restricted to the chemicals of persistent occurrence and manifest health influence defined as "priority contaminants" that are regulated under the required limits promulgated by international organizations as World Health Organization (WHO), U.S. Environmental Protection Agency (EPA), and the European Union (EU) [3]. The EU listed 45 chemical pollutants as priority



contaminants including heavy metals (arsenic, cadmium), industrial byproducts, phenols, halogenated polyaromatics, petroleum derivatives and others [4]. However, many other synthetic organic substances have been up to now unregulated because they belong to one of the following categories: (a) they are newly manufactured and are being recently introduced into water systems from the industrial companies, (b) they were present in the aquatic systems in low amounts and were not detected until advanced analytical techniques were developed (HPLC/MS-MS, hyphenated chemical screening techniques, and bioassays) [5-7], or (c) they were previously detected in the water systems but their health impact was not clear until recent elaborations. Because of recent concern about these substances, they were defined as “emerging contaminants” (ECs), and their emerging status might remain until complete assessment of their acute and chronic toxicity in order to regulate them. These ECs comprise of endocrine disrupting compounds as hormones, pharmaceuticals, illicit drugs, non-controlled drugs, sweeteners, surfactants, personal care products, flame retardants, perfluorinated compounds, some organic solvents, complexing agents, and pesticides [8]. The recent successful detection of ECs has revealed their unavoidable and ubiquitous occurrence in the water bodies including influents and effluents of municipal wastewater treatment plants, surface water, groundwater and even drinking water in many regions throughout the World (US, Latin American countries, Canada, European Countries, Middle East, Asian countries, etc.); therefore, ECs are of universal influence on both aquatic ecology and human health [9-13].

Conventional waste water and water treatment strategies, whether physical or chemical or biological (coagulation, flocculation, sedimentation, filtration, microbial attack, disinfection) have failed to achieve efficient removal of the abovementioned

micropollutants [14]. This limitation has promoted the development of alternative methods of which Advanced Oxidation Processes (AOPs) evolved as one of the most promising routes for oxidizing toxic organic micropollutants into carbon dioxide, water, inorganics, or at least into less hazardous transformation products. Among the micropollutants, the pharmaceuticals are a main interest of study because they are used worldwide and have stable therapeutic structures intractable to be removed or controlled once disposed into the water systems.

## **A. Literature review**

### ***1. Occurrence of Pharmaceuticals***

Pharmaceuticals are medicinal drugs needed for therapeutic purposes either for humans or animals. These drugs have stable structures, a persistent character, and they occur universally in water accommodates; therefore they are menacing to the environmental integrity. A large portion of the consumed drug concentration is retained in its original form and excreted into sewage water systems together with some metabolites [15]. Later the drugs are transported into the influents of a waste water treatment plant, arrived unrecovered to its effluents and could leak after that into surface water, seawater, and groundwater [16] . Although the first detection of pharmaceuticals in the US Sewage Treatment Plants (STPs) was in the 1970's (Clofircic acid detection) [17], the concern of the international scientific community about the pharmaceutical threat on the environment was not until the late 1990's [18]. Recent studies acknowledged that only a few concentrations of pharmaceuticals (parts per billion to parts per trillion) in receiving water and drinking water are suspicious of causing hazardous effects on aquatic life and human health [19, 20]. Some examples of pharmaceuticals, divided into a variety of categories according to their mode of function, are presented in **Table 1** with their corresponding concentrations in some STP effluents of different countries

.

**Table 1.** Measured Concentrations (MCs) of Some Selected Pharmaceuticals in STP Effluents at Specific Sites

Categories	Selected Pharmaceuticals	Measured concentrations (MCs) (ng/ L)	Sites of STP effluents	Reference
Analgesic/ Anti-Inflammatory	Ibuprofen	264	Spain	[21]
Antibiotics	Sulfamethoxazole	191	Germany	[22]
Anti-hypertensive	Hydrochlorothiazide	1949	Spain	[23]
Beta-Blockers	Atenolol	2772	Korea	[24]
Antiulcer	Ranitidine	823	China	[25]
Anticonvulsant	Carbamazepine	1283	UK	[26]
Antifungal	Fluconazole	140	Sweden	[27]

## ***2. Sources of Pharmaceuticals***

The sources of contamination of surface water (rivers, estuaries, lakes) and groundwater by human and veterinary pharmaceuticals can be divided into point sources and non-point sources. Point sources have discrete locations that can be easily identified, whereas non-point sources are without definite locations but rather are spread over wide areas and hence are harder to identify. The main point sources of pharmaceutical pollution are:

- Discharges of Municipal Sewage Treatment Plants [28],
- Discharges from pharmaceutical industries [29],
- Hospital effluents [30],
- Domestic discharges of unused pharmaceuticals through drains [31],
- Excretion from human body of non-metabolized pharmaceuticals [31],
- Leak out of waste disposal sites (landfills, septic tanks) [32, 33].

Pharmaceutical pollution through non-point sources is also called diffuse pollution that poses an indirect threat to ground water. It occurs mainly by:

- Manure application to soil while feeding livestock with drugs as antibiotics [34],
- Urban run-off and leakage from sewage systems [35].

While all of the above examples of sources introduce pharmaceuticals into water bodies, the increase in population, accompanied by more drug manufacturing and more consumption, remains the main factor of pollution.

### ***3. Fate of Pharmaceuticals in the Environment***

The persistence of pharmaceuticals in the environment depends on several factors, listed in **Table 2**, some of which are internal, related to the physico-chemical properties of the pharmaceutical itself (partition, sorption, and distribution coefficients), and some of which are external related to the surrounding environmental media (pH, microbial attack) [36]. As a consequence, the fate of a certain pharmaceutical compound will differ from other compounds as it passes into the waste water treatment plant (WWTP), solid environmental matrices (soil, sediments, and sludge), and aquatic environment.

In the WWTP primary treatment stage, some pharmaceutical compounds that are hydrophobic are adsorbed to sludge; however, those that are hydrophilic, with low partition coefficients, are passed untreated from this stage which has a removal efficiency of not more than 30%. In the secondary stage, some compounds undergo biological degradation resulting in the formation of metabolites, but many other compounds are not readily biodegradable [37].

On another aspect, sludge containing pharmaceuticals is mainly applied to soil. The adsorption/ desorption capability of these pharmaceuticals is related to their binding affinity interpreted by Koc. Nevertheless, soil pH has also an important influence on sorption. For example, acidic pharmaceuticals, which are anions at normal environmental pH (6 to 8), show less sorption to soil (soil organic matter is negatively charged). On the contrary, basic compounds present as cations at normal pH, indicate a very strong sorption to soil [38]. Accordingly, these pharmaceuticals are either accumulated or transported with run-off to surface water.

The resisting compounds to primary and secondary treatments as well those that are leaked from soil can end up in surface water where they may interact with organic matter and

living organisms inducing ecological impairments [39], or they may adsorb onto sediments and retain more in the environment [40], or they may also encounter biotic or abiotic degradation and be transformed into byproducts whose identification and evaluation is cumbersome [41]. Furthermore, those having a high leaching index are more likely to be encountered in groundwater.

Consequently, it is of crucial importance to identify for each compound the associated physico-chemical properties, in addition to the surrounding environmental media, in order to assess their fate and their corresponding impacts.

**Table 2.** Factors Affecting Pharmaceutical Fate: Physico-Chemical Properties and Environmental Factors [36, 39, 42].

Physico-chemical properties		
Symbol	Meaning	Elaboration
Kow	Octanol-water partition coefficient	Log Kow < 4 → hydrophilic (remains in aqueous phase) Log Kow > 4 → hydrophobic (interacts with organic matter)
Sw	Solubility of a compound in water	Sw is high → high solubility and high mobility Sw is low → low solubility and more affinity to sorption
GUS	Groundwater Ubiquity Score Index	Index of leachability → Compounds absent in groundwater have low leaching potential (GUS < 1.8)
Koc	Soil Organic Carbon-Water Partitioning Coefficient	For neutral hydrophobic organic compounds, the distribution coefficient “Kd” between water and soil is normalized to total organic carbon content of the soil. High Koc → less mobility Low Koc → more mobility
List of Environmental Factors		
pH	Temperature	Dissolved Organic Matter
Microbial degradation	Ionic Strength	Ionic Composition (minerals, nitrates)
Light	Salinity	Oxygen Content



#### ***4. Effect of Pharmaceuticals in the Environment***

Pharmaceuticals have biological functions, so they can alter the ecosystem (fauna and flora) when present in the environment. The recognition of their persistence, accumulation, risk assessments, and eco-toxicity is necessary to evaluate their influence. Acute and chronic tests are employed to determine their extent of eco-toxicity [43]. Acute toxicity is assessed by standard tests based on laboratory analysis upon exposing sensitive aquatic organisms as algae, invertebrates, and fish [44, 45], or human embryonic cells [46] to matrices containing pharmaceuticals at different conditions. Deleterious effects on the organisms' biological features, mobility, growth, and mortality were encountered after being exposed to pharmaceuticals of concentrations ranging from mg/L to  $\mu\text{g/L}$  in a time less than 100 hours [45, 47]. On the other hand, tests for chronic toxicity are more complex due to requiring longer exposure time (more than 20 days for example) and investigations over life-time stages. Some of these studies revealed that the long term influence of drugs on organisms affects mainly their reproduction [48, 49], as well as their gene expression accompanied by tissue damage [50], larvae failure [51], the development of bacterial resistance [52], and many other impacts. The accumulation of pharmaceuticals can reach an alarming situation of threatening some species, as example, the decline in the vulture population affected by Diclofenac residues [53]. Some studies argued that the real environmental concentrations of drugs are not toxic enough to affect human health [54], but other studies have indicated that the calculation of the risk potential on humans includes the risk potential of aquatic organisms, such as fish, because they are part of human food consumption [55]. In addition, the continuous introduction of drugs into the environment increases in the possibility of their accumulation inside the aquatic

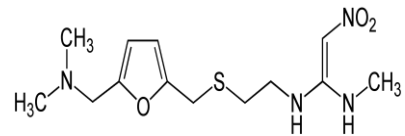
organisms where they may reach high influential concentrations. Moreover, drug-polluted drinking water is another source of influence that poses threat over humans [56]. The assessment of toxicity became more complicated when a mixture of pharmaceuticals occur together [57]. All these troublesome impacts stress on the necessity of improving the treatment plants by including advanced oxidation processes (AOPs) that limit the uncontrolled release of pharmaceuticals into water bodies. In this study, the focus is on an antiulcer pharmaceutical, Ranitidine, which is consumed worldwide and regularly detected throughout different water systems.

### ***5. Properties of Ranitidine***

Ranitidine (RAN) (brand name: Zantac), a gastrointestinal medicine that belongs to histamine H<sub>2</sub>-receptor antagonists, inhibits acid secretions in the stomach and is widely used in treatment of peptic ulcer disease and gastroesophageal reflux disease. Given the essential need of this drug for basic human health [58], it is among the most prescribed pharmaceuticals in the world [59, 60]. RAN is a very soluble compound (**Table 3**); it has therefore the potential of arriving into water ways majorly through excretion, since 30% to 70% of RAN is excreted intact in its parental form [20, 61] with traces of its relevant metabolites. Eventually, RAN has been encountered in the aquatic environment at maximal detected concentration of 1 µg/ L [43]. Particularly, in European and US WWTP effluents, the detected concentration of RAN ranges from 0.2 µg/ L to 0.55 µg/ L [62, 63], and in surface waters it ranges from 1 to 38.5 ng/ L [19, 63] or to higher levels in case the surface water is at the downstream of a WWTP [64]. Because of pervasive identification of RAN in water, recent studies have tested the health side effects it may induce. Evidently the most serious ramification observed was

the formation of N-Nitrosodimethylamine (NDMA), a potent carcinogen, after a process of chloramine disinfection to water containing RAN. The molar conversion from RAN to NDMA has exceeded 77% because its structure contains Dimethylamine (DMA) entity, occurring at C2 to a furan ring donating group, which is very reactive to chloramines [65]. Upon identifying RAN as a carcinogenic precursor, many agencies start to include it in priority compounds list [66]. Furthermore, at environmental concentrations, RAN showed genotoxic and mutagenic activity to aquatic organisms [67], as well as, growth inhibition activity to human cells while participating in a mixture of pharmaceuticals [46]. Moreover, in surface water under direct exposure of sunlight, RAN can be transformed into photo-products that are more stable and of higher risk potential [68]. In conventional WWTPs, RAN showed low biodegradability [69]; therefore, alternative methods are needed to increase its removal efficiency. In this study, RAN degradation has been tested through AOPs by chemically activated persulfate.

**Table 3.** Physiochemical properties of Ranitidine [54, 63, 64]

Therapeutic Group	Compound	Structural Formula	Structure	MW (g mol <sup>-1</sup> )	Log Kow	pKa	S (mg L <sup>-1</sup> ) at 37°C
Antiulcer agent Histamine H <sub>2</sub> -receptor antagonists	Ranitidine	C <sub>13</sub> H <sub>22</sub> N <sub>4</sub> O <sub>3</sub> S		314.4	0.27	8.2 and 2.7	660

MW = Molecular Weight; S = Solubility

## 6. Prior to Advanced Oxidation Processes

### a. $Fe^0 / H_2O$ system

Zero-Valent Iron (ZVI) has been first witnessed as a powerful constituent for contaminant removal in 1972 as reported in the patent literature. Field application wasn't established until the early 1990's by installing Iron Permeable Reactive Barrier ( $Fe^0$  PRB) for in-situ groundwater remediation [70, 71]. ZVI was a promising technology because of low cost and less energy-demand operation and more importantly it was successful in removing different contaminants from water including inorganic metals [72], arsenic [73], nitrates and nitrites [74], halogenated organics [75], and other types of organic compounds [76].

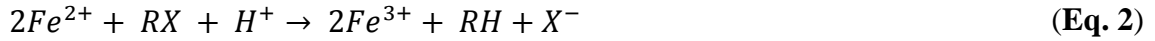
A lot of controversy among the scientific community has developed with respect to the contaminant removal mechanism. The predicted mechanisms of ZVI role can be summed up in two main assumptions: Redox Route, and adsorption/ co-precipitation route.

#### i. Redox Route (Degradation/ Transformation to Less Harmful Byproducts)

- Reduction

Reduction of hazardous contaminants by ZVI is essentially referred to the advantageous corrosion of iron. Based on a thermodynamic argument, this process was majorly attributed so long to the strong reductive capability of ZVI ( $E_{0 (Fe^{2+}/Fe)} = -0.44$  V/ SHE) [77] in reducing halogenated compounds ( $E_{0 (RX/RH)}$  ranges from +0.5 V to +1.5 V at pH 7) [78]. Matheson was the first who proposed the mechanism of this process considering three possibilities of reduction: (a) direct reduction upon surface contact with  $Fe^0$  (**Eq. 1**), (b) indirect reduction by the  $Fe^{2+}$  (**Eq. 2**) generated from

anaerobic and aerobic iron dissolution (**Eqs. 3,4**), (c) or by the hydrogen generated from water reduction (**Eq. 5**) [79].



- Oxidation

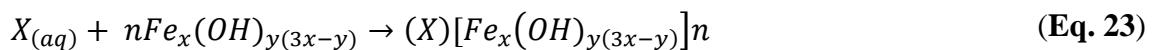
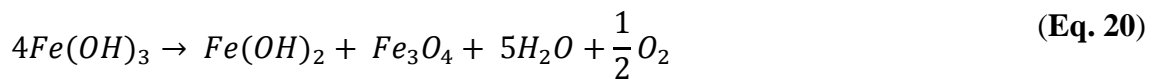
On the other hand, in the presence of dissolved oxygen (DO), ZVI has the potential of generating strongly oxidizing entities mainly hydroxyl radicals (HRs) which prompted contaminant oxidation. The process of  $OH^\bullet$  generation was described as following: (a)  $2e^-$  transfer reaction from ZVI to  $O_2$  results in  $H_2O_2$  formation (Eq. 6), (b)  $4e^-$  transfer reaction reduces  $H_2O_2$  into water (Eq. 7), (c) Fenton reaction (between  $H_2O_2$  and  $Fe^{2+}$ ) produces HRs (Eq. 8) [80]. ZVI oxidative contribution allows successful degradation of a variety of organic compounds as dyes and phenols [81].



## ii. Adsorption/ Co-precipitation Route (Immobilizing)

By contrast, as an alternative approach, Noubactep has reassessed the process of contaminant removal suggesting the concept of adsorption/ co-precipitation of contaminants onto or with the growing oxide layer in the vicinity of  $Fe^0$  [82]. Any further oxidation or reduction is basically occurring to the adsorbed or entrapped species

in the matrix of iron oxides ( $Fe(OH)_2$ ,  $Fe(OH)_3$ ,  $FeOOH$ ,  $Fe_2O_3$ ,  $Fe_3O_4$ ) [83, 84]. The mechanism was proposed by Ghauch and coworkers as following: (a) iron passivation in the presence of oxygen (Eq. 9), (b) followed by iron depassivation (Eqs. 10-12). (c)  $H_2$  production decreases at neutral pH (Eq. 13), (d) therefore  $O_2$  reduction is more favorable (Eq. 14). (e)  $Fe^{2+}$  is oxidized into  $Fe^{3+}$  in the presence of  $O_2$  (Eq. 15). (f) When  $[Fe^{2+}]$  or  $[Fe^{3+}] > 10^{-5} M$  (exceeding the limit of solubility) at  $5 < pH < 10$ , iron hydroxides are formed (Eqs. 16, 17). (g) These iron hydroxides undergo dehydration producing non-protective oxide scales (Eqs. 18-21) that are responsible of contaminant “X” (h) adsorption (Eq. 22), and (i) co-precipitation (Eq. 23) [85].



## 6. Advanced Oxidation Processes (AOPs)

### a. $Fe^0/H_2O_2$ system

Although ZVI in the presence of oxygen could trigger strong oxidants formation (Eqs. 6-8) without the aid of any external reagent, this approach encountered a low yield of less than 5 % of oxidant species converted from iron capable of targeting contaminants. Therefore,  $Fe^0/H_2O$  system was unable to oxidize recalcitrant contaminants [86]. Moreover, ZVI high load application (40 g/ L) is another limitation because more sludge could be formed without reaching full removal extent [87]. An alternative approach suggested oxidant feeding to the  $Fe^0/H_2O$  system, for instance, adding  $H_2O_2$  as an external oxidant to provide faster generation of HRs while using fewer amounts of iron in a less contact time.  $H_2O_2$  together with the generated  $Fe^{2+}$  is called Fenton's reagent. Albeit it is not a new reagent since it was developed in the 1890s [88], but because of its strong oxidizing properties it has been recently utilized for pharmaceutical oxidation [89]. Many studies applied Fenton's reagent in its homogeneous form ( $Fe^{2+}/H_2O_2$ ) [90-92], but ZVI implementation was found to be more advantageous in terms of cost savings, avoiding unnecessary counter ions from the added iron salts, releasing less amount of iron ions in the treated wastewater, and recycling ferric ions at the surface of ZVI [93].

The oxidation processes are crucial at the wastewater treatment plant since they can transform xenobiotics to less refractory and more biodegradable species. Traditional oxidation methods, as ozone or permanganate, revealed many limitations. For example, oxidative reactions via direct ozonation are slow, selective, unstable and incomplete [94], and in the case of potassium permanganate, effectiveness of remediation is limited due to the precipitation of  $MnO_2$  that hinders contact with the contaminant [95]. On the



other hand, AOPs have been found to be successful for the abatement of organic pollutants. In these processes, reactive radicals primarily HRs ( $E^0 = 2.8 \text{ V}$ ) are generated having a very strong oxidizing capability for non-selectively driving the mechanism for degradation at a high rate of the order of  $10^9 \text{ M}^{-1}\text{s}^{-1}$  [93, 96]. Two main constituents that comprise AOPs are: The oxidant and the activator, in this regard, they are  $\text{H}_2\text{O}_2$  and  $\text{Fe}^{2+}/\text{Fe}^0$ , respectively. UV source could be added to the  $\text{Fe}^0/\text{H}_2\text{O}_2$  system for faster generation of HRs and better efficiency. However, this approach increases the cost of the process and consumes more energy. One major limitation in the Fenton and Fenton-Like processes is the requirement of an acidic operable pH ( $\sim 3$ ) [97]. Therefore, a new initiative was launched to find an alternative oxidant that can operate at a wider pH range with higher efficiency even at very low iron load but without increasing the cost of the process.

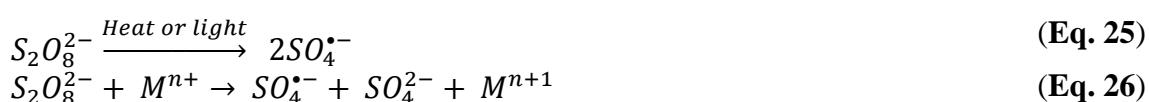
b.  $\text{Fe}^0/\text{PS}$  system

Peroxydisulfate ( $\text{S}_2\text{O}_8^{2-}$ ), which can be simply referred to as persulfate (PS), is the newest oxidant that is being utilized for in situ chemical oxidation (ISCO) in groundwater and soil remediation [98]. The discovery of persulfuric acid ( $\text{H}_2\text{S}_2\text{O}_8$ ) was in 1878 by a French chemist Marcelin Berthelot in a process of electrolysis of sulfate salts [99]. The salts of PS occur usually as sodium, potassium, or ammonium salts. In ISCO the sodium salt is the most preferred because it has the highest water solubility of 56 g / 100 mL at 20°C. PS has received a significant attention as a strong oxidant with a high standard reduction potential,  $E^0 = 2.1 \text{ V}$  according to **Eq. 24**, capable of substituting hydrogen peroxide ( $\text{H}_2\text{O}_2$ ) ( $E^0 = 1.8 \text{ V}$ ). The application of PS has the potential to overcome the limitations of stability and mass transfer of Fenton and

Fenton-like reagents. The half-life of  $H_2O_2$  in the subsurface is not more than 48 hours, on the contrary, PS showed more stability with half-life ranging from 10 to 20 days [100]. These significant properties of PS make it a strong, stable, and soluble oxidant successfully used for remediation of water from a wide range of organic contaminants. However, the kinetics of contaminant degradation by PS is slow and need to be improved [101].



The reactivity of PS is enhanced by various activators including heat [102-105], UV light (**Eq. 25**) [106], peroxide [107] and transition metals (**Eq. 26**) [108, 109]. The cleavage of -O-O- bond in PS generates sulfate radicals (SRs) that are strongly reactive oxidizing agents of higher oxidation potential than the original parent oxidant. These reactive radicals can decompose organic contaminants and mineralize them eventually into  $CO_2$ , water, inorganic species, and less hazardous byproducts.



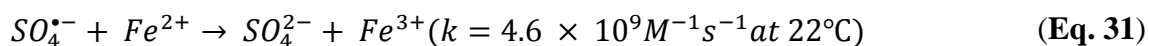
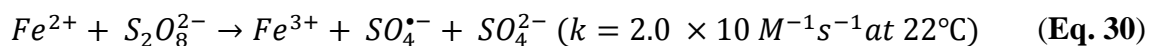
The mechanism of SRs is more selective than HRs toward target contaminants. SRs react more preferably via electron transfer with the organic molecules, whereas HRs degrade the molecules by addition reactions and/ or hydrogen abstraction to form hydroxylated moieties [110]. SRs are stronger oxidants than HRs, as they possess higher standard redox potential (2.5 V-3.1 V) and their reactivity is retained over a wide range of pH values (3 to 8) [111]. The reactivity rates of SR-induced oxidation reactions of

several volatile organic compounds were in the range of  $10^7$ - $10^8$   $M^{-1}s^{-1}$  [112], this is lower compared to the reactivity rates of HRs; however, in activated PS systems both reactive species, SRs and HRs, are coexisting. During PS propagation reactions, HRs are generated particularly under alkaline conditions (**Eqs. 27, 28**).



The PS activation by transition metals is more applicable than by heat and UV light for In-Situ technology. Many metals as Co (II) and Ag (I) conjugated with PS showed effective contaminant decomposition along with successful SR-generation [113], but their toxicity and high cost have significantly limited their application. Analogous to Fenton processes,  $Fe^{2+}$  salts react with PS to generate SRs capable of degrading organic molecules. In a similar manner,  $Fe^{2+}/PS$  efficiency is restricted to low pH. For example, the degradation of polychlorinated biphenyls (PCBs) by PS activated  $Fe^{2+}$  has shifted from complete to partial degradation when the pH was increased from 3 to 5 [114]. ZVI is a good alternative activator for providing  $Fe^{2+}$  given that it can address the pH issue. Beside of the typical dissociation of ZVI under oxic and anoxic conditions (**Eqs. 2, 3**), ZVI oxidation is also attributed to the direct reaction of PS at its surface (**Eq. 29**) [115]. The process of SR generation from PS activation by  $Fe^{2+}$  (**Eq. 30**) can be deactivated by a quenching reaction with excess  $Fe^{2+}$  (**Eq. 31**) [116]. Therefore, the Fe:PS ratio is a key factor that should be optimized to overcome the loss of SRs in the quenching pathway.





Over the last decade, ZVI-activated PS has received increasing attention for the degradation of several types of contaminants. Pharmaceutical degradation has been recently studied under this technology. Ghauch et al. has studied the ZVI-PS activation on an antibiotic compound called Sulfamethoxazole (SMX). His work has demonstrated complete SMX degradation after one hour reaction time and up to 37% mineralization. The efficiency was assessed by the Reaction Stoichiometric Efficiency (RSE) that was calculated as the ratio of the amount of SMX degraded over the amount of PS consumed. The maximum value it reached was 5.2% which requires further improvement [116]. In another study, Ayoub and Ghauch have showed that the efficiency can be improved by plating catalytic metals on the  $Fe^0$  surface as the case of bimetallic and trimetallic systems [117].

In this study, micrometric industrial iron (iFe) waste was used as a heterogeneous metallic system for PS activation. The occurrence of elements other than Fe makes this system similar to iron plated systems. Metals different from Fe could play catalytic role in accelerating the substrate removal; however, Fe remains the main contributor in PS activation.

## B. Objectives

Throughout this investigation, the role of iFe in activating PS and inducing RAN degradation was evaluated. An assessment of PS activation using Fe salt was done to determine the adequate amounts of  $Fe^{2+}$  required for generating SRs that cause full RAN degradation. A comparative study between iFe and cFe was conducted to assess iFe efficiency and sustainability throughout successive treatment runs ( $n = 2$ ), and to comment on sludge formation by the end of the treatment. The impact of environmental conditions as ionic strength and ionic content ( $Cl^-$ ,  $Br^-$ ) on the extent and kinetics of RAN degradation was tested. The parameters that were followed are: rate constant of the degradation reaction, %  $RSE_{av}$ , final total dissolved iron species, initial and final pH, and conductivity. Total organic carbon was tested under different PS: iFe molar ratios and the influence of generated iron corrosion products (ICPs) was elaborated. Byproduct evolution from RAN degradation process was monitored and identified.

## CHAPTER II

### MATERIALS AND METHODS

#### A. Chemicals

Ranitidine hydrochloride ( $C_{13}H_{22}N_4O_3S \cdot HCl$ ), sodium persulfate (PS) ( $Na_2S_2O_8, \geq 99.0\%$ ), and potassium iodide (KI) (puriss, 99.0-100.5%) were purchased from Sigma-Aldrich (India, France, and Germany, respectively). Commercial iron (puriss 99.5%, fine powder  $< 150 \mu m$ ) and iron (II) sulfate heptahydrate ( $FeSO_4 \cdot 7H_2O$ ) (puriss, 99.5-104.5%) were obtained from Riedel-de-Haen (Germany), while iron (II) chloride tetrahydrate ( $FeCl_2 \cdot 4H_2O$ ) (purum  $\geq 98\%$ ) was acquired from Fluka (packed in Switzerland). Industrial iron powders were collected from RYMCO car workshop (Lebanon), grinded and sieved to the size of 53-150  $\mu m$ . Sodium perchlorate monohydrate ( $NaClO_4 \cdot H_2O$ ) (ACS reagent, 98%) was purchased from Sigma-Aldrich (France) and used as a background electrolyte. To assess the ionic additives effect, sodium bromide (NaBr) and sodium chloride (NaCl) were acquired from HIMEDIA and Fluka, respectively. Ammonium acetate ( $C_2H_7NO_2, \geq 98.0\%$ , puriss ACS reagent), sodium hydrogen carbonate ( $NaHCO_3$ ) and hydrochloric acid (HCl) were purchased from Fluka (Netherlands). Methanol of HPLC grade was from Sigma-Aldrich (Germany). Millipore deionized water (DI) was used in the preparation of all solutions employed in this investigation.

#### B. Chemical Analysis

RAN analysis was carried out in duplicates on an Agilent 1100 Series Liquid Chromatography (LC) equipped with a quaternary pump, a vacuum degasser, an

autosampler maintained at 4°C, and a thermostated column compartment set at 30°C. For the separation of RAN and its transformation products, a C18 reversed phase column (5 µm; 4.6 i.d. × 250 mm long) was used along with a security guard column HS C18 (5 µm; 4.0 i.d. 20 mm long) (Discovery, Supleco, USA). The LC was also equipped with two detectors placed in series: a diode-array detector (DAD) for the quantification of RAN, and an extra capacity ion trap mass spectrometer detector (MSD) for the identification of RAN and its transformation products in positive ionization mode. The ionization source used for the MSD is a PhotoMate orthogonal atmospheric pressure photoionization (APPI) spray source (Syagen Technology). Additional details on the LC/MS system have been previously described [89, 102, 104]. The LC mobile phase consisted of Methanol: (10 mM) Ammonium acetate (aq) of (40:60) (v/v) and was kept under isocratic mode at a flow rate of 0.8 mL/ min. The injection volume was 50 µL taken from 0.5 mL aliquots pre-filtered on a 0.45 µm PTFE 13 mm disc filters (Jaytee Biosciences Ltd., UK) and placed in a 2 mL Agilent vial. Under these conditions, RAN was eluted at a retention time of 5.3 min. It revealed two  $\lambda_{\max}$  at 230 nm and 320 nm; the latter was used for RAN detection and quantification. The remaining persulfate anions were determined at  $\lambda_{\max} = 352$  nm based on a calibration curve (**Fig. 1**) of a concentration range extending from 40 to 100 µM using a **Nanodrop 2000c** UV-VIS Spectrophotometer (Thermo Scientific) in accordance with the procedure developed by Liang and collaborators [118]. The concentration of KI used for PS complexation was 100 g/ L. At each time interval, 0.5 mL sample was withdrawn from the reactor and added into 2 mL vial containing 0.5 mL of KI. Samples were kept for 30 min for complete complexation before analysis. Total iron was quantified by flame atomization on a Thermo labsystems Solaar atomic absorption (AA)

spectrometer. Solutions obtained at the final time of the treatment period (e.g.  $t = 60$  min) were homogenized, settled at a magnet to let down the metallic particles, and 5 mL aliquots were withdrawn from each. Adequate amounts of concentrated HCl (e.g. 2 mL) were added to them to ensure complete hydroxide dissolution. Later, samples were diluted to obtain a total volume of 10 mL. In some cases further dilution is required. Quantification was carried out on a calibration curve of a linear dynamic range extending from 2 to 15 ppm prepared from 50 ppm  $FeCl_2 \cdot 4H_2O$  (Fig. 2). Surface analysis of commercial iron and industrial iron were performed by a Scanning Electron Microscope coupled with Energy Dispersive X-ray spectroscopy (SEM/ EDS) (Tescan, Czech Republic) at 20 kV. Mineralization of RAN was assessed by a Total Organic Carbon (TOC) analyzer (GE 5310C) equipped with an auto-sampler and a  $CO_2$  conductivity detector.

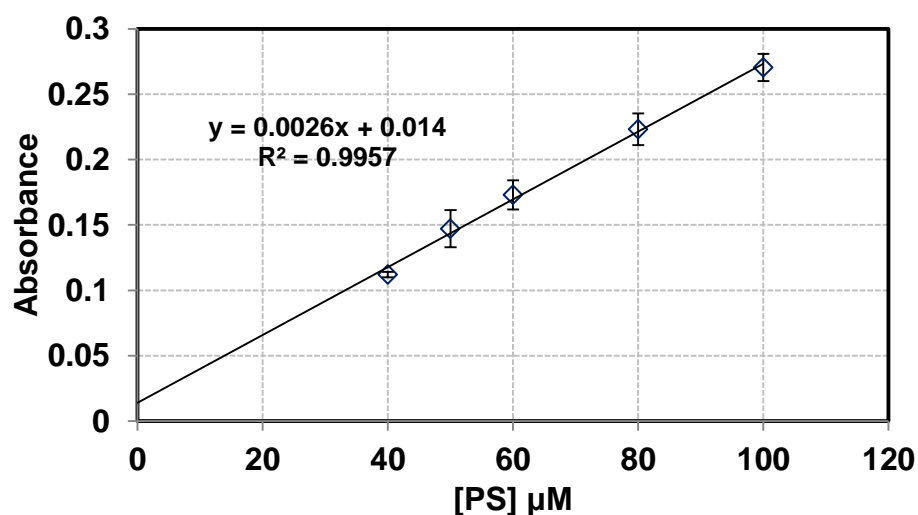


**Fig. 1.** Calibration curve by spectrophotometric method for quantification of PS showing absorbance of the PS-KI complex vs concentration of PS at 40  $\mu\text{M}$ , 50  $\mu\text{M}$ , 60  $\mu\text{M}$ , 80  $\mu\text{M}$ , and 100  $\mu\text{M}$ . Error bars represent standard deviation of six replicates.



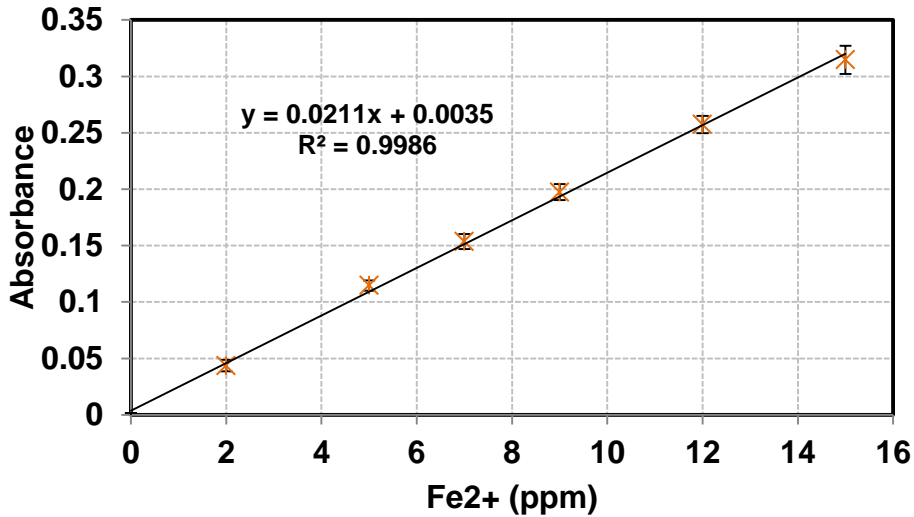


**Fig. 2.** Calibration curve by AA for quantification of dissolved iron species (equivalent  $Fe^{2+}$ ) showing absorbance vs concentration of  $Fe^{2+}$  at 2 ppm, 5 ppm, 7 ppm, 9 ppm, 12 ppm, and 15 ppm. Error bars represent standard deviation of three replicates.

### C. Experimental Setup

#### 1. Industrial Iron Boring Scrap Collection

This investigation aims to introduce industrial iron-based waste as an alternative to commercial iron. It is more affordable, readily available, and can be successfully employed in PS chemical activation processes. The industrial iron boring scrap was collected from a car workshop (RYMCO). It was ejected from the surface of rotor discs during dry cleaning and polishing processes, by which the first layers of the rotor discs were removed to make them smoother before the installation of new brake pads (**Fig. 3**). The estimated weight of the iron scrap was 330 g per two rotor discs. Based on an average of 34 cars per day, the workshop can provide 11 kg of iron-based waste per day for a total of almost 3 tons per year making the material very abundant for large scale application and this with zero cost. For experimental purposes, iron scrap was used without acid washing; however, it went through crushing, grinding, and sieve shaking. The latter was done so as to obtain a size range of 53-150  $\mu\text{m}$  comparable to

the size of the available commercial iron ( $< 150 \mu\text{m}$ ). Based on BET measurements, it was determined that the specific surface area of the sieved fraction of iron waste was about  $4.0 \text{ m}^2/\text{g}$  greater than the one obtained for the available commercial iron e.g.  $2.1 \text{ m}^2/\text{g}$ .



**Fig. 3.** Brake disc skimming and iron boring scrap collection.

## ***2. Batch Experiments***

All solutions were freshly prepared using DI water. The RAN solution was prepared by readily dissolving 20 mg of RAN in a capped 1 L volumetric flask for a  $57 \mu\text{M}$  stock solution. PS stock solution was prepared in a 100 mL volumetric flask by adding 2.381 g to get a PS stock solution at a concentration of 100 mM. The chemical activation reactions were conducted in a set of 20 mL or 40 mL Pyrex vials at room temperature ( $22^\circ\text{C}$ ) under normal atmospheric conditions. Duplicates of reactors were placed on a vortex shaker (IKA<sup>®</sup> Vortex GENIUS) of eight vial-positions. The mixing intensity was moderate.

The initial concentration of RAN in all of the conducted experiments was  $28.5 \mu\text{M}$ . The PS starting concentration was generally  $100 \mu\text{M}$ , however, this was varied in order to study the mineralization of RAN at different concentrations of PS. The addition

of the reagents into the reactor vials was in the following order: RAN, DI water,  $NaClO_4$  (if used), NaCl or NaBr (if used), and then PS as active reagent. The metallic system ( $Fe^{2+}$ , cFe, or iFe) was finally added to initiate PS activation, and therefore RAN degradation.

The sampling method throughout this study was as follow: at each designated time interval the reactor vials were removed from the vortex shaker and placed on a magnet to capture the iron powder. Using a 1 mL BD syringe, aliquots of 0.5 mL were sampled and filtered by 0.45  $\mu$ m filters into 2 mL HPLC vials chilled in an ice bath to stop further reactions post sampling [116, 117]. Later, these aliquots were analyzed by HPLC/ DAD/ MS to follow the degradation process of RAN.

In the case of using  $Fe^{2+}$  as PS activator, different stock solutions of  $FeCl_2$  were prepared, and adequate volumes were added into the reactor solutions to get the desired concentrations of  $Fe^{2+}$  (142  $\mu$ M, 100  $\mu$ M, or 56.4  $\mu$ M). The added volumes of  $Fe^{2+}$  were either spiked entirely at  $t = 0$ , or were divided into equal portions spiked at every 10 min interval for a duration of 1 h. In a two-run-recycling experiment using cFe and iFe, masses of the corresponding iron powders were weighed on a micro-balance (Mettler Toledo) and added into solutions. After 1 h of reaction, the reactor vials were placed on a magnet and the treated solution was completely withdrawn away using a syringe. The left iron powder settled at the bottom of the vial was dried up on a freeze dryer and used in a second 1 h run reaction. Further experiments using iFe were performed in the presence of different ionic matrices composed of  $NaClO_4$ , NaCl, and NaBr obtained from stock solutions at concentrations of 2 M, 500 mM, and 100 mM, respectively. Fe analysis was conducted at the end of the reactions according to a previously described procedure [117].

The initial and the final pH and conductivity values were measured using a Metrohm device equipped with tiamo 2.3-workplace software and connected to pH and conductivity modules. Control experiments were performed throughout this study.

## CHAPTER III

### RESULTS AND DISCUSSION

#### A. Characterization of Iron-Based Particles

##### 1. Commercial Iron (*cFe*)

**Fig. 4a** is a picture of a sample of commercial iron (*cFe*) powder used in this investigation. The SEM morphology in **Fig. 4b** reveals that the particles of iron are irregular. They are fine and porous, and their diameters don't exceed 150  $\mu\text{m}$ . Their elemental composition was confirmed to be 100% Fe by the EDS analysis shown in **Fig. 4c**.

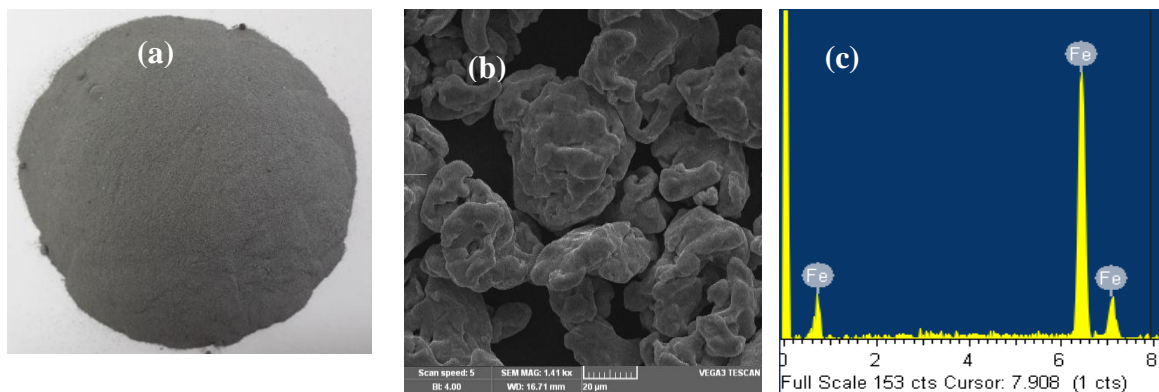


**Fig. 4.** (a) Picture, (b) SEM image, and (c) EDS analysis of commercial iron powder.

##### 2. Industrial Iron Waste (*iFe*)

A picture of non-sieved cast iron borings scrap collected from a rotor disc is presented in **Fig. 5a**. These *iFe* borings have a color darker than that of *cFe* particles (**Fig. 4a**) indicating that a mixture of elements other than iron might be present in their composition. Their texture is slightly rough compared to smooth *cFe* texture. Their structures appear as circular longitudinal hollow entities (**Fig. 5b**), and not rounded like *cFe* (**Fig. 4b**), typically due to the action of skimming exerted on a brake disc set under

rotation for renewing its friction surface. The SEM image in **Fig. 5c** reveals a close view of the surface wall of one of those circular entities. Apparently the surface is composed of superimposed layers with spiral-shaped metallic deposits randomly distributed all over. A magnified SEM image of one of those deposits is depicted in **Fig. 5d**.

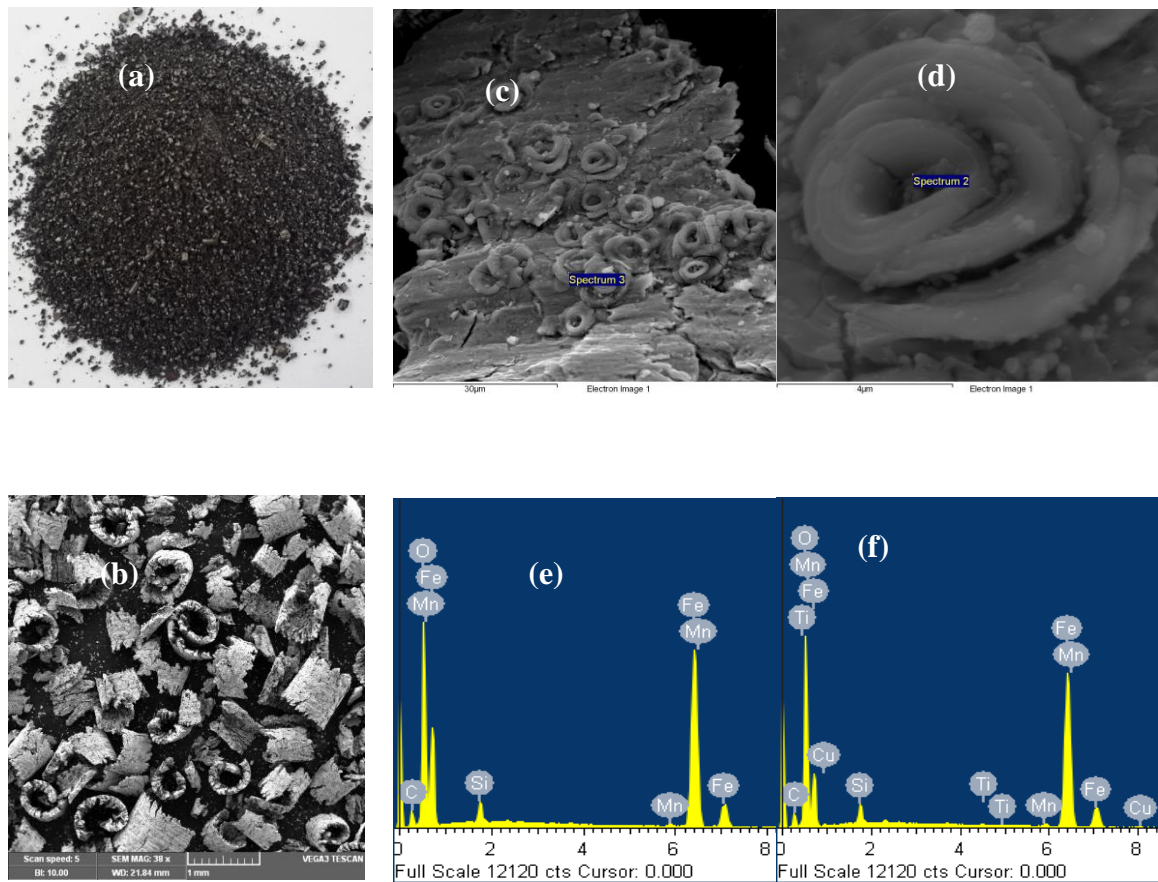


**Fig. 5.** (a) Picture and (b) SEM image of non-sieved iron boring scrap from a rotor disc. (c, d) SEM images and (e, f) EDS analysis of the surface of this industrial iron and of the spiral deposit present on it, respectively.

In addition to the general physical properties in terms of irregularity in morphology and difference in particle sizes, elemental constituents of iFe appeared to be heterogeneously distributed. However, Fe is the major constituent. The shown

elemental analysis of the iFe sample in **Fig. 5e** corresponds to a particular point in **Fig. 5c** noted as “spectrum 3”. As determined by EDS, the predominant elements at that site of the iFe sample were iron followed by oxygen. Fewer amounts of other elements, such as carbon, manganese, and silicon, were also observed. Moreover, the elemental analysis (**Fig. 5f**) of the magnified spiral-shaped metallic deposit obtained at the surface of the iFe sample was shown particularly for the point noted as “spectrum 2” on **Fig. 5d**. It was similarly indicative of the presence of iron, oxygen, carbon, manganese, and silicon. Traces of titanium and copper were also identified. All of the above mentioned elements detected by EDS were summarized in **Table 4** with their corresponding emission energies.

**Table 4.** The emission energies of the elements detected by EDS in industrial iron boring scrap

Elements	Emission Energies (keV)	
Fe	$K_{\alpha} = 6.3996$	$L_{\alpha} = 0.7048$
O	$K_{\alpha} = 0.5249$	
C	$K_{\alpha} = 0.2774$	
Si	$K_{\alpha} = 1.7398$	
Mn	$K_{\alpha} = 5.8951$	$L_{\alpha} = 0.6374$
Ti	$K_{\alpha} = 4.5089$	$L_{\alpha} = 0.4522$
Cu	$K_{\alpha} = 8.0413$	$L_{\alpha} = 0.9297$

The braking system is usually composed of cast iron where Fe is the major constituent and carbon and silicon are present at trace levels. Some metallic alloys could be added to improve its mechanical properties. The oxygen element could be present in the form of metal oxides due to the oxide layer formation at the pad-brake interface [119]. The advantage of having Fe intermixing with other elements is useful for different applications, where in this study it is being tested on PS activation processes.

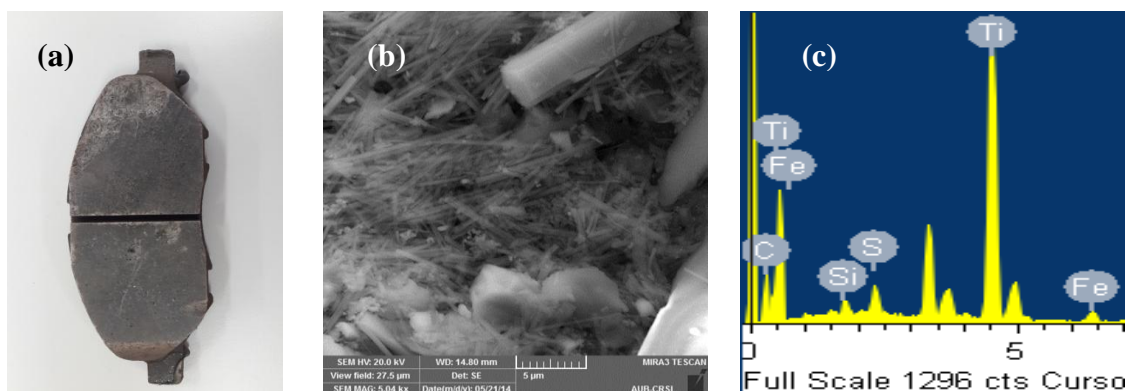


**Fig. 6.** (a) Picture of a brake pad. (b) SEM image of a sample taken from the top of the brake pad, and its corresponding (c) EDS analysis.

The development of heterogeneous catalysis oxidation has recently attracted a great deal of attention in PS technology. Heterogeneous systems have advantageous properties, such as stability and durability. In addition, they are cost-effective and easy to recover [120]. Combining transition metals may increase the efficiency of oxidation. In this investigation, the collected iFe exhibited some transition metals (Mn, Ti, and Cu) in combination with Fe. Ti is also observed among the elements that are present in the brake pad (**Fig. 6a, b, c**). Ti is known for its high strength and high resistance to corrosion. Some research has introduced transition metals ( $M$ ) into magnetites ( $Fe_{3-x}M_xO_4$ ) and ferrites ( $MFe_2O_4$ ) in order to catalytically improve the contaminant degradation [120]. In that regard, the combination of other elements with iron, as the case of iFe, provides an enhancement in the catalytic activity. In this study, iFe was used as PS activator and compared to pure iron under the same experimental conditions.



## B. Optimization of $Fe^{2+}$ :PS Ratio

### 1. $FeCl_2$ vs. $FeSO_4$

The aim of the following experiment is to determine the optimal molar ratio of  $Fe^{2+}$  to PS in RAN/PS/ $Fe^{2+}$  systems.  $Fe^{2+}$  was obtained from  $FeCl_2 \cdot 4H_2O$  instead of  $FeSO_4 \cdot 7H_2O$ , since in the presence of sulfate counter ions the extent of RAN degradation was decreasing especially at high ferrous salt concentrations (**Fig. 7**). For example at 892  $\mu$ M of  $FeSO_4 \cdot 7H_2O$  the % of RAN degradation was about 40%, while at the same concentration of  $FeCl_2 \cdot 4H_2O$  the % of RAN degradation was 84%. This discrepancy tended to be less at lower salt concentrations. Notice that the reactions of generating HRs from SRs are reversible (**Eqs. 27, 28**) [121], so an excess addition of sulfate anions favors the reversible pathway where HRs are consumed and SRs are generated. In that regard, an excess amount of sulfate anions can react with HRs and compete for their incorporation in the substrate oxidation. Moreover, the excess generation of SRs could lead to SR-SR quenching. As a result, RAN degradation gets lower in the presence of excess sulfate anions.

Note that % RAN degradation =  $(1 - [RAN]_t / [RAN]_0) \times 100$  where  $[RAN]_t / [RAN]_0$  is equivalent to Peak Area (RAN)<sub>t</sub> / Peak Area (RAN)<sub>0</sub> as resulted from HPLC chromatograms.

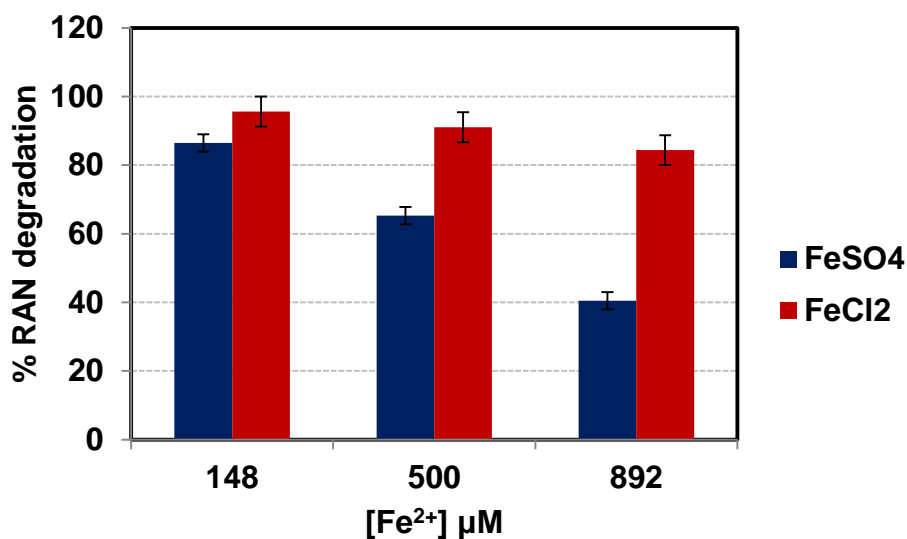


**Fig. 7.** Comparison between the percentages of RAN degradation after 10 min of injecting  $FeSO_4 \cdot 7H_2O$  and  $FeCl_2 \cdot 4H_2O$  at concentrations of 148  $\mu M$ , 500  $\mu M$ , and 892  $\mu M$ . Error bars represent standard deviation of two replicates.

In this experiment, RAN degradation and PS consumption was tested under single and sequential  $Fe^{2+}$  injections over a reaction time of one hour. At a constant RAN concentration of 28.5  $\mu M$ , three different  $Fe^{2+}$ :PS ratios were compared: (a) ~ 0.5:1, (b) 1:1, (c) ~ 1.4:1, where  $[Fe^{2+}] = 56.4 \mu M$ , 100  $\mu M$ , and 142  $\mu M$ , respectively, and  $[PS] = 100 \mu M$ .

## 2. Single $Fe^{2+}$ Additions

**Fig. 8** represents a comparison among the levels of RAN degradation and PS consumption after single  $Fe^{2+}$  injections. Immediate drop of the concentration of RAN was instantly noticed right after introducing  $Fe^{2+}$  into contact with RAN/ PS solution. Nearly the whole degradation occurred at  $t = 0$  before vortex agitation, then it almost stalled. This observation is similar to what was previously reported by Liang in

TCE/PS/ $Fe^{2+}$  system [122]. The rapid RAN drop was a consequence of the high reactivity of SRs generated according to **Eq. 30**.

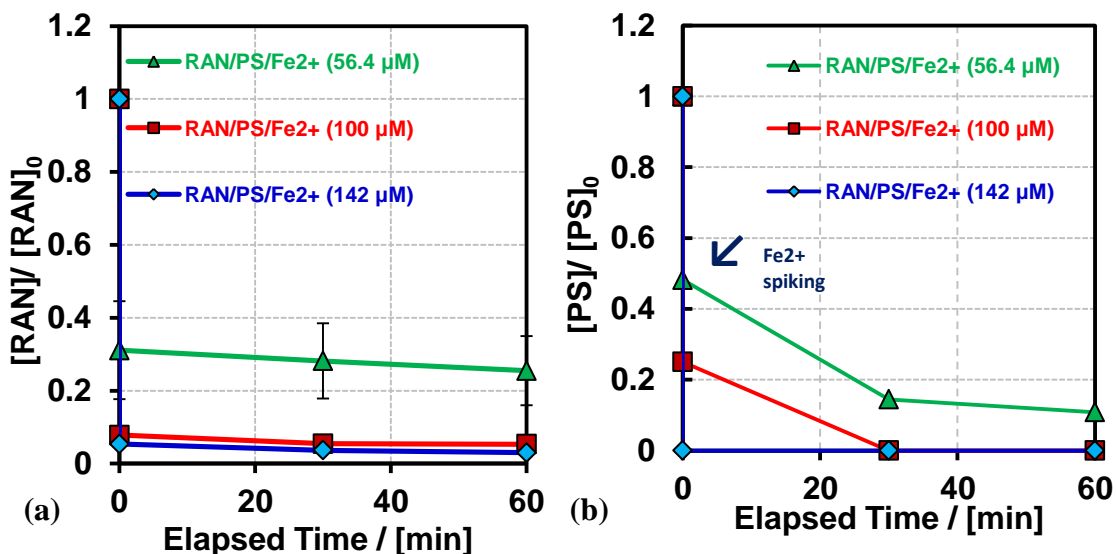


**Fig. 8.** Variations of (a) RAN and (b) PS due to single  $Fe^{2+}$  injections. Experimental conditions:  $[Fe^{2+}]_0 = 56.4 \mu M, 100 \mu M, \text{ and } 142 \mu M$ ,  $[RAN]_0 = 28.5 \mu M$ ,  $[PS]_0 = 100 \mu M$ .  $pH_i = 6.42$ ,  $pH_f$  (case of  $56.4 \mu M$ ) = 4.51,  $pH_f$  (case of  $100 \mu M$ ) = 3.84,  $pH_f$  (case of  $142 \mu M$ ) = 3.83. Error bars represent standard deviation of two replicates.

In the case of a  $Fe^{2+}$ :PS molar ratio of 0.5:1, instantaneous RAN degradation and PS consumption were 69% and 52%, respectively. After one hour of vortex mixing, their values had relatively improved into 75% and 89%, respectively. The limiting amount of  $Fe^{2+}$  compared to PS prevented complete PS consumption and the released SRs weren't enough to exert full RAN degradation. Increasing the  $Fe^{2+}$  content from a  $Fe^{2+}$ :PS molar ratio of 0.5:1 to 1:1 and 1.4:1 resulted in almost a complete RAN degradation. For example, after a one hour reaction, RAN degradation was 95% in the case of a  $Fe^{2+}$ :PS molar ratio of 1:1, and 97% in the case of a  $Fe^{2+}$ :PS molar ratio of 1.4:1, where in both cases PS consumption reached completion. This indicated that the formed SRs were sufficient to induce successful RAN depletion and that no significant quenching of SRs was exerted even at  $Fe^{2+}$ :PS molar ratio of 1.4:1. However, by increasing the concentration of the injected  $Fe^{2+}$  to 148  $\mu M$ , 500  $\mu M$ , and 892  $\mu M$ , RAN degradation decreased to 95%, 91%, and 84%, respectively (**Fig. 7**). This

indicates that the higher the  $Fe^{2+}$  compared to PS, the more the quenching process is important (Eq.31).

### 3. Sequential $Fe^{2+}$ Additions

Since iFe is the activator utilized in this study, the effect of sequential spiking of  $Fe^{2+}$  was tested in accordance to mimic the  $Fe^0$  way of generating  $Fe^{2+}$  into solution. **Fig. 9** represents the variations of RAN and PS due to sequential  $Fe^{2+}$  injections. The overall molar ratios of  $Fe^{2+}$ :PS were the same as for single injections (0.5:1, 1:1, 1.4:1), but this time the addition of  $Fe^{2+}$  was performed sequentially in 6 equally spaced episodes with 10 min intervals between each addition for a total time of one hour. At each time, two samples were taken, one before and one after the  $Fe^{2+}$  injection. A ladder-trend decline was observed for both RAN and PS, exhibiting their immediate decrease upon introducing  $Fe^{2+}$ , followed by a semi-steady state maintained up to the next  $Fe^{2+}$  spiking and this sequence is repeated until the end of the treatment period.

In the case of  $Fe^{2+}$ :PS total molar ratio of 0.5:1 (**Fig.9 a, b**), after one hour, RAN degradation reached 91% indicating a 16% improvement compared to single injections. This is because smooth formation of SRs is more advantageous toward the degradation process. PS didn't achieve complete consumption, but rather 16% of PS had remained at the end of the treatment.

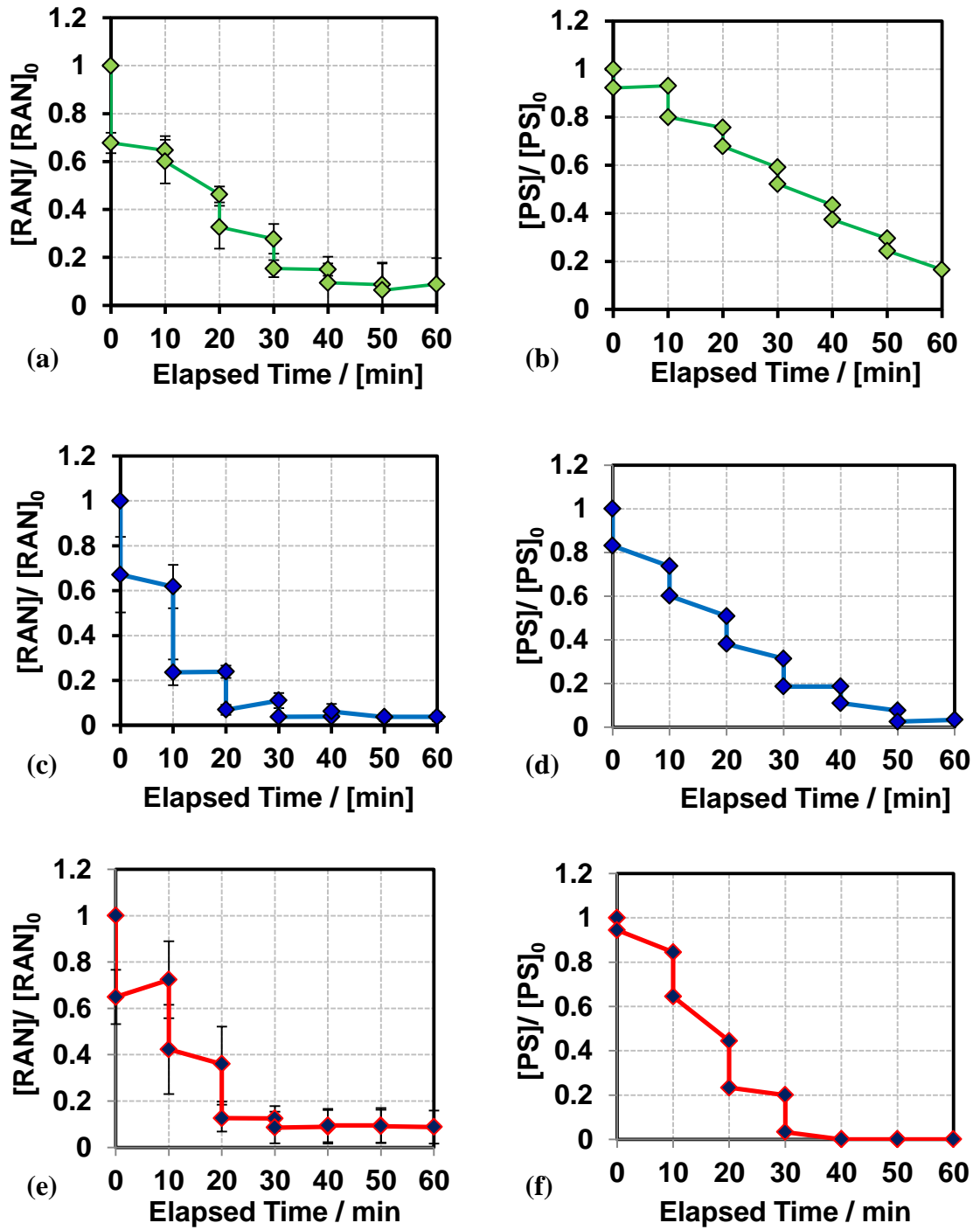


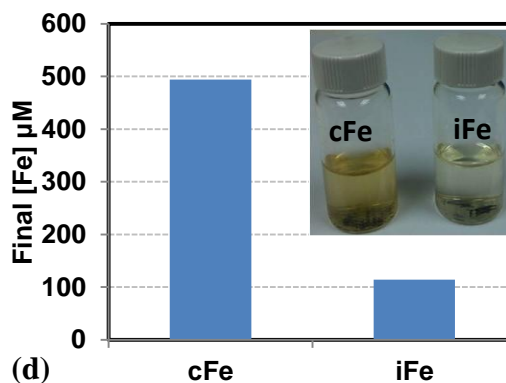
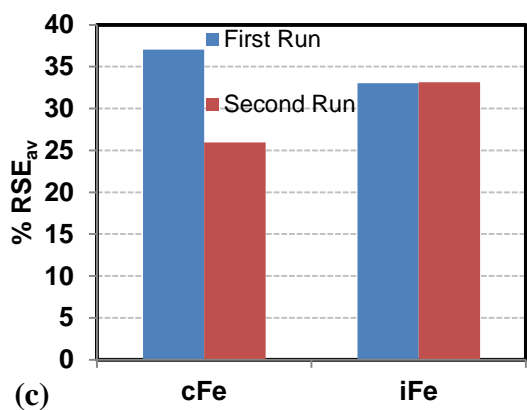
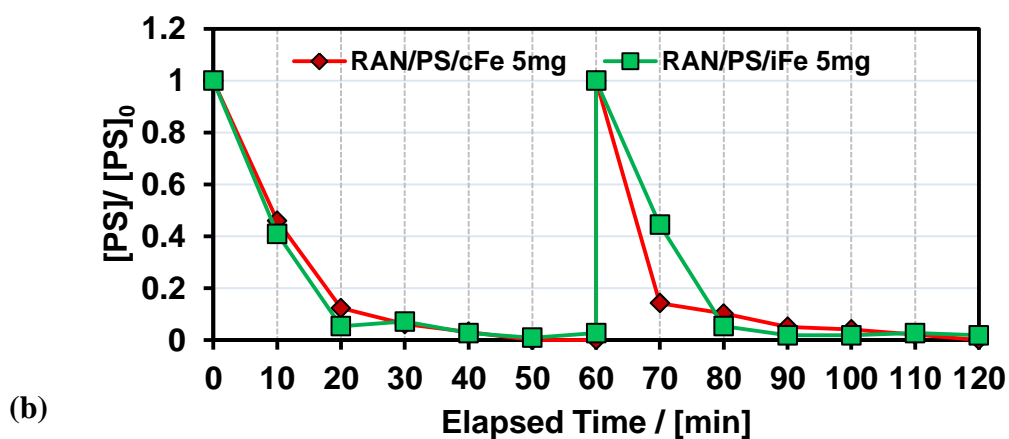
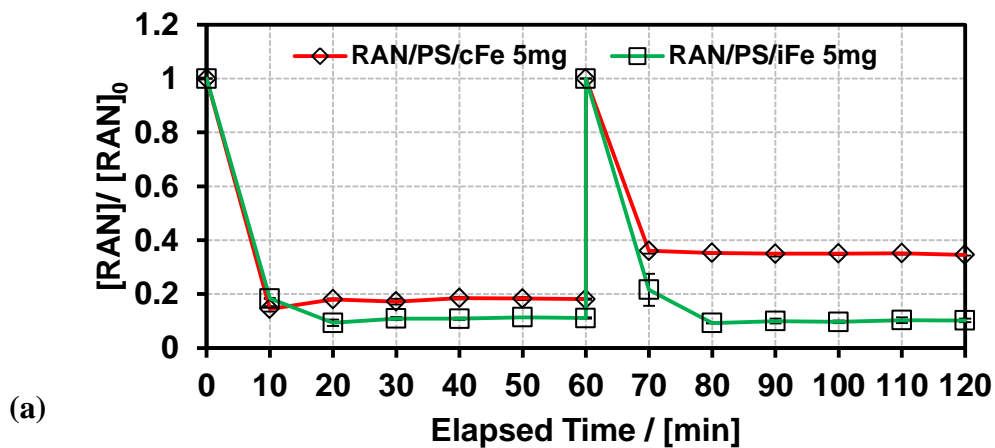
**Fig. 9.** Variation of (a, c, e) RAN and (b, d, f) PS due to sequential  $Fe^{2+}$  injections. Experimental conditions:  $[Fe^{2+}]_{total} = 56.4 \mu M$  (a,b),  $100 \mu M$  (c,d),  $142 \mu M$  (e,f),  $[RAN]_0 = 28.5 \mu M$ ,  $[PS]_0 = 100 \mu M$ .  $pH_i = 6.45$ ,  $pH_f$  (case of  $56.4 \mu M$ ) =  $3.7$ ,  $pH_f$  (case of  $100 \mu M$ ) =  $3.61$ ,  $pH_f$  (case of  $142 \mu M$ ) =  $3.95$ . Error bars represent standard deviation of two replicates.

In the case of  $Fe^{2+}$ :PS total molar ratio of 1:1 (**Fig. 9 c, d**), RAN degradation was 96% close to what resulted upon single  $Fe^{2+}$  injections. PS consumption was complete at  $t = 60$  min when the total added amount of  $Fe^{2+}$  ( $100 \mu\text{M}$ ) reacted to  $100 \mu\text{M}$  of PS. This confirms that one  $Fe^{2+}$  with one PS induces a complete reaction whether at a single injection or at successive additions.

In the case of  $Fe^{2+}$ :PS total molar ratio of 1.4:1 (**Fig. 9 e, f**), RAN degradation was 91%, lower by 6% than when  $Fe^{2+}$  was injected at once. By comparison, PS was completely consumed at the moment of injection upon single injection of  $Fe^{2+}$ , while it was consumed at  $t = 40$  min upon sequential additions of  $Fe^{2+}$ . At this time, a total of  $95 \mu\text{M}$  of  $Fe^{2+}$  was introduced, which is equivalent to the  $Fe^{2+}$ :PS of 1:1 molar ratio. Also, at  $t = 40$  min, RAN degradation was 91% and wasn't improved by the later  $Fe^{2+}$  additions. This is because when PS was completely consumed, the additional  $Fe^{2+}$  would rather target SRs instead of PS. This had deprived sequential additions from reaching the same degradation extent as for single injections. Moreover, it is not an advantage to add an excessive amount of  $Fe^{2+}$ , but rather it is important to just introduce the adequate amount.

In conclusion, the optimal molar ratio of  $Fe^{2+}$ :PS was found to be 1:1 in the RAN/ PS/  $Fe^{2+}$  systems. This finding is in agreement to what was reported in other studies, such as a study by Seok-Young Oh about polyvinyl alcohol oxidation in the presence of  $Fe^{2+}$  and PS [115]. This tells that  $100 \mu\text{M}$  of  $Fe^{2+}$ , whether injected at once or sequentially, can successfully consume  $100 \mu\text{M}$  of PS in one hour reaction, and the formed SRs were adequate for almost full RAN degradation of concentration of  $28.5 \mu\text{M}$ . Throughout this study,  $Fe^{2+}$  generated by iFe was compared to this optimal case.

### C. Evaluation of iFe Efficiency, Sustainability, and Corrosivity





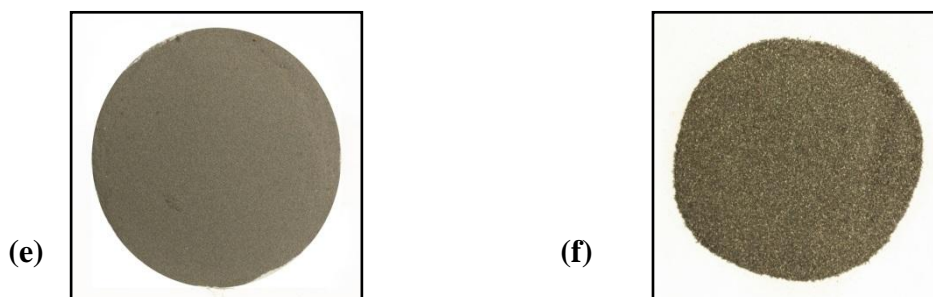


**Fig. 10.** Variation of (a) RAN and (b) PS in 2 runs of 5 mg of cFe ( $< 150 \mu\text{m}$ ) vs 5 mg of iFe (53- 150  $\mu\text{m}$ ). (c) The % of average RSE for each run. (d) Concentration of iron species (equivalent  $Fe^{2+}$ ) at the end of the reaction. Inset: Picture of the solutions at  $t = 120 \text{ min}$ . Pictures of (e) cFe vs (f) sieved iFe. Experimental conditions:  $[\text{RAN}]_0 = 28.5 \mu\text{M}$ ,  $[\text{PS}]_0 = 100 \mu\text{M}$ ,  $[\text{cFe}]_0 = [\text{iFe}]_0 = 5 \text{ mg} / 20 \text{ mL} = 4.46 \text{ mM}$ .  $\text{pH}_i = 6.5$ ,  $\text{pH}_f$  (case of cFe) = 6.26,  $\text{pH}_f$  (case of iFe) = 6.21. Error bars represent standard deviation of two replicates.

In order to check the possibility of iFe in activating PS thereby degrading RAN, a load of 5 mg / 20 mL of iFe was added to a RAN (28.5  $\mu\text{M}$ )/PS (100  $\mu\text{M}$ ) solution, where its efficiency was compared to that of cFe. **Fig. 10a, b** shows a decrease of RAN concentration accompanied by PS consumption with respect to iFe and cFe. As it can be noticed, more than 80% of RAN degradation was achieved upon using both iFe or cFe in just 10 min of the first experimental run. After that time, a halt in degradation was observed at a level that was less than complete. At 60 min of reaction, almost 89% of RAN has disappeared against 97% of PS for the system of iFe, while 82% of RAN has disappeared against full PS consumption for the system of cFe. The higher degradation accomplished by iFe system indicated that iFe is not only successful for applications of contaminant degradation in persulfate activation processes, but is also competitive to cFe.

By the end of the first experimental run, the treated solution was discarded by means of a syringe and the remaining iron powder was dried up by a freeze dryer. The dried iron was used again in the second experimental run with a new RAN/ PS solution

at same concentrations as before in another one hour reaction. The results showed that the extent of RAN degradation in the presence of reused iFe was maintained as in the first run (89%); however, it was 17% less in the presence of reused cFe (65%). Moreover, the average of % RSE (calculated for all selected times 10-60 min) (**Fig. 10c**) was maintained at 33% after recycling iFe, but it decreased from 37% to 26% after recycling cFe. Therefore, the treatment efficiency was more successfully sustained while using iFe.

Iron corrosion was assessed in three different aspects: the final pH, the final color of the solutions, and the final total iron analyzed by AA after acidification.

The pH of the solutions was 6.5 initially and by the end of the recycling experiment it became 6.26 and 6.21 for cFe and iFe cases, respectively, showing a slight but not significant decrease in pH. Since most PS was consumed early in the first 20 min, later, PS was no longer contributing to the pH change, but rather, the iron dissolution in water (**Eqs. 3, 4**) was the main influential factor on pH. This is because of the formation of hydroxide anions that undermined the acidity exerted by PS decomposition and raised up the pH again to a value close to what it was initially.

Moreover, the yellow color appearing at the end of the recycling experiment confirmed the formation of hydroxides. The discrepancy between both activators was more obvious since a dark yellow color appeared in the case of cFe and a very pale yellow color appeared in the case of iFe, indicating that more hydroxides were formed using cFe.

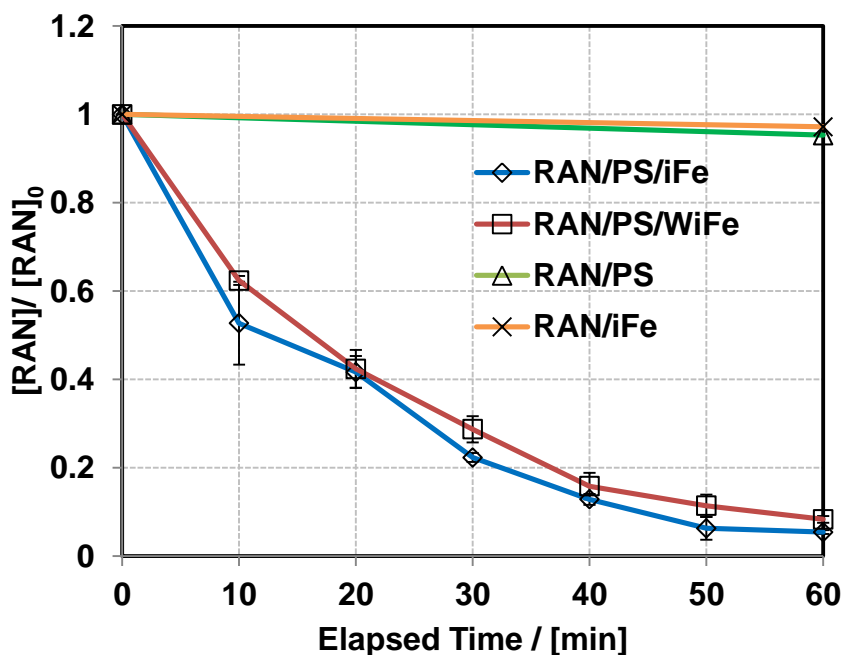
Furthermore, since the activation of PS by  $Fe^0$  is referred majorly to the dissolved ferrous ions released from  $Fe^0$ , a control experiment was performed to estimate the ferrous ions released into solution by iFe and cFe in the absence of RAN

and PS. A high load of iron activators was used (50 mg / 20 mL) to overcome detection limits. Final total iron content was analyzed for the treated solutions after acidification to convert all possibly formed iron hydroxides into dissolved iron ions. The results showed that more iron ions were released by cFe than by iFe with respective amounts of 29.46  $\mu\text{M}$  and 23.57  $\mu\text{M}$  after 1 hour of vortex mixing of the iron activators in only DI water. However, in RAN/ PS systems with an iron load of about 5 mg / 20 mL (**Fig. 10d**), higher amounts of dissolved iron species were released in the presence of PS e.g. 494  $\mu\text{M}$  vs 114  $\mu\text{M}$  from cFe and iFe, respectively, due to the fact of its direct activity at the surface of  $\text{Fe}^0$  (**Eq. 29**). More iron corrosion was obtained for cFe compared to iFe. This was reasonable since cFe composition was almost 100% atomic Fe, while iFe showed elements other than Fe in its composition such as Mn and Si as previously shown by the SEM/ EDS analysis (**Fig. 5**). Interestingly, with less  $\text{Fe}^{2+}$  released, iFe has achieved similar RAN degradation extent as cFe. Furthermore, the excessive release of iron ions, as in the case of cFe, was leading to sludge formation after PS was consumed. Controlling the iron ions fed into persulfate activation systems is the key factor in accomplishing successful contaminant degradation. It is always important to provide the adequate amounts of ferrous ions that can participate in activation without leaving high iron residual amounts in water by the end of the treatment. The released iron species from iFe of 114  $\mu\text{M}$  gives with 100  $\mu\text{M}$  of PS a case equivalent to  $\text{Fe}^{2+}$ :PS of 1:1 molar ratio. The trend of degradation was a direct decline rather than gradual over one hour. This is because PS is decomposing by both the direct reaction at the surface of  $\text{Fe}^0$  and the sulfate radical generating reaction with  $\text{Fe}^{2+}$ . Therefore, less than 100  $\mu\text{M}$  of  $\text{Fe}^{2+}$  is sufficient to consume PS (100  $\mu\text{M}$ ) entirely. Accordingly, a lower load of iFe was further assessed and tested under different ionic matrices.

## D. Application of iFe at Low Iron Load in Different Water Matrices Containing Chlorides and Bromides (the Main Sea Water Components)

### 1. Optimization of Ionic Strength (RAN/PS/iFe/NaClO<sub>4</sub> Systems)

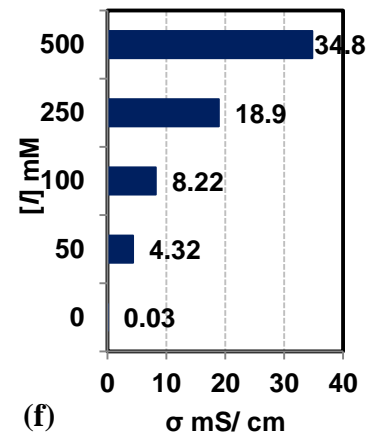
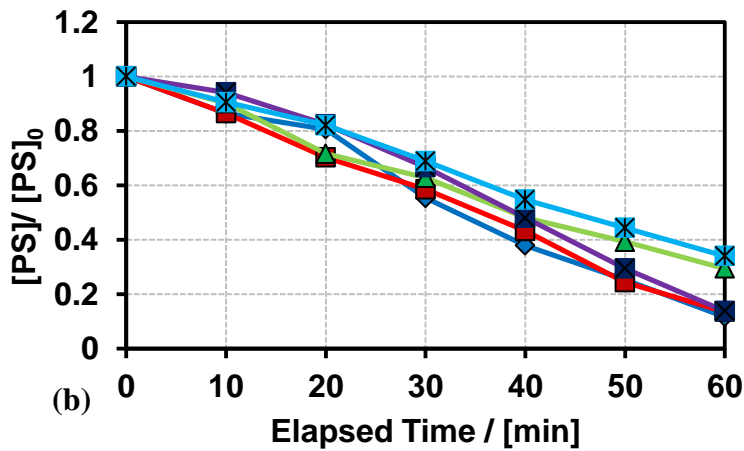
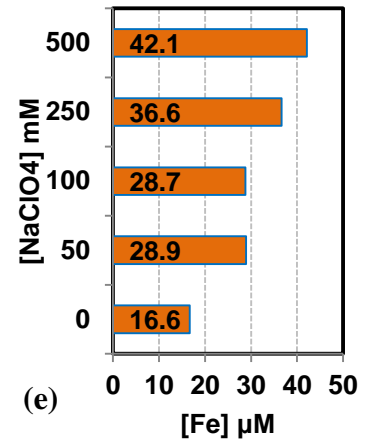
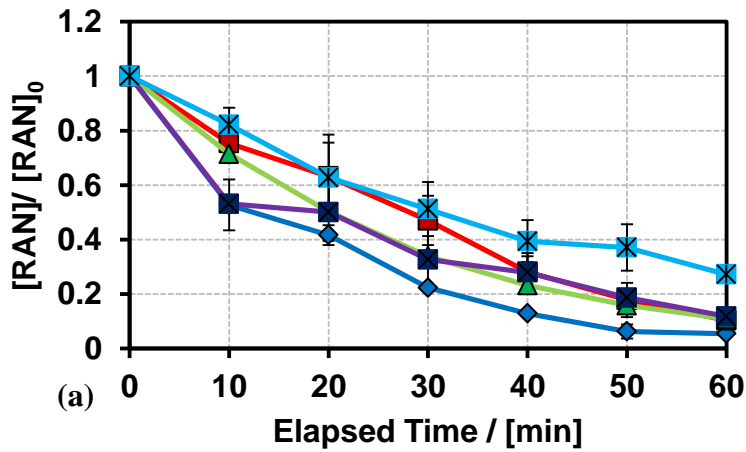
#### a. Non-Controlled Ionic Strength System



**Fig. 11.** Variation of RAN in the presence of washed iFe (RAN/PS/WiFe) and non-washed iFe (RAN/PS/iFe). Experimental conditions:  $[RAN]_0 = 28.5 \mu\text{M}$ ,  $[PS]_0 = 100 \mu\text{M}$ ,  $[WiFe] = [iFe] = 1 \text{ mg} / 20 \text{ mL} = 892 \mu\text{M}$ .  $\text{pH}_i = 6.5$ ,  $\text{pH}_f (\text{WiFe}) = \text{pH}_f (\text{iFe}) = 3.9$ . Additional control experiments without PS or iFe gives  $\text{pH}_f (\text{RAN/PS}) = 6.6$  and  $\text{pH}_f (\text{RAN/iFe}) = 7.01$ . Error bars represent standard deviation of two replicates.

In all experimental systems iFe was used without acid washing, since the acid washed iFe showed a similar RAN degradation as the non-washed iFe (**Fig. 11**). Control experiments containing RAN (28.5  $\mu\text{M}$ )/ PS (100  $\mu\text{M}$ ) induced a minimal decline in RAN level (less than 5%) after one hour of agitation. The same was encountered in another control experiment containing RAN (28.5  $\mu\text{M}$ )/ iFe (1 mg / 20 mL) (**Fig. 11**). This indicates that RAN degradation isn't successful with non-activated PS systems or

with low iFe load systems. Further control experiments containing PS (100  $\mu\text{M}$ ) / iFe (1 mg / 20 mL) induced only 15% decomposition of PS showing that in the absence of RAN less consumption of the generated SRs causes less PS decomposition.



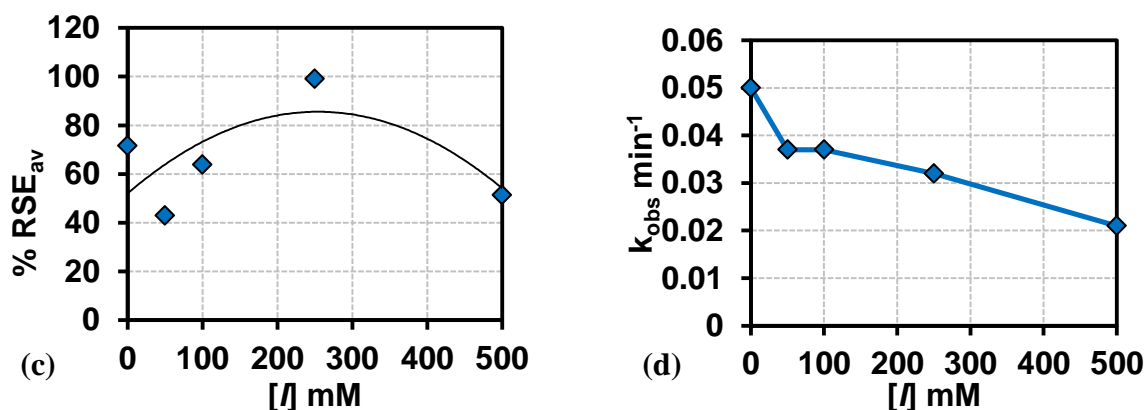


**Fig. 12.** Variation of (a) RAN, (b) PS, (c) % RSE<sub>av</sub>, and (d)  $k_{obs}$  at different ionic strength conditions in the presence of different concentrations of  $NaClO_4$  where  $[I] = [NaClO_4]$ . (e) Concentration of iron species (equivalent  $Fe^{2+}$ ) at the end of the reaction. (f) Conductivities with respect to ionic strength values. Experimental conditions:  $[RAN]_0 = 28.5 \mu M$ ,  $[PS]_0 = 100 \mu M$ ,  $[iFe]_0 = 1 \text{ mg} / 20 \text{ mL} = 892 \mu M$ ,  $[NaClO_4] = 0, 50 \text{ mM}, 100 \text{ mM}, 250 \text{ mM}, 500 \text{ mM}$ ,  $pH_i = 6.5$  and  $pH_f = 4.4 \pm 0.1$ . Error bars represent standard deviation of two replicates.

**Fig. 12a, b.** reveals the variation of RAN degradation against PS consumption in the presence of different concentrations of a neutral electrolyte sodium perchlorate ( $NaClO_4$ ). The ionic strength was considered negligible in the RAN/PS/iFe system and the concentration of  $NaClO_4$  added directly reflects  $[I]$ . In this investigation, iFe was utilized at a low load of 1 mg / 20 mL in order to provide adequate PS activation with less ferrous residual amounts. For example, in the case of perchlorate-free system, gradual RAN degradation was encountered with a satisfactory extent of removal at about 95% (**Fig. 12a**) and a remaining of 12% of PS (**Fig. 12b**). This shows an improvement from the case of using a high load of iFe (5 mg / 20mL), where the extent of removal was 89% and PS was almost totally consumed (**Fig. 10a, b**). Therefore, the process at a low load of iFe is characterized by the sustainability of PS oxidation with less quenching of SRs. The final acidic pH was due to  $HSO_4^-$  formation from the

decomposition of PS that was still in progress throughout the one hour reaction (**Eqs. 32, 33**).



As can be displayed from **Fig. 12c**, before controlling ionic strength, % RSE<sub>av</sub> has reached 72%, providing an enhancement of 39% in the stoichiometric efficiency with respect to the high load case where % RSE<sub>av</sub> was 33% (**Fig. 10c**). The increase in RSE<sub>av</sub> while using a low load of iFe indicated that SRs generated from PS were more successfully targeting RAN rather than being quenched by radical sinks as water,  $Fe^{2+}$ , or other SRs (**Eqs. 27, 31, 34**).



A previous study about sulfamethoxazole (SMX) removal by iron activated PS has also revealed that this removal can be enhanced by adding lower iron loads because of more sustainability of PS (1 mM) [116]. However, the maximum RSE reached was only 5.2% which is very low compared to the RSE in this study (72%). Even after plating iron particles with Ag and Co to activate persulfate for removing SMX, % RSE didn't exceed 10% [117]. Basically, SMX and RAN are different probes and have different reactivity toward SRs; hence their RSE values are varied. However, the employment of low persulfate content (100  $\mu$ M) for the RAN case was advantageous

toward increasing RSE. **Fig. 12d** shows the influence of ionic strength on the RAN degradation rate. The process of RAN degradation was observed to fit pseudo-first-order kinetic model well ( $[RAN]/[RAN]_0 = \exp(-k_{\text{obs}}t)$ ), where  $k_{\text{obs}}$  represents a pseudo-first-order rate constant determined from the slope of the plot  $\ln([RAN]/[RAN]_0)$  vs time (min) with a correlation coefficient  $R^2$  value greater than 0.94. For example, in the perchlorate-free system,  $k_{\text{obs}}$  was  $0.05 \text{ min}^{-1}$ . **Fig. 12e** shows the total iron ions analyzed after 60 min of the reaction. Interestingly, in the perchlorate-free system, only about  $16.6 \mu\text{M}$  of iron ions (equivalent to  $Fe^{2+}$ ) were released. This indicates that  $Fe^{2+}$  at an amount that is about 6 times less than the initial PS amount ( $100 \mu\text{M}$ ) was sufficient to induce successful PS activation and almost full RAN degradation. This is attributed to the regeneration ability of  $Fe^{2+}$  from the reaction of  $Fe^{3+}$  at the surface of  $Fe^0$  (**Eq. 35**).



**Fig. 12f** shows the conductivities at different ionic strength conditions, where the perchlorate-free system has a low conductivity of  $0.03 \text{ mS/cm}$ .

#### b. Controlled Ionic Strength Systems

Different ionic strength conditions were investigated to study the effect of the water matrix on the performance of iFe in activating PS for the degradation of RAN. The ionic strength was controlled by sodium perchlorate ( $NaClO_4$ ) .i.e.  $[I] = [NaClO_4]$ . The aim is to determine the optimal ionic strength value and adjust it for the later



experiments. **Fig. 12a,b** reveals that at increasing the ionic strength values,  $[I] = 50$  mM, 100 mM, 250 mM, and 500 mM, the degradation extent of RAN decreased to levels less than 95% (case of perchlorate-free system) to reach 90%, 89%, 88%, and 72%, against 87%, 71%, 86%, and 66% of PS consumed, respectively.

**Fig. 12c** shows that a maximum of 100%  $RSE_{av}$  was obtained at  $[I] = 250$  mM. From  $[I] = 50$  mM to  $[I] = 100$  mM, %  $RSE_{av}$  increased from 44% to 64%. After reaching optimum at  $[I] = 250$  mM, %  $RSE_{av}$  decreased to reach 51% at  $[I] = 500$  mM. In comparison to the %  $RSE_{av}$  of the perchlorate-free system (72%), the condition of  $[I] = 100$  mM was observed to have the closest %  $RSE_{av}$  among the other ionic strength conditions. Furthermore, as seen in **Fig. 12d**, a decline in the degradation rate constant ( $k_{obs}$ ) from  $0.05 \text{ min}^{-1}$  initially to  $0.037 \text{ min}^{-1}$ ,  $0.037 \text{ min}^{-1}$ ,  $0.032 \text{ min}^{-1}$ , and  $0.021 \text{ min}^{-1}$  was occurring while increasing the ionic strength to  $[I] = 50$  mM, 100 mM, 250 mM, and 500 mM, respectively. As can be deduced, the increase of ionic strength has a negative salt effect on the reactivity of PS. This is in coherence with previous studies [101, 123].

Therefore, the rate of RAN degradation decreased as ionic strength increased. As can be noticed, from  $[I] = 50$  mM to  $[I] = 100$  mM,  $k_{obs}$  was apparently stable. However, after exceeding  $[I] = 100$  mM,  $k_{obs}$  started to decrease. For this reason,  $[I] = 100$  mM was observed as a limiting edge that should not be exceeded in order to preserve the degradation rate. **Fig. 12e** reveals that more corrosion of iFe is occurring at higher ionic strength conditions. For example, at  $[I] = 50$  mM, 100 mM, 250 mM, and 500 mM, the total dissolved iron species at  $t = 60$  min was  $28.9 \mu\text{M}$ ,  $28.7 \mu\text{M}$ ,  $36.6 \mu\text{M}$ , and  $42.1 \mu\text{M}$ , respectively. Although at elevated ionic strength conditions more  $Fe^{2+}$  was released, less RAN degradation rate was encountered since the effect of ionic

matrix slows down SRs attack on RAN and decreases its rate of degradation. As represented in **Fig. 12f**, the conductivity is certainly in direct relation with  $[I]$ , such that, at  $[I] = 50$  mM, 100 mM, 250 mM, and 500 mM,  $\sigma = 4.32$  mS/ cm, 8.22 mS/ cm, 18.9 mS/ cm, and 34.8 mS/ cm, respectively. For later experiments, where iFe performance was evaluated in the presence of chlorides and bromides, ionic strength was optimized at  $[I] = 100$  mM because of three reasons: (1) RAN degradation extent at the selected  $[I]$  and in the perchlorate-free system were very close e.g. 89% vs 95%. (2) The calculated %  $RSE_{av}$  at the selected  $[I]$  and in the perchlorate-free system were close as well e.g. 64% vs 72%. (3) The rate of RAN degradation tended to decrease dramatically at  $[I] > 100$  mM, so this selected ionic strength was considered as a limit above which the rate was no longer sustained.

The knowledge about the feasibility of iFe-PS activation under different ionic interferences in natural water, e.g. seawater, is important in order to evaluate the fulfillment of the process. Seawater contains around 65 mg/ L bromide equivalent to 0.813 mM and 19000 mg/ L chloride equivalent to 535 mM [124]. In this study, chlorides and bromides were evaluated at levels close to that obtained in brackish water and seawater, respectively, in order to do a comparative assessment between both halides in iFe-PS activated systems.

## ***2. Application of iFe in the Presence of Chlorides at Concentrations as that in Brackish Water (RAN/PS/iFe/NaClO<sub>4</sub>/NaCl Systems)***

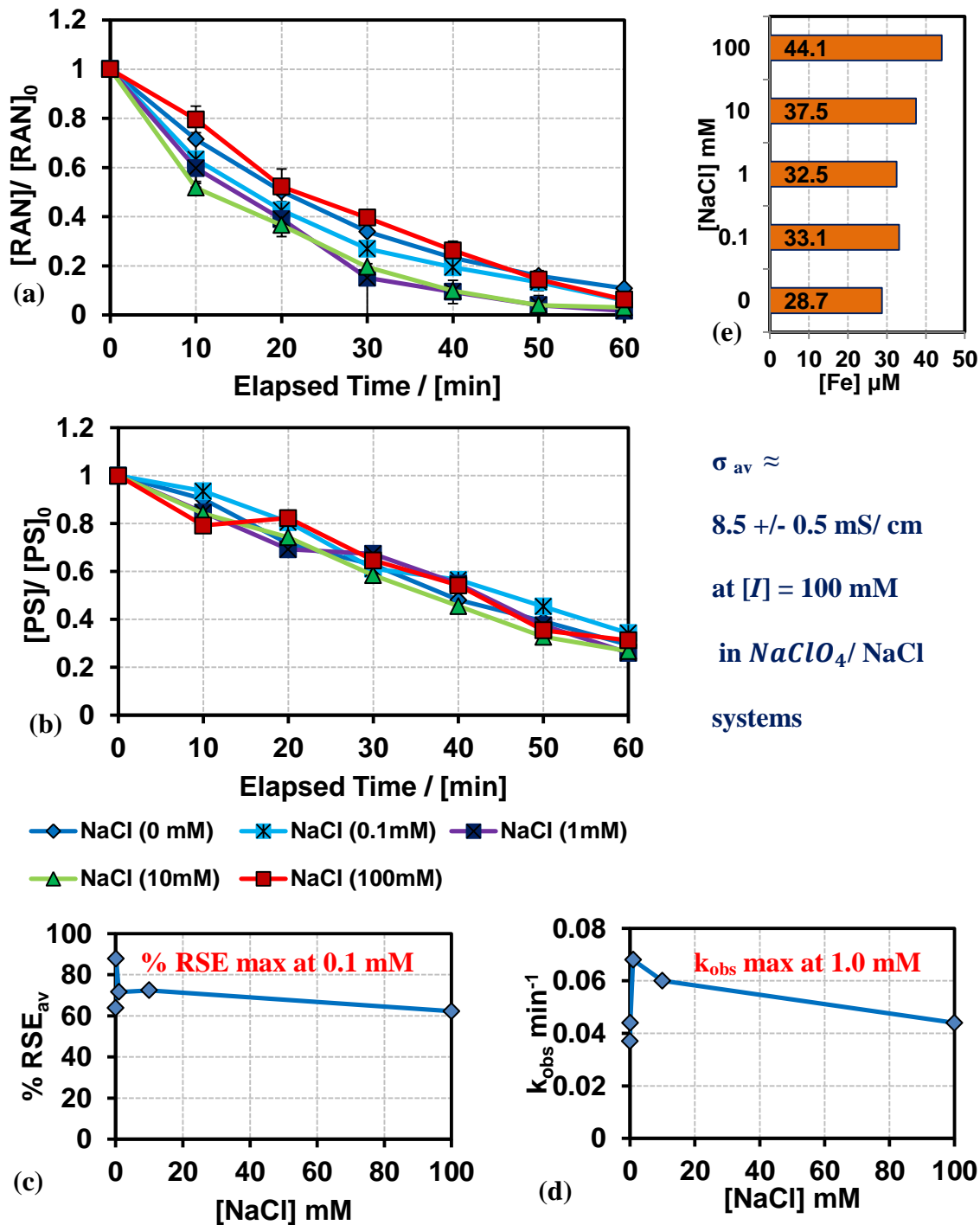
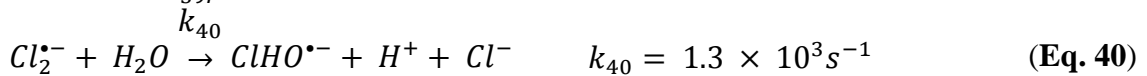
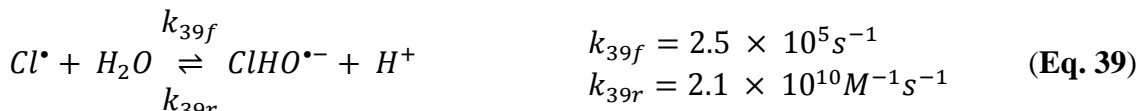
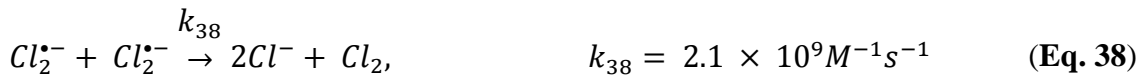
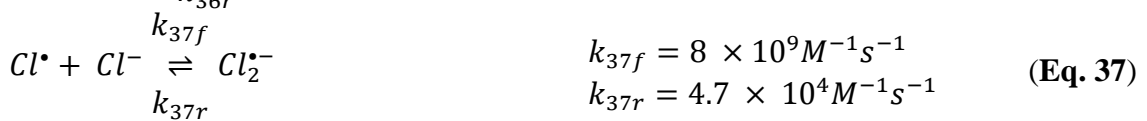
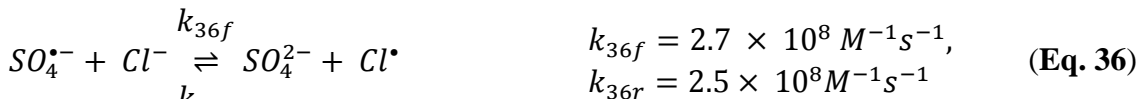


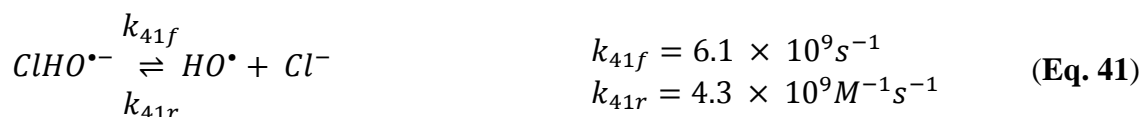
**Fig. 13.** Variation of (a) RAN, (b) PS, (c) %  $RSE_{av}$ , and (d)  $k_{obs}$  at different  $[NaCl]$  at  $[I] = 100 \text{ mM}$ . (e) Concentration of iron species (equivalent  $Fe^{2+}$ ) at the end of the reaction. Experimental conditions:  $[RAN]_0 = 28.5 \text{ }\mu\text{M}$ ,  $[PS]_0 = 100 \text{ }\mu\text{M}$ ,  $[iFe]_0 = 1 \text{ mg} / 20 \text{ mL} = 892 \text{ }\mu\text{M}$ ,  $[NaClO_4] = 100 \text{ mM}$ ,  $[NaCl] = 0, 0.1 \text{ mM}, 1 \text{ mM}, 10 \text{ mM}, 100 \text{ mM}$ .  $pH_i = 6.5$  and  $pH_f = 4.0 \pm 0.1$ . Error bars represent standard deviation of two replicates.

In these series of experiments, ionic strength was optimized at 100 mM, i.e.  $[I] = [NaClO_4] + [NaCl]$ , and the conductivity was about 8.5 +/- 0.5 mS/cm. **Fig. 13a, b** shows the influence of chloride ions on the degradation of RAN against PS consumption at chloride concentrations ranging from 0 to 100 mM. As it can be recognized, the extent of degradation reached a maximum of 98% at 1 mM NaCl against 74% of PS consumed. However, when the concentration exceeded 1 mM, RAN degradation was decreased to 97% and 93% against 73% and 69% of PS consumed at 10 mM and 100 mM of NaCl, respectively. It was noticed that the effect of NaCl in the whole studied range (0.1 mM-100 mM) showed an improvement from chloride-free system (89%). This indicates that chloride can exhibit an enhancing effect in iron activated persulfate processes. However, NaCl at concentrations greater than 1 mM can induce a quenching effect that is more significant at higher chloride levels. Therefore, chloride ions can have a dual effect, enhancing and quenching, depending on their concentrations. **Fig. 13c** shows that the highest  $RSE_{av}$  (88%) was at 0.1 mM NaCl, where the enhancing role of NaCl is still of crucial importance. The high RSE is attributed to high RAN degradation achieved with less PS consumption. **Fig. 13d** shows that the optimum rate of degradation ( $k_{obs} = 0.068 \text{ min}^{-1}$ ) was achieved at 1 mM NaCl. It should be noted that the addition of chloride (0.1 mM- 100 mM) has enhanced the rate of degradation compared to the chloride-free system where  $k_{obs}$  was  $0.037 \text{ min}^{-1}$ . Furthermore, as seen in **Fig. 13e**, the addition of chloride contributed to increasing the iron corrosion. The dissolved iron species released after 60 min of reaction reached 44.1  $\mu\text{M}$  at 100 mM of NaCl. This is due to the pitting action chloride may exert on  $\text{Fe}^0$ .

The chemistry of chloride ions in PS activation processes was described by several authors [125-128]. However, few works were made to test their effects in metal

activated PS systems. It was traditionally assumed that chlorides exert a quenching effect on SRs in PS oxidation processes. The principal reaction taking place between SR and chloride is shown in **Eq. 36** [129, 130]. The forward reaction is considered a scavenging reaction that lowers the oxidation efficiency. However, the reverse reaction between the formed chloride radical and the sulfate anion can regenerate SR and conserve the oxidation efficiency. The content of chloride in solution is the main factor that contributes in the direction of this reaction. If chloride ions are present at a high level, a scavenging reaction is favored. Moreover, chloride radical can later enter in chain reactions. For example, it can react with chloride anion to give  $Cl_2^{\bullet-}$  (**Eq. 37**) [129, 131]. The reaction between two  $Cl_2^{\bullet-}$  can regenerate chloride anion and form chlorine (**Eq. 38**) [132]. Both  $Cl^{\bullet}$  and  $Cl_2^{\bullet-}$  can complex in water to form  $ClHO^{\bullet-}$  (**Eqs. 39, 40**) [133, 134]. The decomposition of  $ClHO^{\bullet-}$  gives HR (**Eq. 41**) [134]. By that regard, the process can be shifted from SR-based AOPs to HR-based AOPs at elevated concentrations of chloride ions.





Recently, studies are considering that chloride can play an enhancing role in PS-induced-contaminant oxidation. For example, 1mM of chloride was found to have an enhancing effect on the rate of degradation of p-nitrosodimethylaniline (RNO) at 65°C, and 5-50 mM of chloride was observed to increase the rate of RNO bleaching under alkaline conditions. However, up to 28 mM of chloride, no effect was detected on the overall oxidation efficiency using iron activation for RNO removal [126]. The produced chlorine radicals can be considered as reactive radicals if they can cause a direct attack toward the contaminant present, or if they induce propagation reactions that give more SRs. In addition to the external experimental conditions (pH, temperature, or the method of PS activation applied), the internal properties of the contaminant itself are of crucial importance in order to determine whether chlorine radicals are reactive to it or not. For example, olefins with C=C functional group shows a higher rate of reaction with  $Cl_2^{\bullet-}$  than their aromatic and alkane analogues [127]. In this investigation, the studied compound (RAN) exhibited a C=C attached to a nitro group and a furan ring with dimethylamine at its C2 position (**Table 3**). The increase in the rate of degradation of RAN in the presence of chloride may be related to the occurrence of electron density entities in the RAN structure. However, there is no evidence that reactive chlorine radicals have directly attacked RAN.

### **3. Application of *i*Fe in the Presence of Bromides at Concentrations as that for Sea Water (RAN/PS/*i*Fe/NaClO<sub>4</sub>/NaBr Systems)**

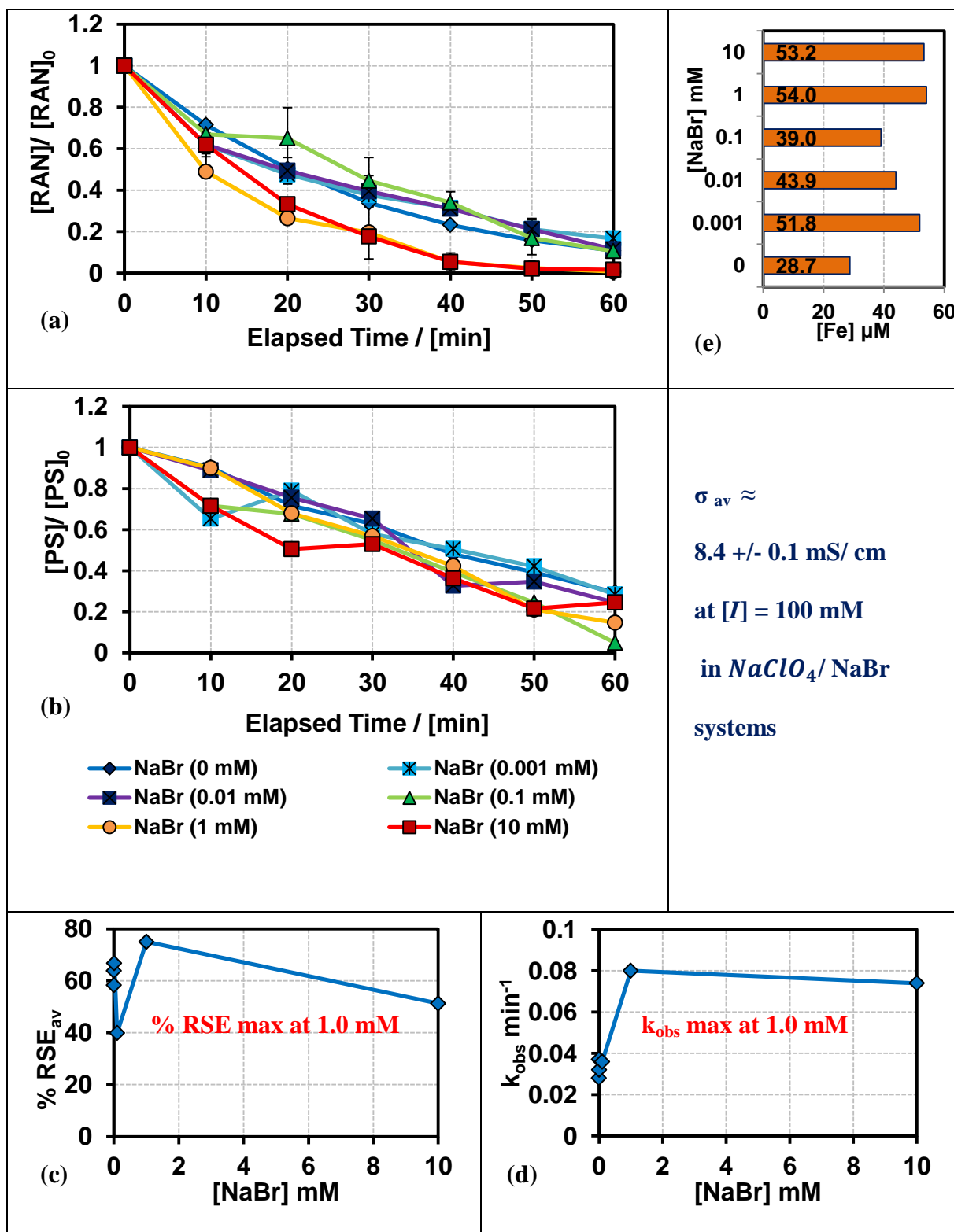


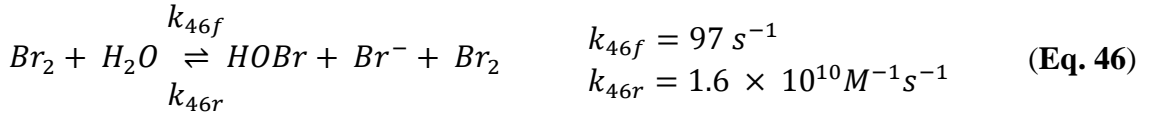
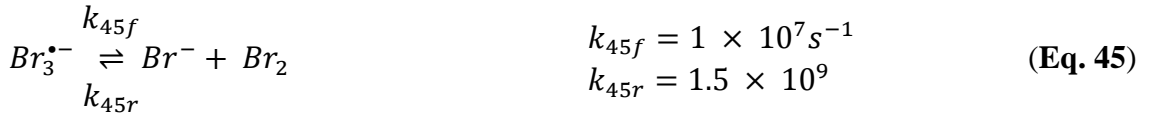
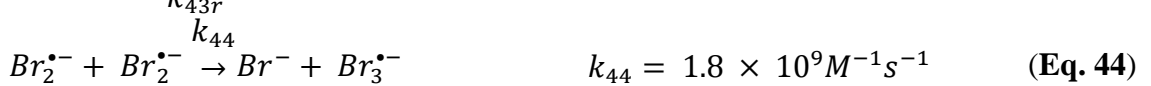
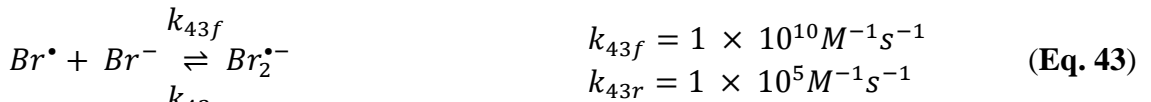
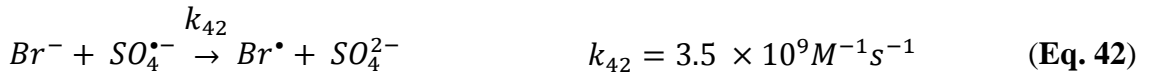
**Fig. 14.** Variation of (a) RAN, (b) PS, (c) % RSE<sub>av</sub>, and (d) k<sub>obs</sub> at different [NaBr] at [I] = 100 mM. (e) Concentration of iron species (equivalent Fe<sup>2+</sup>) at the end of the reaction. Experimental conditions: [RAN]<sub>0</sub> = 28.5 μM, [PS]<sub>0</sub> = 100 μM, [iFe]<sub>0</sub> = 1 mg / 20 mL = 892 μM, [NaClO<sub>4</sub>] = 100 mM, [NaBr] = 0, 0.001 mM, 0.01mM, 0.1 mM, 1 mM, 10 mM. pH<sub>i</sub> = 6.5 and pH<sub>f</sub> = 3.9 ± 0.1. Error bars represent standard deviation of two replicates.

Another series of experiments were conducted in the presence of NaBr, where the ionic strength was also optimized at 100 mM, i.e.  $[I] = [NaClO_4] + [NaBr]$  and the conductivity was about 8.4 +/- 0.1 mS/ cm. **Fig. 14a, b** shows the effect of bromide ions on the degradation of RAN against PS consumption at bromide concentrations ranging from 0 to 10 mM. As can be seen, at trace amounts of bromide (0.001 mM- 0.1 mM) no significant change in the level of RAN degradation was observed; it was about 89%, the same as that in bromide-free system. However, at 1 mM and 10 mM of NaBr, RAN dropped to reach almost full degradation at about 99% and 98% against 85% and 75% of PS consumption. Similar to chloride ions, bromide ions can also have an enhancing effect in metal activated PS systems with optimum at 1 mM NaBr.

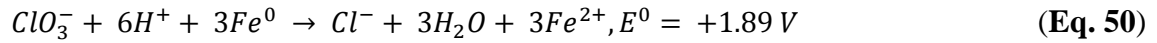
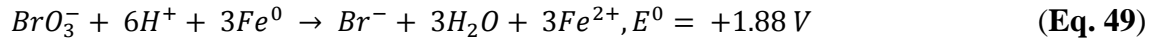
The highest %  $RSE_{av}$  was 75% (**Fig. 14c**) and the highest rate of degradation  $k_{obs}$  was  $0.08 \text{ min}^{-1}$  (**Fig. 14d**), both at 1 mM NaBr. By comparison to the bromide-free system where  $k_{obs}$  was  $0.037 \text{ min}^{-1}$ , it can be clearly revealed that bromide ions were increasing the speed of PS oxidation and RAN depletion. Furthermore, by comparison to chloride additions, the case of bromide additions showed higher reaction rate constants. For example, at 1 mM of NaCl and NaBr,  $k_{obs}$  was  $0.068 \text{ min}^{-1}$  and  $0.08 \text{ min}^{-1}$ , respectively, and at 10 mM of NaCl and NaBr,  $k_{obs}$  was  $0.06 \text{ min}^{-1}$  and  $0.074 \text{ min}^{-1}$ , respectively (**Fig. 13d, Fig. 14d**). It was shown that both halides can speed up the depletion reaction, but bromide ions have exhibited slightly higher enhancing effect. **Fig. 14e** shows the total dissolved iron species after 60 min of reaction of the RAN/PS/iFe/ $NaClO_4$  systems in the presence of bromide. The highest dissolved iron amount was 54  $\mu\text{M}$  in the presence of 1 mM NaBr, showing that bromide is more reactive than chloride toward iron corrosion.



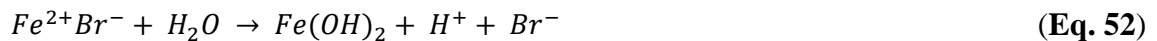
The reaction of SR plus bromide is a very fast reaction ( $k = 3.5 \times 10^9 M^{-1} s^{-1}$ ). This reaction leads to the formation of  $Br^\bullet$  (**Eq. 42**) [135] that is a primary reactive radical that propagates to give  $Br_2^{\bullet-}$  and  $Br_3^{\bullet-}$  as secondary radicals (**Eqs. 43, 44**) [136, 137]. Bromide is regenerated by the decomposition of  $Br_3^{\bullet-}$  and bromine is formed (**Eq. 45**) [138]. The hydrolysis of bromine gives hypobromous acid (HOBr) (**Eq. 46**) [138], which is a requisite intermediate and precursor for bromate ( $BrO_3^-$ ) formation.



However, a study has revealed the lack of  $BrO_3^-$  in UV-activated PS systems due to formation of superoxide anion ( $O_2^{\bullet-}$ ) that reduced HOBr and induced bromide reformation [139]. Another study showed that  $Fe^0$  can electrochemically reduce oxo-anions as bromate and chlorate back to bromide and chloride. It also revealed that the rate of reduction was higher for bromate (**Eq. 47-50**) [140]. Similarly, in this study, the possible involvement of  $Fe^0$  in reducing the formed oxo-anions can be the reason why more iron ions were released and their levels were higher in the presence of bromide rather than chloride.



Furthermore, the addition of halides promotes  $Fe^0$  corrosion due to a pitting action that removes the passivating oxide layer from the surface of  $Fe^0$ . The development of (oxy) hydroxides layer at the surface of  $Fe^0$  as a result of oxidation and precipitation can prevent electron flow and reduce its reactivity in treatment applications. Chlorides and bromides can penetrate into pores of the oxide layer and increase its permeability. Although halides can also adsorb on the iron film, this process doesn't reduce metal dissolution. On the contrary, halides favor hydration of the metal ions and promote their continual dissolving at a high rate (**Eqs. 51, 52**) [141].



Moreover, chlorides and bromides impact the efficiency of  $Fe^{2+}$  oxidation reactions not only as radical scavengers but also as metal complexing agents. As the stability of the ion pair formed increases, the rate of oxidation of  $Fe^{2+}$  decreases [142]. For example,  $FeCl^+$  is stronger than  $FeBr^+$ . As a consequence, the rate of  $Fe^{2+}$  oxidation is greater in the presence of  $Br^-$  than  $Cl^-$ . This may affect the rate of  $Fe^{2+}$ -PS activation reaction and subsequently the rate of substrate depletion.

The enhancing/ scavenging effect of halides is complicated but halides should not be strictly considered as scavengers.

### E. TOC Analysis at Different PS:iFe Molar Ratios

The effect of PS content and iFe amount on the total organic carbon (TOC) is tested at  $[I] = 100 \text{ mM}$  under two cases. Case # 1 where the  $n(\text{PS}):n(\text{iFe})$  is constant at 0.112, such that at elevated  $[\text{PS}]$ , iFe amount added was increased proportionally to keep the molar ratio constant. The aim is to find out by keeping the same molar ratio of PS:iFe but increasing  $[\text{PS}]$  and mass of iFe, whether this gives the same final TOC results or not. Case # 2 where the  $n(\text{PS}):n(\text{iFe})$  is increasing from 0.112 to 22.4, such that at elevated  $[\text{PS}]$ , iFe was kept constant at  $2 \text{ mg} / 40 \text{ mL}$ . The aim is to check the feasibility of removing TOC from water with a low load of iFe.

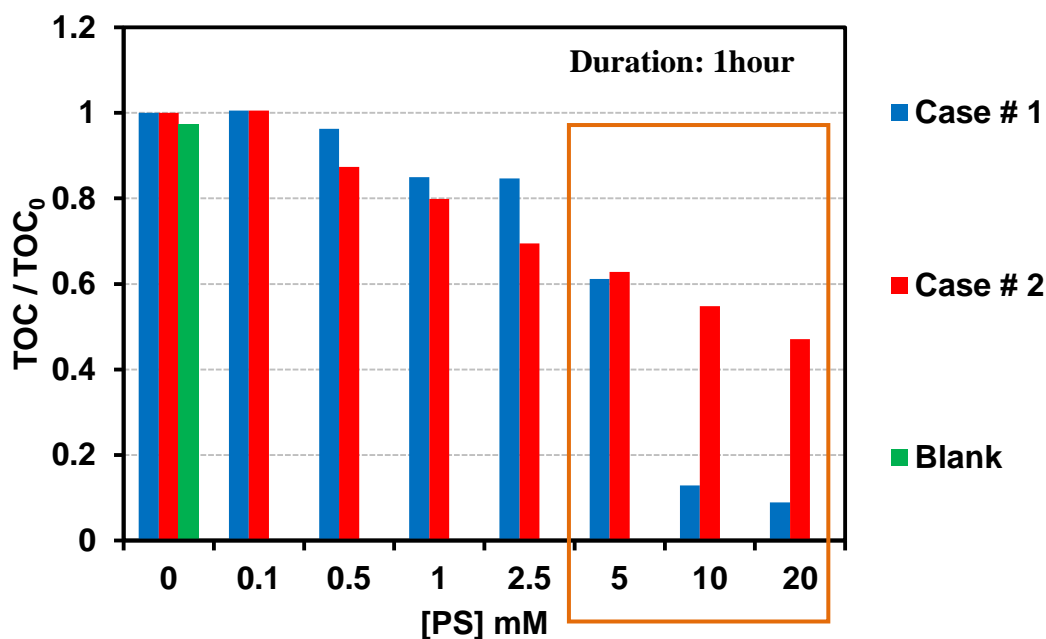


**Fig. 15.** Variation of the Total Organic Carbon (TOC) obtained after one hour reaction in several systems of RAN/PS/ $\text{NaClO}_4$ /iFe where  $[\text{RAN}] = 28.5 \mu\text{M}$  and  $[\text{NaClO}_4] = 100 \text{ mM}$ . Case # 1: different concentrations of  $[\text{PS}]$  at different masses of iFe. Case # 2: different  $[\text{PS}]$  at same masses of iFe.  $\text{pH}_i = 6.5$  for both cases. Experimental conditions are summarized in **Table 5**. Blank solution contains RAN/ iFe ( $400 \text{ mg} / 40 \text{ mL}$ ) gives  $\text{pH}_f = 8.8$ .

**Table 5.** Experimental conditions corresponding for Case # 1 and Case #2 of **Fig. 11**: [PS] (mM), iFe (mg/ 40 mL), n(PS):n(iFe), and pH<sub>f</sub>.

<b>Case # 1</b>								
[PS] mM	0	0.1	0.5	1	2.5	5	10	20
iFe (mg/ 40 mL)	0	2	10	20	50	100	200	400
n(PS):n(iFe)		0.112	0.112	0.112	0.112	0.112	0.112	0.112
pH <sub>f</sub>	6.5	4.37	3.36	3.15	2.93	2.81	5.26	5.92
<b>Case # 2</b>								
[PS] mM	0	0.1	0.5	1	2.5	5	10	20
iFe (mg/ 40 mL)	0	2	2	2	2	2	2	2
n(PS):n(iFe)		0.112	0.56	1.12	2.8	5.6	11.2	22.4
pH <sub>f</sub>	6.5	4.37	3.75	3.47	3.21	3.07	2.84	2.75

**Fig. 15** shows the variation of TOC after 1 hour of reaction in RAN/PS/NaClO<sub>4</sub>/iFe systems at Case # 1 and Case # 2. Control system containing RAN with a very high amount of iFe at 400 mg / 40 mL shows only 2% removal of TOC revealing that high amount of iFe in the absence of PS can incorporate in the removal process of TOC but with very minimal efficiency. Results show that in the system where [PS] = 0.1 mM and [iFe] = 2 mg / 40 mL no removal of TOC was obtained, although at similar conditions RAN has reached 89% degradation (**Fig. 12a**). This indicates that at low PS and low iFe concentrations RAN has transformed into by-products, however, mineralization was not taking place. While keeping the same molar ratio of PS:iFe at 0.112 and increasing the concentrations of both PS and iFe (Case # 1), TOC removal has increased from 3% to 38% at [PS] = 0.5-5mM and [iFe] = 10 mg / 40 mL - 100 mg / 40 mL, respectively. Interestingly, TOC removal has reached 87% at [PS] = 10 mM and [iFe] = 200 mg / 40 mL and 91% at [PS] = 20 mM and [iFe] = 400 mg / 40 mL. This implies that a system with the same PS:iFe molar ratio doesn't necessarily induce the same TOC removal extent. It is revealed that a high amount of iFe reacting with a high amount of PS can generate iron corrosion products (ICPs) that are involved in activation of PS on one side and sequestration of organic compounds

(RAN and its byproducts) on another side. Two possible processes were hypothesized: the first hypothesis relates the presence of high amounts of PS and iFe to the excessive and rapid generation of SRs, so that the oxidation power is high enough to cause almost complete mineralization of organic compounds into water and CO<sub>2</sub>. The second hypothesis is the concept of co-precipitation where high amounts of PS and iFe produce abundant ICPs that are responsible for sequestering organic compounds during their formation and removing them from aqueous systems by their precipitation. It was noticed that more ICPs were formed when higher amounts of iron were used. The same experiment was repeated with a low load of iFe at 2 mg / 40 mL (Case # 2) to minimize the amount of ICPs present, therefore minimizing the effect of co-precipitation. Results showed that while increasing [PS] from 0.1 to 20 mM the TOC removal was improving on an average of 8% between each increase in PS. However, in the range of low concentrations of PS (0.1 mM-2.5 mM) TOC removal (12%-30%) was slightly higher than Case # 1. At [PS] = 5 mM TOC removal was 37% close to what was obtained in Case # 1. At higher PS concentrations, 10mM and 20 mM, TOC removal was 45 % and 52 %, respectively, much lower than what was achieved in Case # 1. This can tell that the use a low iFe load favors the oxidation approach of the removal mechanism, so that when [PS] is increased, more SRs are generated and mineralization is higher. On the contrary, at increasing amounts of iFe with elevated [PS], more ICPs are formed, mainly from the reaction of PS at the surface of iron. This case favors co-precipitation whose effect appeared largely from the sudden drop of TOC between [PS] of 5 mM and 10 mM accompanied by excessive increase of iFe from 100 mg / 40 mL to 200 mg / 40 mL (Case # 1). The formation of excessive amounts of ICPs between these conditions is

followed by a  $\text{pH}_f$  increase from 2.81 to 5.26. However, at a low  $\text{iFe}$  load (Case # 2),  $\text{pH}_f$  keeps decreasing as PS increases due to the effect of PS decomposition.

#### **F. Study of Iron Corrosion Products (ICPs)**

Additional work was done on the three systems of Case # 1 marked in **Fig. 15**. After the reaction was over in 1 hour, the supernatant was removed and centrifuged. The formed ICPs were accumulated at the bottom of the centrifuge tube. The formed ICPs were weighed by difference. **Fig. 16** shows the results of the collected masses of ICPs (mg) with respect to the [PS] added initially to the solutions. A linear relationship was obtained with a regression of 0.99 between the weight of the ICPs collected and the concentrations of PS in solution as well the masses of  $\text{iFe}$ . By comparing sys 1 (RAN/ $\text{iFe}$ ) at  $[\text{iFe}] = 200 \text{ mg} / 40 \text{ mL}$  with sys 3 (RAN/ PS/  $\text{NaClO}_4$ / $\text{iFe}$ ) at  $[\text{PS}] = 10 \text{ mM}$  and  $[\text{iFe}] = 200 \text{ mg} / 40 \text{ mL}$ , it is noticed that  $\text{iFe}$  alone, without the presence of PS, has formed about 5 mg of ICPs, while in the presence of PS the mass was more than 15 mg. This proves that PS is encouraging more  $\text{Fe}^{2+}$  release from  $\text{iFe}$  as well as more ICP formation.

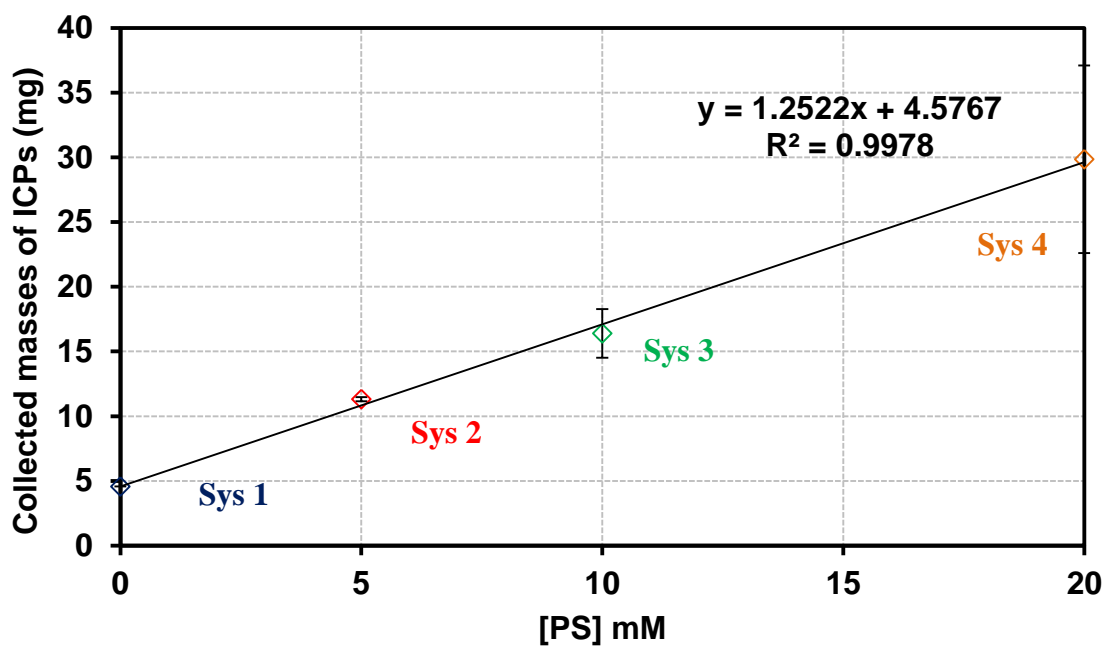


**Fig. 16.** Collected masses of ICPs in different systems of RAN/PS/ $NaClO_4$ /iFe. Experimental conditions:  $[RAN] = 28.5 \mu M$ ,  $[NaClO_4] = 100 \text{ mM}$ ,  $[PS](\text{mM}):iFe(\text{mg}/40 \text{ mL})$  is 0:200, 5:100, 10:200, and 20:400 for Sys 1, Sys 2, Sys 3, and Sys 4, respectively. Error bars represent standard deviation of two replicates.

SEM images of the corresponding precipitates of ICPs show how the interference of PS can change the image of ICPs from being connected to complete deterioration. EDS reveals that the only new element being added to ICPs in PS containing systems is S, coming from PS and activated PS (**Fig. 17**).

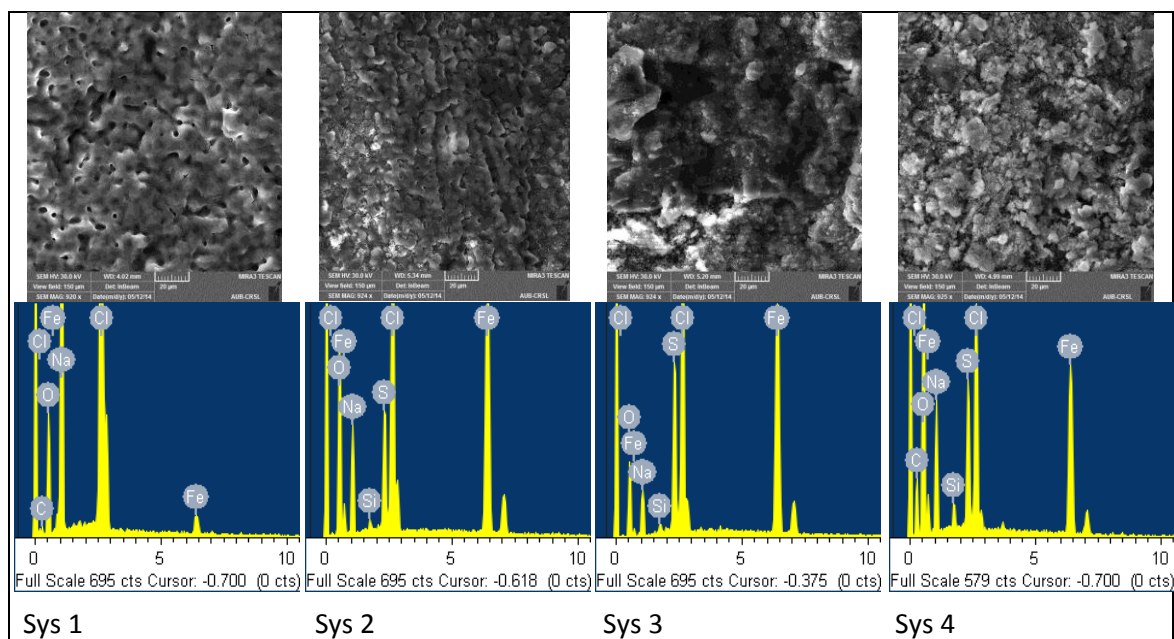


**Fig. 17.** SEM images and EDS analysis for the collected ICPs precipitates from solutions of RAN/PS/ $NaClO_4$ /iFe systems. Experimental conditions: [RAN] = 28.5  $\mu$ M and [ $NaClO_4$ ] = 100 mM. Sys 1: [PS]:[iFe] is 0:200. Sys 2: [PS]:[iFe] is 5:100. Sys 3: [PS]:[iFe] is 10:200. Sys 4: [PS]:[iFe] is 20:400. [PS] in mM and [iFe] in mg/ 40 mL.

### G. Characterization of iFe (53-150 $\mu$ M) after Reaction

Further analysis was done on the surface and elemental composition of iFe after running an experiment. RAN (28.5  $\mu$ M)/ $NaClO_4$  (100 mM)/PS (5 mM)/ iFe (100 mg / 40 mL) was the system under study. Before reaction the elements present were mainly Fe, Mn and Si (**Fig. 18a, c**). However, after 1h reaction, as can be seen in **Fig. 18b, d**, elements as oxygen, sulfur, and chlorine has appeared due to the direct reaction of the surface of iFe with  $S_2O_8^{2-}$  in the presence of  $NaClO_4$ .



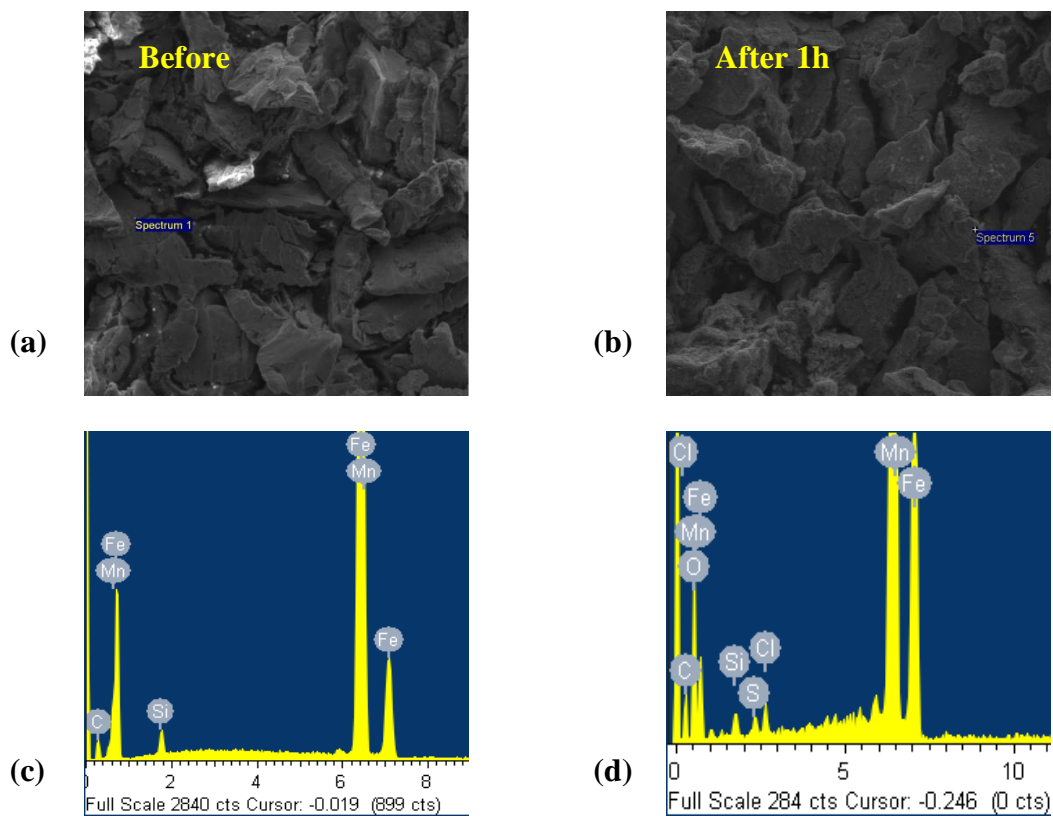


**Fig. 18.** (a, b) SEM images and (c, d) EDS analysis showing elemental composition of iFe (53-150  $\mu\text{M}$ ) before and after 1h reaction, respectively. Experimental conditions:  $[\text{RAN}] = 28.5 \mu\text{M}$ ,  $[\text{NaClO}_4] = 100 \text{ mM}$ ,  $[\text{PS}] = 5 \text{ mM}$  and  $\text{iFe} = 100 \text{ mg} / 40 \text{ mL} = 44.64 \text{ mM}$ .

The above sample taken after 1h reaction was kept exposed to air for 1 week. Then SEM/ EDS analysis was done again to it. **Fig. 19** reveals the expansion of the surface of iFe at particular sites where the pitting action of SRs or PS was occurring.

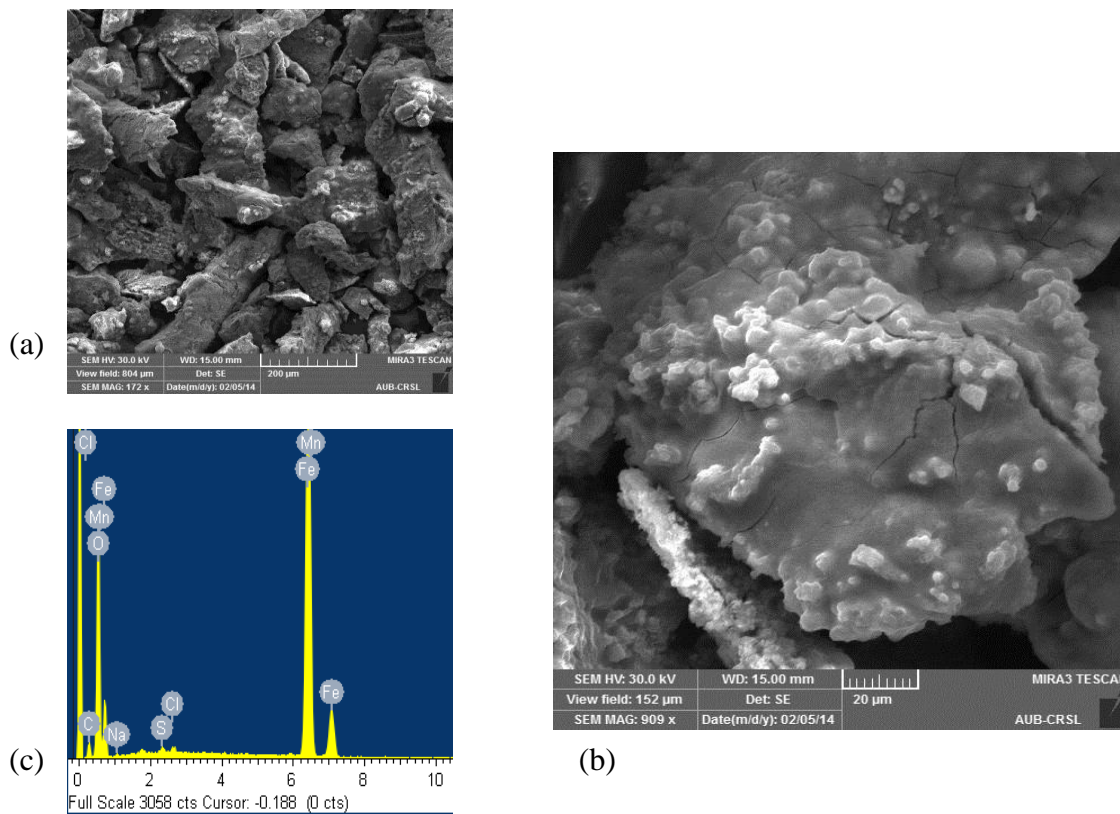


**Fig. 19.** SEM images of iFe (53-150  $\mu\text{M}$ ), after 1 week of the 1h reaction is over, at (a) low magnification and (b) high magnification with corresponding (c) EDS analysis. Experimental conditions:  $[\text{RAN}] = 28.5 \mu\text{M}$ ,  $[\text{NaClO}_4] = 100 \text{ mM}$ ,  $[\text{PS}] = 5 \text{ mM}$  and  $\text{iFe} = 100 \text{ mg} / 40 \text{ mL} = 44.64 \text{ mM}$ .

A higher magnification was done at one of the spots where expansion was observed. **Fig. 20** shows the difference of elemental composition between the spot of expansion and the nearby surface. As can be seen, oxygen element is higher at the spot of expansion showing that it corresponds to iron oxide formation. Therefore, pitting corrosion nucleation is formed at the weak points in the passive film.

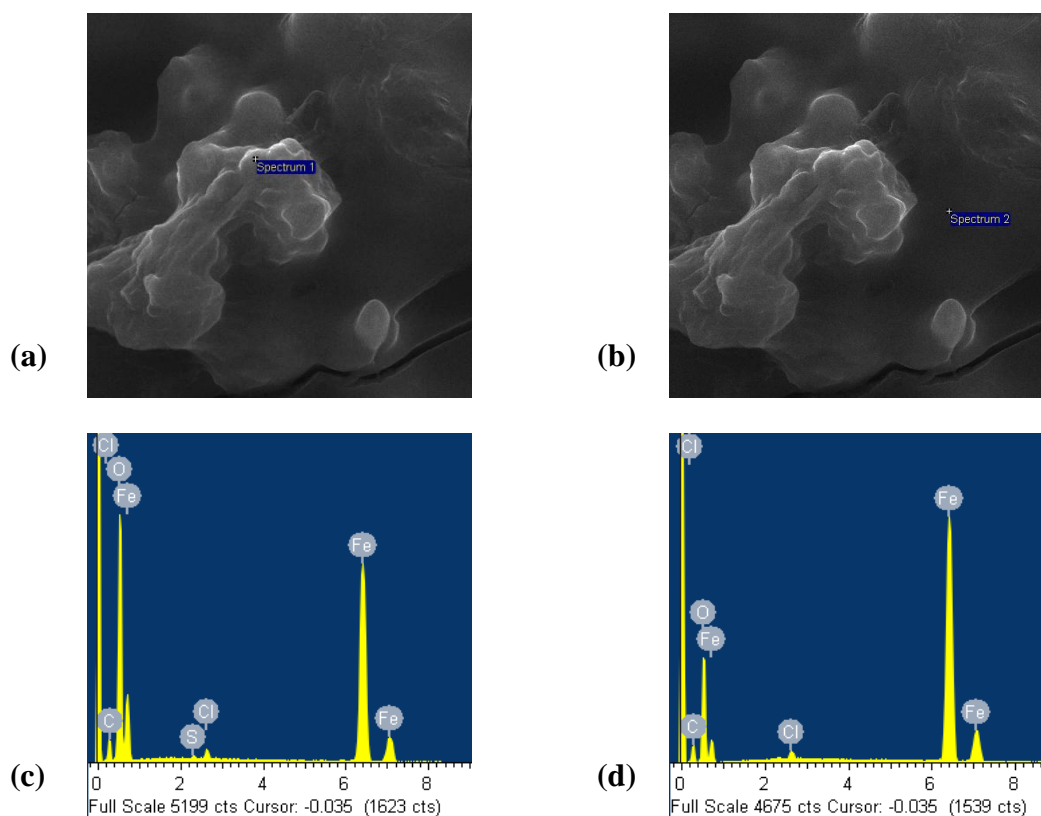


**Fig. 20.** (a, b) SEM images of the magnification of the metallic oxide expansion of Fig. 17 where EDS analysis is considering (c) the expansion and (d) the nearby surface, respectively. Experimental conditions: [RAN] = 28.5  $\mu$ M, [PS] = 5mM, [NaClO<sub>4</sub>] = 100 mM, and iFe = 100 mg / 40 mL = 44.64 mM.

## H. Identification of Transformation Products and Proposed Degradation Scheme.

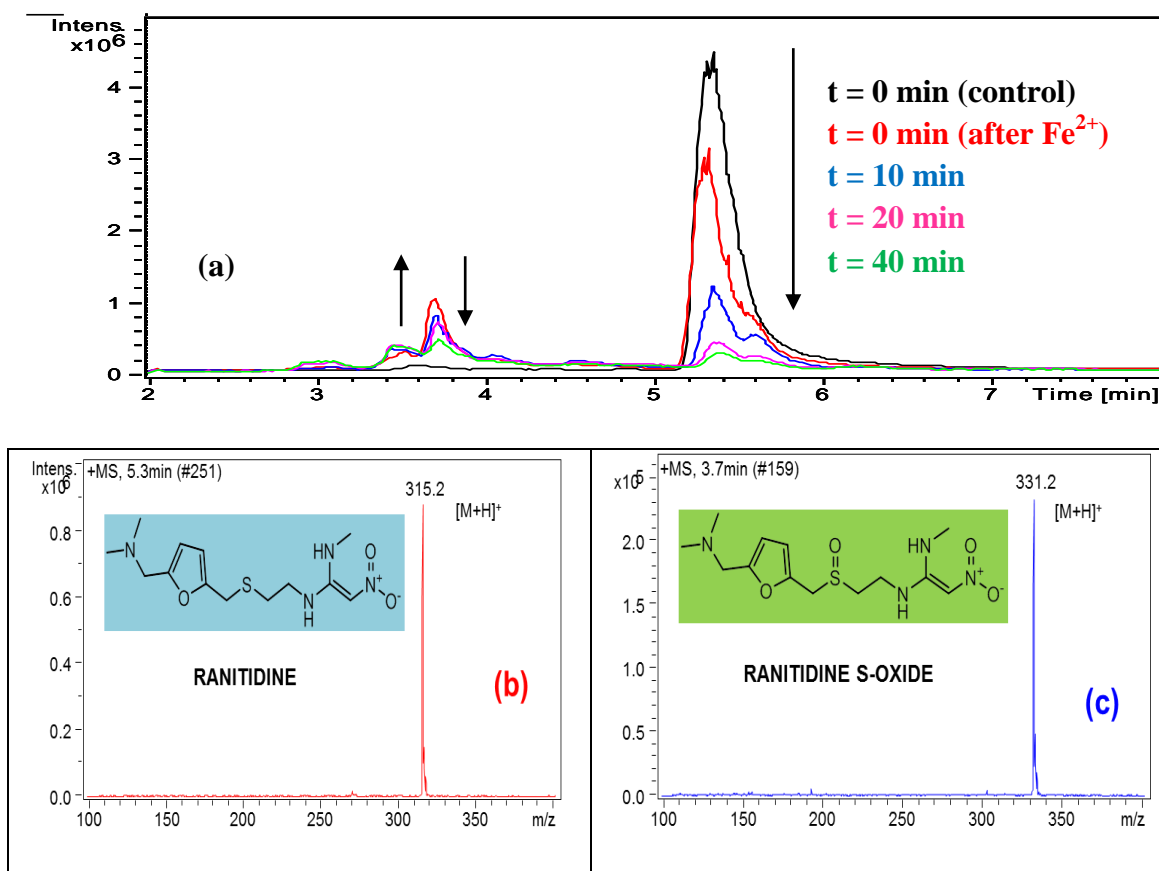


**Fig. 21.** (a) HPLC Chromatogram showing RAN degradation in the RAN/PS/ $Fe^{2+}$  (sequentially spiked) system: 28.5  $\mu$ M/ 100  $\mu$ M/ 100  $\mu$ M. Presence of an oxidation byproduct initially formed and later disappeared after repetitive  $Fe^{2+}$  spiking. (b, c) MS spectra showing RAN peak at 315.2 m/z and the oxidation byproduct peak at 331.2 m/z with their corresponding structures.

The LC/MS analysis of RAN and its transformation products (**Fig. 21a**) represents the case of RAN/PS/ $Fe^{2+}$  (sequentially added) at 28.5  $\mu$ M/ 100  $\mu$ M/ 100  $\mu$ M whose RAN degradation and PS decomposition was shown in **Fig. 9**. The chromatogram shows that RAN in the presence of PS was dissipating gradually upon successive  $Fe^{2+}$  additions. It also reveals that RAN oxidation products were initially formed and later disappeared after additional  $Fe^{2+}$  spiking and continuous activation of PS. The MS spectrum of RAN presented a molecular ion  $[M+H]^+$  in positive ionization

mode at 315 m/z (**Fig. 21b**). A transformation product has appeared at a retention time of 3.7 min showing a molecular ion  $[M+H]^+$  in positive ionization at 331 m/z (**Fig. 21c**). The increase by 16 amu in the mass of RAN during oxidation is referred to the addition of an oxygen atom. The oxidation byproduct was predicted to be Ranitidine S-oxide, which is also one of the RAN metabolites [61]. Non-activated PS, as an oxidant, could be responsible of some RAN oxidation. However, this oxidation was accelerated when PS was activated and SRs were generated just after  $Fe^{2+}$  initial spiking (**Eq. 30**). After successive  $Fe^{2+}$  spiking, the continuous generation of SRs was not only targeting RAN, but also the formed oxidation products as well, leading to their gradual degradation starting from  $t = 10$  min.

The DAD UV spectrum of RAN ( $r_t = 5.3$  min) shows two absorption peaks at 320 nm and 230 nm, which are related to nitroethenediamine moiety and the furanyl group, respectively [143]. The DAD UV spectrum of the oxidation byproduct ( $r_t = 3.7$  min) was similar to that of RAN with a slight bathochromic effect (red shift of  $\Delta\lambda = 4$  nm) indicating a transformation in the RAN molecule (**Fig. 22**).

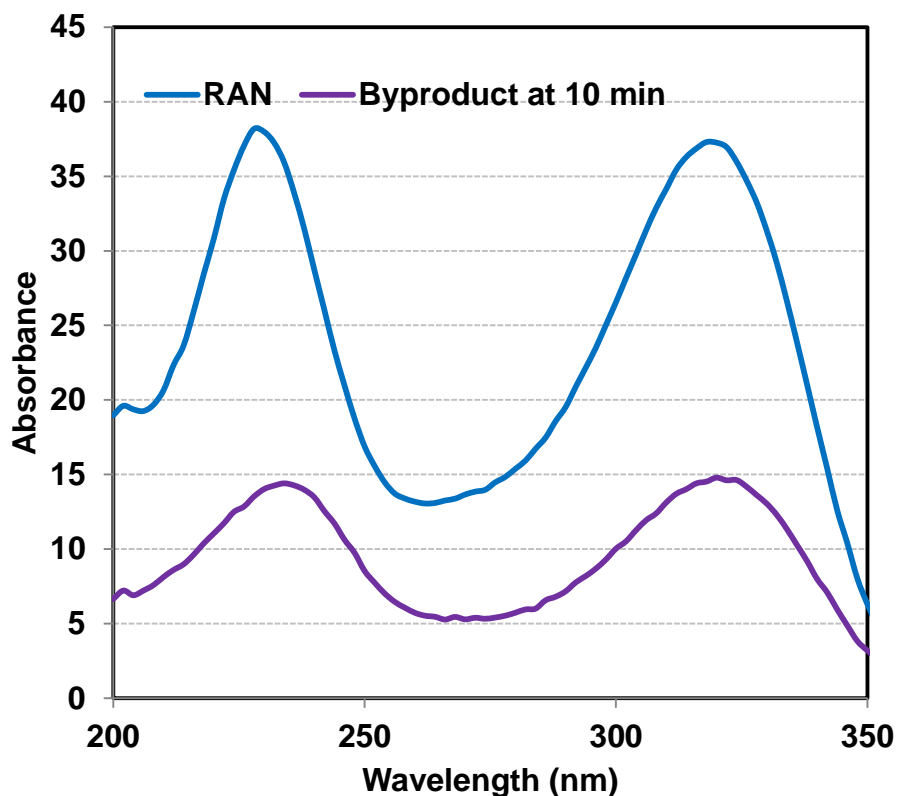


**Fig. 22.** DAD absorption spectrum of RAN (at  $t = 0$  min) and the oxidation product obtained at 3.7 min (at  $t = 10$  min).

SRs react more frequently by  $e^-$  abstraction from organic molecules [110]. For example, a SR can abstract an electron from aromatic derivatives forming aromatic cationic radicals that can later undergo hydroxylation with water [144]. The predicted mechanism of the oxidation product formation in the presence of SRs is depicted in **Fig. 23**. The reactive entities of the RAN molecule that can be subjected to electron transfer are: S, N, O, and the furan ring. The comparison of the ionization energies of each entity is useful to determine the least IE which corresponds to higher electron transfer possibility. The furan ring indicates the lower IE at 857.4 kJ/mol ( $71673\text{ cm}^{-1}$ ) [145], followed by S (IE = 999.6 kJ/mol), then O (IE = 1313.9 kJ/mol), and N (1402.3 kJ/mol). Since the primary oxidation byproduct ( $[M+H]^+$  331 m/z) has a furan ring

(noticed from 230 nm absorption band), then the byproduct has an electron transfer from S rather than furan ring. After removing an  $e^-$  from S atom by a SR, S was oxygenated probably by an attack of another SR. Furthermore, electron transfer from furan ring is also plausible and there is a possibility of ring opening, but transformation products were not identified. Other oxidation products may be formed and they may later be fragmented or mineralized.

In SR-based AOPs, both SRs and HRs are coexisting (**Eq. 27**). The experimental pH was below 6.5 in most experiments. At this slightly acidic condition, SRs are dominating but HRs are still existing at lower amounts. HRs react more preferably by H-abstraction from C-H bond or addition to unsaturated moieties [146]. The predicted mechanism of the oxidation product formation in the presence of HRs is depicted in **Fig. 24**.  $OH^\bullet$  can abstract hydrogen atoms from several positions of the target molecule. The most favored H-abstraction can be from the carbon positioned between the sulfur atom and the furan ring, since the formed radical is stabilized by resonance with the d-lone pair of the sulfur atom and with the  $\pi$  -electrons of the furan ring. The radical delocalization on the furan ring makes it very unstable with a high tendency for ring cleavage. On the other side, the radical delocalization on the sulfur atom increases the possibility of an OH radical attack on S, followed by tautomerization to give Ranitidine S-oxide that was detected by MS at 331 m/z. Further oxidation of this transformation product can lead to the formation of other byproducts, not identified by this study, which can achieve mineralization.

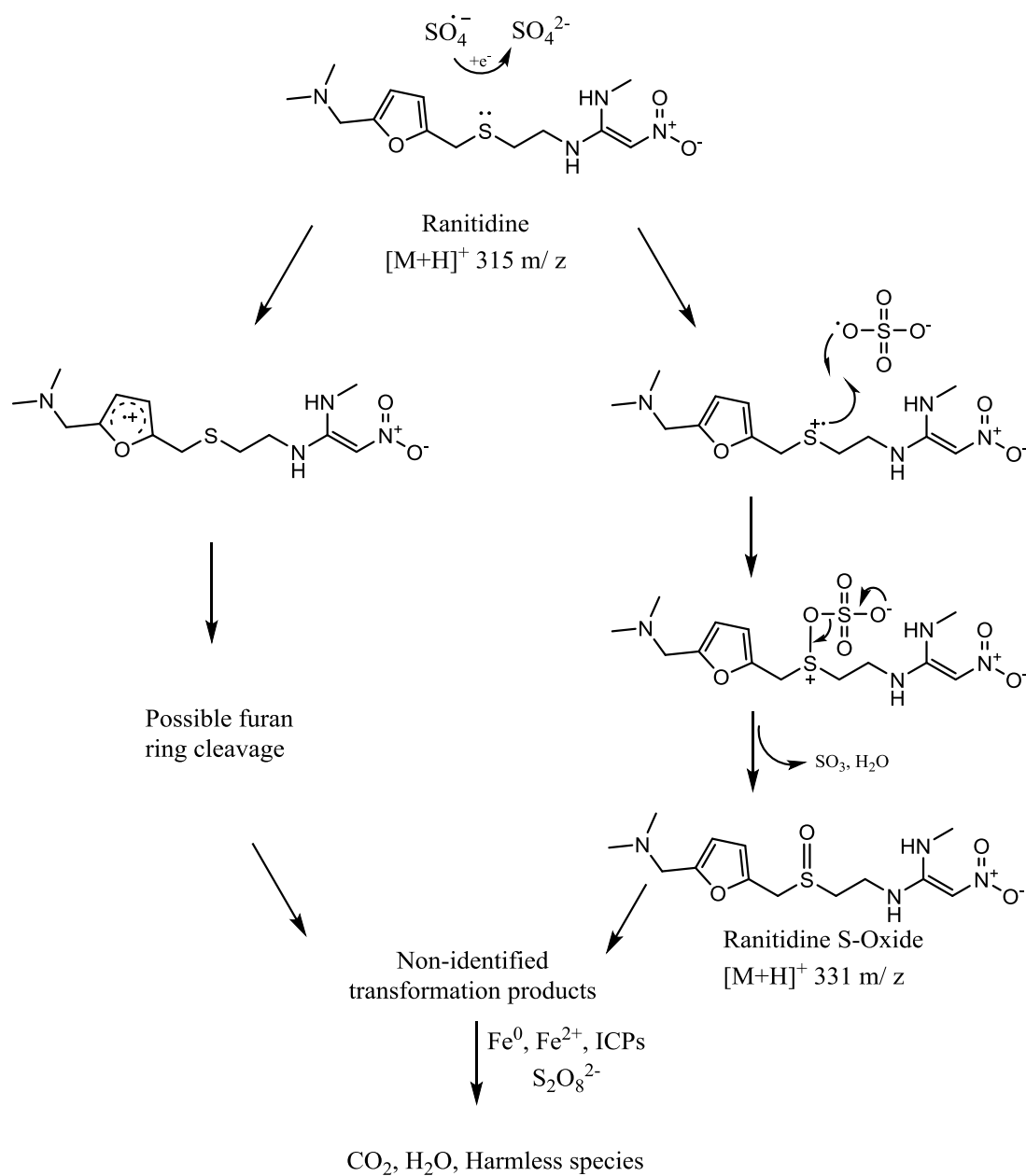


**Fig. 23.** Proposed degradation mechanism of RAN by sulfate radicals in PS/  $\text{Fe}^{2+}$  systems at room temperature.



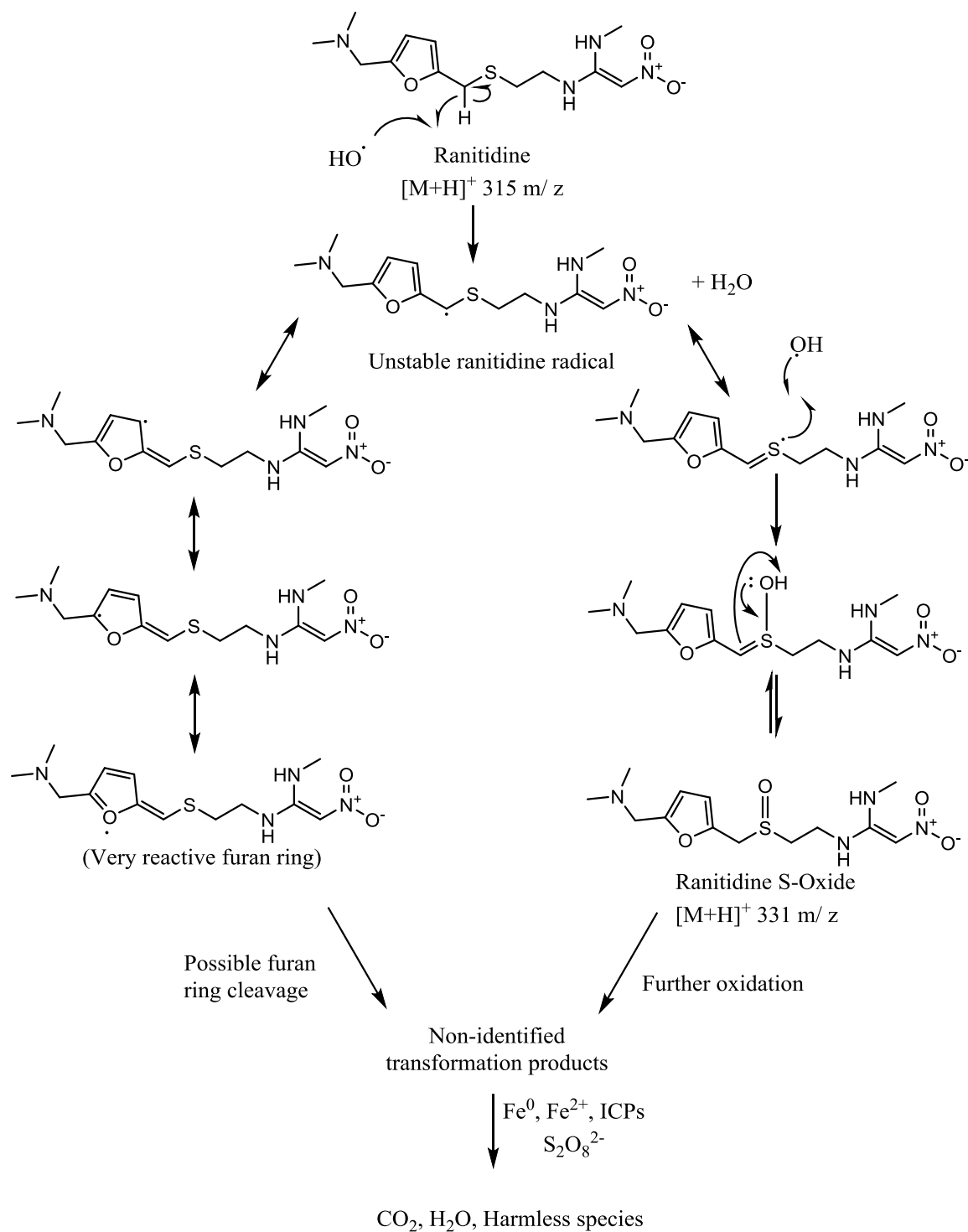


**Fig. 24.** Proposed degradation mechanism of RAN by hydroxyl radicals in PS/ $\text{Fe}^{2+}$  systems at room temperature.

## CHAPTER IV

### CONCLUSION

Industrial iron (iFe) is an abundant and an available metallic scrap collected from a car workshop with a zero cost. This work has demonstrated a successful employment of iFe as a PS activator for RAN degradation in aqueous systems. iFe has indicated a sustained RSE and a less iron hydroxide sludge compared to cFe. iFe is composed mainly of atomic Fe and other elemental constituents (e.g. Si, O, C, Mn, Ti, Cu). The  $Fe^{2+}$  produced from iFe oxidation is responsible for PS activation by which oxidative SRs are generated. The optimal molar ratio of  $Fe^{2+}$ :PS was observed to be 1:1. A low load of iFe ( 1 mg / 20 mL) with 100  $\mu$ M of PS was sufficient to induce almost a complete RAN removal over 1 h reaction accompanied by the release of only few amounts of  $Fe^{2+}$ , i.e.  $Fe^{2+}$ :PS is 0.166:1. %  $RSE_{av}$  obtained in this system was about 72% and has reached 100% at  $[I] = 250$  mM. On the contrary, at a higher load of iFe (5 mg / 20 mL), %  $RSE_{av}$  was only 33%. Although oxidative degradation was successful at this low load of iFe, but mineralization was negligible. TOC removal was improved by increasing the iFe amounts and the PS concentrations, proportionally, due to the fact that the process of co-precipitation became more significant at high loads of iFe and PS. A removal of 91% of TOC was reached at  $[PS] = 20$  mM and  $[iFe] = 400$  mg / 40 mL. Furthermore, in the ionic strength controlled systems, it was revealed that as ionic strength increases, the rate of RAN degradation decreases. However, ionic strength of 100 mM was considered as a limiting edge that should not be exceeded in order to sustain an acceptable rate of RAN degradation. The addition of halides ( $Cl^-$  and  $Br^-$ ) showed an improvement in the rate of RAN degradation at optimum

concentration of 1 mM each, but  $Br^-$  denoted higher kobs than  $Cl^-$ . This was in consistency with more iFe corrosion and greater dissolved iron species at the end of the treatment period. The enhancing effect was attributed to the pitting action halides may exert on the surface of iFe. However, at  $[Cl^-]$  or  $[Br^-] > 1$  mM, the effect of SR quenching became more significant. During the treatment a RAN intermediate was detected by HPLC/ MS at 331 m/ z which dissipated gradually. Further progress can be directed toward studying the efficiency of AOPs in real water samples (seawater, underground water). In addition, because of the successful application of a very low load of iFe toward RAN oxidation, further research targeting metallic nanoparticles in chemical-activated PS technology is important in order to elaborate more the oxidation/ co-precipitation processes and their relation to metallic load.

## BIBLIOGRAPHY

- [1] E.G. Primel, S.S. Caldas, A.L.V. Escarrone, Multi-residue analytical methods for the determination of pesticides and PPCPs in water by LC-MS/MS: a review, *Central European Journal of Chemistry*, 10 (2012) 876-899.
- [2] J.C. Crittenden, H. Montgomery Watson, I. Books24x, MWH's water treatment: principles and design, third edition, John Wiley & Sons, Hoboken, N.J, 2012.
- [3] M. Beretta, V. Britto, T.M. Tavares, S.M.T. da Silva, A.L. Pletsch, Occurrence of pharmaceutical and personal care products (PPCPs) in marine sediments in the Todos os Santos Bay and the north coast of Salvador, Bahia, Brazil, *Journal of Soils and Sediments*, 14 (2014) 1278-1286.
- [4] J. Robles-Molina, F.J. Lara-Ortega, B. Gilbert-Lopez, J.F. Garcia-Reyes, A. Molina-Diaz, Multi-residue method for the determination of over 400 priority and emerging pollutants in water and wastewater by solid-phase extraction and liquid chromatography-time-of-flight mass spectrometry, *Journal of Chromatography A*, 1350 (2014) 30-43.
- [5] F.W. Rabii, P.A. Segura, P.B. Fayad, S. Sauvé, Determination of six chemotherapeutic agents in municipal wastewater using online solid-phase extraction coupled to liquid chromatography-tandem mass spectrometry, *The Science of the total environment*, 487 (2014) 792-800.
- [6] A. Jakimska, A. Kot-Wasik, J. Namiesnik, The Current State-of-the-Art in the Determination of Pharmaceutical Residues in Environmental Matrices Using Hyphenated Techniques, *Critical Reviews in Analytical Chemistry*, 44 (2014) 277-298.
- [7] W. Brand, C.M. de Jongh, S.C. van der Linden, W. Mennes, L.M. Puijker, C.J. van Leeuwen, A.P. van Wezel, M. Schriks, M.B. Heringa, Trigger values for investigation of hormonal activity in drinking water and its sources using CALUX bioassays, *Environment international*, 55 (2013) 109-118.
- [8] C.J. Houtman, Emerging contaminants in surface waters and their relevance for the production of drinking water in Europe, *Journal of Integrative Environmental Sciences*, 7 (2010) 271-295.
- [9] T.A. Ternes, Occurrence of drugs in German sewage treatment plants and rivers, *Water Research*, 32 (1998) 3245-3260.
- [10] M. Carballa, F. Omil, J.M. Lema, M. Llombart, C. García-Jares, I. Rodríguez, M. Gómez, T. Ternes, Behavior of pharmaceuticals, cosmetics and hormones in a sewage treatment plant, *Water Research*, 38 (2004) 2918-2926.
- [11] A. Pal, K.Y.-H. Gin, A.Y.-C. Lin, M. Reinhard, Impacts of emerging organic contaminants on freshwater resources: review of recent occurrences, sources, fate and effects, *The Science of the total environment*, 408 (2010) 6062-6069.
- [12] O.A. Jones, J.N. Lester, N. Voulvoulis, Pharmaceuticals: a threat to drinking water?, *Trends in biotechnology*, 23 (2005) 163-167.
- [13] D.J. Lapworth, N. Baran, M.E. Stuart, R.S. Ward, Emerging organic contaminants in groundwater: A review of sources, fate and occurrence, *Environmental pollution (Barking, Essex : 1987)*, 163 (2012) 287-303.
- [14] P.E. Stackelberg, E.T. Furlong, M.T. Meyer, S.D. Zaugg, A.K. Henderson, D.B. Reissman, Persistence of pharmaceutical compounds and other organic wastewater contaminants in a conventional drinking-water-treatment plant, *Science of the Total Environment*, 329 (2004) 99-113.

- [15] M. Winker, D. Faika, H. Gulyas, R. Otterpohl, A comparison of human pharmaceutical concentrations in raw municipal wastewater and yellowwater, *Science of the Total Environment*, 399 (2008) 96-104.
- [16] A. Nikolaou, S. Meric, D. Fatta, Occurrence patterns of pharmaceuticals in water and wastewater environments, *Analytical and bioanalytical chemistry*, 387 (2007) 1225-1234.
- [17] T. Heberer, Occurrence, fate, and removal of pharmaceutical residues in the aquatic environment: a review of recent research data, *Toxicology letters*, 131 (2002) 5-17.
- [18] C.G. Daughton, I.S. Ruhoy, Environmental footprint of pharmaceuticals: the significance of factors beyond direct excretion to sewers, *Environmental toxicology and chemistry / SETAC*, 28 (2009) 2495.
- [19] D.W. Kolpin, E.T. Furlong, M.T. Meyer, Pharmaceuticals, hormones, and other organic wastewater contaminants in U.S. streams, 1999-2000: a national reconnaissance, *Environmental Science & Technology* [H.W. Wilson - GS], 36 (2002) 1202.
- [20] P.K. Jjemba, Excretion and ecotoxicity of pharmaceutical and personal care products in the environment, *Ecotoxicology and Environmental Safety*, 63 (2006) 113-130.
- [21] R. Rodil, J.B. Quintana, E. Concha-Graña, P. López-Mahía, S. Muniategui-Lorenzo, D. Prada-Rodríguez, Emerging pollutants in sewage, surface and drinking water in Galicia (NW Spain), *Chemosphere*, 86 (2012) 1040-1049.
- [22] J. Rossmann, S. Schubert, R. Gurke, R. Oertel, W. Kirch, Simultaneous determination of most prescribed antibiotics in multiple urban wastewater by SPE-LC-MS/MS, *Journal of Chromatography B-Analytical Technologies in the Biomedical and Life Sciences*, 969 (2014) 162-170.
- [23] M. Gros, M. Petrović, D. Barceló, Tracing pharmaceutical residues of different therapeutic classes in environmental waters by using liquid chromatography/quadrupole-linear ion trap mass spectrometry and automated library searching, *Analytical chemistry*, 81 (2009) 898-912.
- [24] S.K. Behera, H.W. Kim, J.-E. Oh, H.-S. Park, Occurrence and removal of antibiotics, hormones and several other pharmaceuticals in wastewater treatment plants of the largest industrial city of Korea, *Science of the Total Environment*, 409 (2011) 4351-4360.
- [25] K. Yu, B. Li, T. Zhang, Direct rapid analysis of multiple PPCPs in municipal wastewater using ultrahigh performance liquid chromatography-tandem mass spectrometry without SPE pre-concentration, *Analytica chimica acta*, 738 (2012) 59-68.
- [26] K. Maskaoui, J.L. Zhou, Colloids as a sink for certain pharmaceuticals in the aquatic environment, *Environmental science and pollution research international*, 17 (2010) 898-907.
- [27] R.H. Lindberg, J. Fick, M. Tysklind, i. Kemiska, f. Teknisk-naturvetenskapliga, u. Umeå, Screening of antimycotics in Swedish sewage treatment plants – Waters and sludge, *Water Research*, 44 (2010) 649-657.
- [28] M.J.M. Bueno, M.J. Gomez, S. Herrera, M.D. Hernando, A. Agüera, A.R. Fernández-Alba, Occurrence and persistence of organic emerging contaminants and priority pollutants in five sewage treatment plants of Spain: Two years pilot survey monitoring, *Environmental Pollution*, 164 (2012) 267-273.
- [29] A.Y.-C. Lin, C.-F. Lin, T.-H. Yu, Pharmaceutical contamination in residential, industrial, and agricultural waste streams: Risk to aqueous environments in Taiwan, *Chemosphere*, 74 (2008) 131-141.
- [30] P. Verlicchi, A. Galletti, M. Petrovic, D. Barceló, Hospital effluents as a source of emerging pollutants: An overview of micropollutants and sustainable treatment options, *Journal of Hydrology*, 389 (2010) 416-428.
- [31] K. Kümmerer, The presence of pharmaceuticals in the environment due to human use-- present knowledge and future challenges, *Journal of environmental management*, 90 (2009) 2354-2366.

- [32] J.V. Holm, K. Rugge, P.L. Bjerg, T.H. Christensen, Occurrence and distribution of pharmaceutical organic compounds in the groundwater downgradient of a landfill (Grindsted, Denmark), *Environmental Science & Technology*, 29 (1995) 1415.
- [33] J.A. Dougherty, P.W. Swarzenski, R.S. Dinicola, M. Reinhard, Occurrence of herbicides and pharmaceutical and personal care products in surface water and groundwater around Liberty Bay, Puget Sound, Washington, *Journal of environmental quality*, 39 (2010) 1173.
- [34] N. Watanabe, B.A. Bergamaschi, K.A. Loftin, M.T. Meyer, T. Harter, Use and environmental occurrence of antibiotics in freestall dairy farms with manured forage fields, *Environmental science & technology*, 44 (2010) 6591-6600.
- [35] A. Jurado, E. Vázquez-Suñé, J. Carrera, M. López de Alda, E. Pujades, D. Barceló, Emerging organic contaminants in groundwater in Spain: a review of sources, recent occurrence and fate in a European context, *The Science of the total environment*, 440 (2012) 82.
- [36] R. Meffe, I. de Bustamante, Emerging organic contaminants in surface water and groundwater: A first overview of the situation in Italy, *Science of the Total Environment*, 481 (2014) 280-295.
- [37] Y. Luo, W. Guo, H.H. Ngo, L.D. Nghiem, F.I. Hai, J. Zhang, S. Liang, X.C. Wang, A review on the occurrence of micropollutants in the aquatic environment and their fate and removal during wastewater treatment, *The Science of the total environment*, 473-474 (2014) 619-641.
- [38] S.C. Monteiro, A.B.A. Boxall, Occurrence and fate of human pharmaceuticals in the environment, *Reviews of environmental contamination and toxicology*, 202 (2010) 53-154.
- [39] O. Jones, N. Voulvoulis, J. Lester, Potential Ecological and Human Health Risks Associated With the Presence of Pharmaceutically Active Compounds in the Aquatic Environment, *Critical Reviews in Toxicology*, 34 (2004) 335-350.
- [40] O.B. Samuelsen, B.T. Lunestad, A. Ervik, S. Fjelde, Stability of antibacterial agents in an artificial marine aquaculture sediment studied under laboratory conditions, *Aquaculture*, 126 (1994) 283-290.
- [41] A.Y.-C. Lin, M.H. Plumlee, M. Reinhard, Natural attenuation of pharmaceuticals and alkylphenol polyethoxylate metabolites during river transport: photochemical and biological transformation, *Environmental toxicology and chemistry / SETAC*, 25 (2006) 1458-1464.
- [42] M.S. Díaz-Cruz, M.a.J. López de Alda, D. Barceló, Environmental behavior and analysis of veterinary and human drugs in soils, sediments and sludge, *Trends in Analytical Chemistry*, 22 (2003) 340-351.
- [43] H. Zhou, Q. Zhang, X. Wang, Q. Zhang, L. Ma, Y. Zhan, Systematic screening of common wastewater-marking pharmaceuticals in urban aquatic environments: implications for environmental risk control, *Environmental Science and Pollution Research*, 21 (2014) 7113-7129.
- [44] C. Vannini, G. Domingo, M. Marsoni, F. De Mattia, M. Labra, S. Castiglioni, M. Bracale, Effects of a complex mixture of therapeutic drugs on unicellular algae *Pseudokirchneriella subcapitata*, *Aquatic Toxicology*, 101 (2011) 459-465.
- [45] Y. Kim, K. Choi, J. Jung, S. Park, P.-G. Kim, J. Park, Aquatic toxicity of acetaminophen, carbamazepine, cimetidine, diltiazem and six major sulfonamides, and their potential ecological risks in Korea, *Environment international*, 33 (2007) 370-375.
- [46] F. Pomati, S. Castiglioni, E. Zuccato, Effects of a Complex Mixture of Therapeutic Drugs at Environmental Levels on Human Embryonic Cells, *Environmental Science & Technology [H.W. Wilson - GS]*, 40 (2006) 2442.
- [47] D.J. Johnson, H. Sanderson, R.A. Brain, C.J. Wilson, K.R. Solomon, Toxicity and hazard of selective serotonin reuptake inhibitor antidepressants fluoxetine, fluvoxamine, and sertraline to algae, *Ecotoxicology and environmental safety*, 67 (2007) 128-139.
- [48] M.J. Winter, T.H. Hutchinson, A.D. Lillicrap, J.E. Caunter, C. Schaffner, A.C. Alder, M. Ramil, T.A. Ternes, E. Giltrow, J.P. Sumpter, Defining the chronic impacts of atenolol on embryo-larval

development and reproduction in the fathead minnow ( *Pimephales promelas*), *Aquatic Toxicology*, 86 (2008) 361-369.

[49] E. Minagh, R. Hernan, K. O'Rourke, F.M. Lyng, M. Davoren, Aquatic ecotoxicity of the selective serotonin reuptake inhibitor sertraline hydrochloride in a battery of freshwater test species, *Ecotoxicology and Environmental Safety*, 72 (2009) 434-440.

[50] A.C. Mehinto, E.M. Hill, C.R. Tyler, Uptake and biological effects of environmentally relevant concentrations of the nonsteroidal anti-inflammatory pharmaceutical diclofenac in rainbow trout (*Oncorhynchus mykiss*), *Environmental science & technology*, 44 (2010) 2176-2182.

[51] B.t. Ferrari, N. Paxéus, R.L. Giudice, A. Pollio, J. Garric, Ecotoxicological impact of pharmaceuticals found in treated wastewaters: study of carbamazepine, clofibric acid, and diclofenac, *Ecotoxicology and Environmental Safety*, 55 (2003) 359-370.

[52] M. Crane, C. Watts, T. Boucard, Chronic aquatic environmental risks from exposure to human pharmaceuticals, *The Science of the total environment*, 367 (2006) 23-41.

[53] J.L. Oaks, M. Arshad, S. Mahmood, A. Ali, A.A. Khan, M. Gilbert, M.Z. Virani, R.T. Watson, C.U. Meteyer, B.A. Rideout, H.L. Shivaprasad, S. Ahmed, M.J.I. Chaudhry, Diclofenac residues as the cause of vulture population decline in Pakistan, *Nature*, 427 (2004) 630-633.

[54] F.M. Christensen, Pharmaceuticals in the environment--a human risk?, *Regulatory Toxicology and Pharmacology*, 28 (1998) 212-221.

[55] O.A.H. Jones, Potential Ecological and Human Health Risks Associated With the Presence of Pharmaceutically Active Compounds in the Aquatic Environment, *Critical Reviews in Toxicology*, 34 (2004) 335-350.

[56] S. Webb, T. Ternes, M. Gibert, K. Olejniczak, Indirect human exposure to pharmaceuticals via drinking water, *Toxicology Letters*, 142 (2003) 157-167.

[57] M. Cleuvers, Aquatic ecotoxicity of pharmaceuticals including the assessment of combination effects, *Toxicology Letters*, 142 (2003) 185-194.

[58] Anonymous, WHO Model List of Essential Medicines, *WHO Drug Information*, 19 (2005) 222.

[59] L. Sera, M.L. McPherson, H.M. Holmes, Commonly prescribed medications in a population of hospice patients, *The American journal of hospice & palliative care*, 31 (2014) 126-131.

[60] T. Buckley, A. Cashin, M. Stuart, G. Browne, S.V. Dunn, Nurse practitioner prescribing practices: the most frequently prescribed medications, *Journal of Clinical Nursing*, 22 (2013) 2053-2063.

[61] P.F. Carey, L.E. Martin, P.E. Owen, Determination of ranitidine and its metabolites in human urine by reversed-phase ion-pair high-performance liquid chromatography, *Journal of Chromatography B: Biomedical Sciences and Applications*, 225 (1981) 161-168.

[62] A.L. Batt, M.S. Kostich, J.M. Lazorchak, Analysis of ecologically relevant pharmaceuticals in wastewater and surface water using selective solid-phase extraction and UPLC-MS/MS, *Analytical chemistry*, 80 (2008) 5021-5030.

[63] E. Zuccato, S. Castiglioni, R. Fanelli, G. Reitano, R. Bagnati, C. Chiabrando, F. Pomati, C. Rossetti, D. Calamari, Pharmaceuticals in the environment in Italy: causes, occurrence, effects and control, *Environmental science and pollution research international*, 13 (2006) 15-21.

[64] M. Gros, M. Petrović, D. Barceló, Wastewater treatment plants as a pathway for aquatic contamination by pharmaceuticals in the ebro river basin (northeast Spain), *Environmental toxicology and chemistry / SETAC*, 26 (2007) 1553-1562.

[65] R. Shen, S.A. Andrews, Demonstration of 20 pharmaceuticals and personal care products (PPCPs) as nitrosamine precursors during chloramine disinfection, *Water research*, 45 (2011) 944-952.

[66] M. Isidori, A. Parrella, P. Pistillo, F. Temussi, Effects of ranitidine and its photoderivatives in the aquatic environment, *Environment International*, 35 (2009) 821-825.

- [67] L. Rocco, G. Frenzilli, D. Fusco, C. Peluso, V. Stingo, Evaluation of zebrafish DNA integrity after exposure to pharmacological agents present in aquatic environments, *Ecotoxicology and Environmental Safety*, 73 (2010) 1530-1536.
- [68] M. Bergheim, R. Gieré, K. Kümmerer, Biodegradability and ecotoxicity of tramadol, ranitidine, and their photoderivatives in the aquatic environment, *Environmental science and pollution research international*, 19 (2012) 72-85.
- [69] A. Carucci, G. Cappai, M. Piredda, Biodegradability and toxicity of pharmaceuticals in biological wastewater treatment plants, *Journal of environmental science and health. Part A, Toxic/hazardous substances & environmental engineering*, 41 (2006) 1831-1842.
- [70] S.F. O'Hannesin, R.W. Gillham, Long-term performance of an in situ "iron wall" for remediation of VOCs, *GROUND WATER*, 36 (1998) 164-170.
- [71] R.W. Puls, C.J. Paul, R.M. Powell, The application of in situ permeable reactive (zero-valent iron) barrier technology for the remediation of chromate-contaminated groundwater: a field test, *Applied Geochemistry*, 14 (1999) 989-1000.
- [72] K.J. Cantrell, D.I. Kaplan, T.W. Wietsma, Zero-valent iron for the in situ remediation of selected metals in groundwater, *Journal of Hazardous Materials*, 42 (1995) 201-212.
- [73] C. Su, R.W. Puls, Arsenate and arsenite removal by zerovalent iron: kinetics, redox transformation, and implications for in situ groundwater remediation, *Environmental science & technology*, 35 (2001) 1487-1492.
- [74] J.L. Ginner, P.J.J. Alvarez, S.L. Smith, M.M. Scherer, Nitrate and Nitrite Reduction by Fe<sub>0</sub>: Influence of Mass Transport, Temperature, and Denitrifying Microbes, *Environmental Engineering Science*, 21 (2004) 219-229.
- [75] K. Praveena Juliya Dorathi Palanivelu, Dechlorination of chlorophenols by zero valent iron impregnated silica, *环境科学学报：英文版*, 24 (2012) 765-773.
- [76] W.J. Epolito, H. Yang, L.A. Bottomley, S.G. Pavlostathis, Kinetics of zero-valent iron reductive transformation of the anthraquinone dye Reactive Blue 4, *Journal of Hazardous Materials*, 160 (2008) 594-600.
- [77] S.G. Bratsch, Standard electrode-potentials and temperature coefficients in water at 298.15-K, *Journal of Physical and Chemical Reference Data*, 18 (1989) 1-21.
- [78] T.M. Vogel, C.S. Criddle, P.L. McCarty, Transformations of halogenated aliphatic compounds, *Environmental Science & Technology*, 21 (1987) 722-736.
- [79] L.J. Matheson, P.G. Tratnyek, Reductive dehalogenation of chlorinated methanes by iron metal, *Environmental science & technology*, 28 (1994) 2045-2053.
- [80] A.J. Feitz, S.H. Joo, J. Guan, Q. Sun, D.L. Sedlak, T. David Waite, Oxidative transformation of contaminants using colloidal zero-valent iron, *Colloids and Surfaces A: Physicochemical and Engineering Aspects*, 265 (2005) 88-94.
- [81] F. Fu, D.D. Dionysiou, H. Liu, The use of zero-valent iron for groundwater remediation and wastewater treatment: a review, *Journal of hazardous materials*, 267 (2014) 194-205.
- [82] C. Noubactep, Characterizing the effects of shaking intensity on the kinetics of metallic iron dissolution in EDTA, *Journal of Hazardous Materials*, 170 (2009) 1149-1155.
- [83] A. Ghauch, A. Tuqan, Reductive destruction and decontamination of aqueous solutions of chlorinated antimicrobial agent using bimetallic systems, *Journal of Hazardous Materials*, 164 (2009) 665-674.
- [84] A. Ghauch, H. Abou Assi, A. Tuqan, Investigating the mechanism of clofibrac acid removal in Fe<sub>0</sub>/H<sub>2</sub>O systems, *Journal of Hazardous Materials*, 176 (2010) 48-55.
- [85] A. Ghauch, H. Abou Assi, S. Bdeir, Aqueous removal of diclofenac by plated elemental iron: Bimetallic systems, *Journal of Hazardous Materials*, 182 (2010) 64-74.



- [86] C. Lee, C.R. Keenan, D.L. Sedlak, Polyoxometalate-enhanced oxidation of organic compounds by nanoparticulate zero-valent iron and ferrous ion in the presence of oxygen, *Environmental science & technology*, 42 (2008) 4921-4926.
- [87] A. Ghauch, H. Baydoun, A. Tuqan, G. Ayoub, S. Naim, Submicrometric iron particles for the removal of pharmaceuticals from water: Application to b-lactam antibiotics, in: M. Soueidan, M. Roumie, P. Masri (Eds.) *Advances in Innovative Materials and Applications*, Trans Tech Publications Ltd, Stafa-Zurich, 2011, pp. 485-488.
- [88] V. Homem, L. Santos, Degradation and removal methods of antibiotics from aqueous matrices – A review, *Journal of Environmental Management*, 92 (2011) 2304-2347.
- [89] A. Ghauch, H. Baydoun, P. Dermesropian, Degradation of aqueous carbamazepine in ultrasonic/Fe<sup>0</sup>/H<sub>2</sub>O<sub>2</sub> systems, *Chemical Engineering Journal*, (2011).
- [90] M. San Sebastián, amp, x, N. nez, J.F. Fernández, amp, x, guls, X.F. Segura, A.S. Ferrer, Pre-oxidation of an extremely polluted industrial wastewater by the Fenton's reagent, *Journal of Hazardous Materials*, 101 (2003) 315-322.
- [91] I. Arslan-Alaton, S. Dogruel, Pre-treatment of penicillin formulation effluent by advanced oxidation processes, *Journal of Hazardous Materials*, 112 (2004) 105-113.
- [92] H. Tekin, O. Bilkay, S.S. Ataberk, T.H. Balta, I.H. Ceribasi, F.D. Sanin, F.B. Dilek, U. Yetis, Use of Fenton oxidation to improve the biodegradability of a pharmaceutical wastewater, *Journal of Hazardous Materials*, 136 (2006) 258-265.
- [93] H.Y. Li, Y.H. Gong, Q.Q. Huang, H. Zhang, Degradation of orange II by UV-assisted advanced fenton process: response surface approach, degradation pathway, and biodegradability, *Industrial & Engineering Chemistry Research*, 52 (2013) 15560-15567.
- [94] J. Nawrocki, B. Kasprzyk-Hordern, The efficiency and mechanisms of catalytic ozonation, *Applied Catalysis B, Environmental*, 99 (2010) 27-42.
- [95] S.H. Conrad, R.J. Glass, W.J. Peplinski, Bench-scale visualization of DNAPL remediation processes in analog heterogeneous aquifers: surfactant floods and in situ oxidation using permanganate, *Journal of Contaminant Hydrology*, 58 (2002) 13-49.
- [96] Y. Segura, F. Martínez, J.A. Melero, R. Molina, R. Chand, D.H. Bremner, Enhancement of the advanced Fenton process (Fe<sup>0</sup>/H<sub>2</sub>O<sub>2</sub>) by ultrasound for the mineralization of phenol, *Applied Catalysis B, Environmental*, 113-114 (2012) 100-106.
- [97] A Fenton-like Oxidation Process Using Corrosion of Iron Metal Sheet Surfaces in the Presence of Hydrogen Peroxide: A Batch Process Study Using Model Pollutants, *Environmental Technology*, 26 (2005) 341-352.
- [98] In Situ Chemical Oxidation of Contaminated Soil and Groundwater Using Persulfate: A Review, *Critical Reviews in Environmental Science and Technology*, 40 (2010) 55-91.
- [99] I.M. Kolthoff, I.K. Miller, The Chemistry of Persulfate. I. The Kinetics and Mechanism of the Decomposition of the Persulfate Ion in Aqueous Medium<sup>1</sup>, *Journal of the American Chemical Society*, 73 (1951) 3055-3059.
- [100] R.J. Watts, Enhanced Reactant-Contaminant Contact through the Use of Persulfate In Situ Chemical Oxidation (ISCO), SERDP Project ER-1489 Washington State University, (2011).
- [101] D.A. House, Kinetics and Mechanism of Oxidations by Peroxydisulfate, *Chemical Reviews*, 62 (1962) 185-203.
- [102] A. Ghauch, A.M. Tuqan, Oxidation of bisoprolol in heated persulfate/H<sub>2</sub>O systems: Kinetics and products, *Chemical Engineering Journal*, 183 (2012) 162-171.
- [103] A. Ghauch, A.M. Tuqan, N. Kibbi, Ibuprofen removal by heated persulfate in aqueous solution: A kinetics study, *Chemical Engineering Journal*, 197 (2012) 483-492.
- [104] A. Ghauch, A.M. Tuqan, N. Kibbi, S. Geryes, Methylene blue discoloration by heated persulfate in aqueous solution, *Chemical Engineering Journal*, 213 (2012) 259-271.
- [105] K.-C. Huang, R.A. Couttenye, G.E. Hoag, Kinetics of heat-assisted persulfate oxidation of methyl tert-butyl ether (MTBE), *Chemosphere*, 49 (2002) 413-420.

- [106] Y.-q. Gao, N.-y. Gao, Y. Deng, Y.-q. Yang, Y. Ma, Ultraviolet (UV) light-activated persulfate oxidation of sulfamethazine in water, *Chemical Engineering Journal*, 195-196 (2012) 248-253.
- [107] Experimental Evaluation of Catalyzed Hydrogen Peroxide and Sodium Persulfate for Destruction of BTEX Contaminants, *Soil and Sediment Contamination: An International Journal*, 16 (2007) 29-45.
- [108] G.P. Anipsitakis, D.D. Dionysiou, Radical generation by the interaction of transition metals with common oxidants, *Environmental science & technology*, 38 (2004) 3705-3712.
- [109] C.S. Liu, K. Shih, C.X. Sun, F. Wang, Oxidative degradation of propachlor by ferrous and copper ion activated persulfate, *Science of the Total Environment*, 416 (2012) 507-512.
- [110] S.P. Forsey, In situ chemical oxidation of creosote/coal tar residuals: Experimental and numerical investigation, in, ProQuest, UMI Dissertations Publishing, 2004.
- [111] J. Zhao, Y. Zhang, X. Quan, S. Chen, Enhanced oxidation of 4-chlorophenol using sulfate radicals generated from zero-valent iron and peroxydisulfate at ambient temperature, *Separation and Purification Technology*, 71 (2010) 302-307.
- [112] C. George, H.E. Rassy, J.M. Chovelon, Reactivity of selected volatile organic compounds (VOCs) toward the sulfate radical (SO<sub>4</sub><sup>•-</sup>), *International Journal of Chemical Kinetics*, 33 (2001) 539-547.
- [113] P. Nfodzo, H. Choi, Triclosan decomposition by sulfate radicals: Effects of oxidant and metal doses, *Chemical Engineering Journal*, 174 (2011) 629.
- [114] A. Rastogi, S.R. Al-Abed, D.D. Dionysiou, Sulfate radical-based ferrous–peroxymonosulfate oxidative system for PCBs degradation in aqueous and sediment systems, *Applied Catalysis B, Environmental*, 85 (2009) 171-179.
- [115] S.-Y. Oh, H.-W. Kim, J.-M. Park, H.-S. Park, C. Yoon, Oxidation of polyvinyl alcohol by persulfate activated with heat, Fe<sup>2+</sup>, and zero-valent iron, *Journal of hazardous materials*, 168 (2009) 346-351.
- [116] A. Ghauch, G. Ayoub, S. Naim, Degradation of sulfamethoxazole by persulfate assisted micrometric Fe<sup>0</sup> in aqueous solution, *Chemical Engineering Journal*, 228 (2013) 1168-1181.
- [117] G. Ayoub, A. Ghauch, Assessment of bimetallic and trimetallic iron-based systems for persulfate activation: Application to sulfamethoxazole degradation, *Chemical Engineering Journal*, 256 (2014) 280-292.
- [118] C. Liang, C.-F. Huang, N. Mohanty, R.M. Kurakalva, A rapid spectrophotometric determination of persulfate anion in ISCO, *Chemosphere*, 73 (2008) 1540-1543.
- [119] W. Österle, I. Urban, Third body formation on brake pads and rotors, *Tribology International*, 39 (2006) 401-408.
- [120] B.-T. Zhang, Y. Zhang, Y. Teng, M. Fan, Sulfate Radical and its Application in Decontamination Technologies, *Critical Reviews in Environmental Science and Technology*, (2014).
- [121] R. Matthews, H. Mahlman, T. Sworski, Elementary processes in the radiolysis of aqueous sulfuric acid solutions. Determinations of both GOH and GSO<sub>4</sub>, *The Journal of Physical Chemistry*, 76 (1972) 1265-1272.
- [122] C. Liang, C.J. Bruell, M.C. Marley, K.L. Sperry, Persulfate oxidation for in situ remediation of TCE. I. Activated by ferrous ion with and without a persulfate–thiosulfate redox couple, *Chemosphere*, 55 (2004) 1213-1223.
- [123] C. Liang, C.J. Bruell, Thermally Activated Persulfate Oxidation of Trichloroethylene: Experimental Investigation of Reaction Orders, *Industrial & Engineering Chemistry Research*, 47 (2008) 2912-2918.
- [124] R.S. Magazinovic, B.C. Nicholson, D.E. Mulcahy, D.E. Davey, Bromide levels in natural waters: its relationship to levels of both chloride and total dissolved solids and the implications for water treatment, *Chemosphere*, 57 (2004) 329-335.

- [125] C. Liang, Z.-S. Wang, N. Mohanty, Influences of carbonate and chloride ions on persulfate oxidation of trichloroethylene at 20 °C, *Science of The Total Environment*, 370 (2006) 271-277.
- [126] L.R. Bennedsen, J. Muff, E.G. Søgaaard, Influence of chloride and carbonates on the reactivity of activated persulfate, *Chemosphere*, 86 (2012) 1092-1097.
- [127] Y. Yang, J.J. Pignatello, J. Ma, W.A. Mitch, Comparison of halide impacts on the efficiency of contaminant degradation by sulfate and hydroxyl radical-based advanced oxidation processes (AOPs), *Environmental science & technology*, 48 (2014) 2344.
- [128] H.V. Lutze, N. Kerlin, T.C. Schmidt, Sulfate radical-based water treatment in presence of chloride: Formation of chlorate, inter-conversion of sulfate radicals into hydroxyl radicals and influence of bicarbonate, *Water Research*, (2014).
- [129] W.J. McElroy, A laser photolysis study of the reaction of sulfate(1-) with chloride and the subsequent decay of chlorine(1-) in aqueous solution, *The Journal of Physical Chemistry*, 94 (1990) 2435-2441.
- [130] R.E. Huie, C.L. Clifton, P. Neta, Electron transfer reaction rates and equilibria of the carbonate and sulfate radical anions, *International Journal of Radiation Applications & Instrumentation. Part C, Radiation Physics & Chemistry*, 38 (1991) 477-481.
- [131] V. Nagarajan, R.W. Fessenden, Flash photolysis of transient radicals. 1. X<sup>2-</sup> with X = Cl, Br, I, and SCN, *The Journal of Physical Chemistry*, 89 (1985) 2330-2335.
- [132] X.-Y. Yu, Z.-C. Bao, J.R. Barker, Free Radical Reactions Involving Cl•, Cl<sub>2</sub>-•, and SO<sub>4</sub>-• in the 248 nm Photolysis of Aqueous Solutions Containing S<sub>2</sub>O<sub>8</sub><sup>2-</sup> and Cl, *The Journal of Physical Chemistry A*, 108 (2004) 295-308.
- [133] G.V. Buxton, M. Bydder, G. Arthur Salmon, Reactivity of chlorine atoms in aqueous solution Part 1 The equilibrium CIMNSbd+Cl-Cl<sub>2</sub>, *Journal of the Chemical Society, Faraday Transactions*, 94 (1998) 653-657.
- [134] G.G. Jayson, B. Parsons, A.J. Swallow, Some simple, highly reactive, inorganic chlorine derivatives in aqueous solution. Their formation using pulses of radiation and their role in the mechanism of the Fricke dosimeter, *Journal of the Chemical Society, Faraday Transactions 1*, 1973 (1973) 1597.
- [135] J.L. Redpath, R.L. Willson, Chain Reactions and Radiosensitization: Model Enzyme Studies, *International Journal of Radiation Biology*, 27 (1975) 389-398.
- [136] D. Zehavi, J. Rabani, Oxidation of aqueous bromide ions by hydroxyl radicals. Pulse radiolytic investigation, *The Journal of Physical Chemistry*, 76 (1972) 312-319.
- [137] A.B. Ross, P.j.a. Neta, C. United States. Dept. of, S. United States. National Bureau of, Rate constants for reactions of inorganic radicals in aqueous solution, 1979.
- [138] R.C. Beckwith, T.X. Wang, D.W. Margerum, Equilibrium and kinetics of bromine hydrolysis, *Inorganic Chemistry*, 35 (1995) 995.
- [139] H.V. Lutze, R. Bakkour, N. Kerlin, C. von Sonntag, T.C. Schmidt, Formation of bromate in sulfate radical based oxidation: mechanistic aspects and suppression by dissolved organic matter, *Water research*, 53 (2014) 370.
- [140] P. Westerhoff, Reduction of Nitrate, Bromate, and Chlorate by Zero Valent Iron (Fe<sup>0</sup>), *Journal of Environmental Engineering*, 129 (2003) 10-16.
- [141] J.S. Kim, J.-E. Kim, P.J. Shea, J.E. Yang, Halide salts accelerate degradation of high explosives by zerovalent iron, *Environmental Pollution*, 147 (2007) 634-641.
- [142] F.J. Millero, M. Izaguirre, Effect of ionic strength and ionic interactions on the oxidation of Fe(II), *Journal of Solution Chemistry*, 18 (1989) 585-599.
- [143] M. Mirmehrabi, S. Rohani, K.S.K. Murthy, B. Radatus, Solubility, dissolution rate and phase transition studies of ranitidine hydrochloride tautomeric forms, *International Journal of Pharmaceutics*, 282 (2004) 73-85.

- [144] J.A. Rosso, P.E. Allegretti, D.O. Mártire, M.C. Gonzalez, Reaction of sulfate and phosphate radicals with  $\alpha,\alpha,\alpha$ -trifluorotoluene, *Journal of the Chemical Society, Perkin Transactions 2*, (1999) 205-210.
- [145] T. Ridley, K.P. Lawley, M.H.S.N. Al-Kahali, R.J. Donovan, Determination of the first ionization energy of furan (C<sub>4</sub>H<sub>4</sub>O) from an extrapolation of two nd Rydberg series observed in the mass-resolved (2 + 1) resonance enhanced multiphoton ionization spectrum, *Chemical Physics Letters*, 390 (2004) 376-379.
- [146] The Hydroxyl Radical, in, Springer Berlin Heidelberg, Berlin, Heidelberg, 2006, pp. 47-75.